DESIGN OF AN ORIGAMI PATTERNED PRE-FOLDED THIN WALLED

TUBULAR STRUCTURE FOR CRASHWORTHINESS

A Thesis

Submitted to the Faculty

of

Purdue University

by

Prathamesh Chaudhari

In Partial Fulfillment of the

Requirements for the Degree

of

Master of Science in Mechanical Engineering

May 2019

Purdue University

Indianapolis, Indiana

THE PURDUE UNIVERSITY GRADUATE SCHOOL
STATEMENT OF COMMITTEE APPROVAL

Dr. Andres Tovar, Chair

     Department of Mechanical and Energy Engineering

Dr. Khosrow Nematollahi

     Department of Mechanical and Energy Engineering

Dr. Hazim A El-Mounayri

     Department of Mechanical and Energy Engineering

Approved by:

     Dr. Sohel Anwar

          Chair of the Graduate Program

Dedicated to my parents and especially to my younger sister Aishwarya.

ACKNOWLEDGMENTS

TABLE OF CONTENTS

LIST OF TABLES

LIST OF FIGURES

SYMBOLS

m mass

v velocity

w width of tube

t Thickness of tube

M Number of Modules

θ Dihedral Angle

L Length of Tube

E Young's Modules

μ Friction coefficient

ν Poisson ratio

ρ Material density

σ_y Yield stress

σ_u Ultimate stress

ABBREVIATIONS

$PEEQ$ Equivalent Plastic Strain

MCF Mean Crushing Force

PCF Peak Crushing Force

SEA Specific Energy Absorption

CFE Crushing Force Efficiency

A_{max} Peak Deceleration

A_{mean} Mean Deceleration

SE Strain Energy

ms Milli Seconds

kN Kilo Newton

mps Meters per second

mph Miles per hour

ABSTRACT

Chaudhari, Prathamesh. M.S.M.E., Purdue University, May 2019. Design of an Origami Patterned Pre-Folded Thin Walled Tubular Structure for Crashworthiness. Major Professor: Andres Tovar.

Thin walled tubular structures are widely used in the automotive industry because of its weight to energy absorption advantage. A lot of research has been done in different cross sectional shapes and different tapered designs, with design for manufacturability in mind, to achieve high specific energy absorption.

In this study a novel type of tubular structure is proposed, in which predesigned origami initiators are introduced into conventional square tubes. The crease pattern is designed to achieve extensional collapse mode which results in decreasing the initial buckling forces and at the same time acts as a fold initiator, helping to achieve a extensional collapse mode. The inuence of various design parameters of the origami pattern on the mechanical properties (crushing force and deceleration) are extensively investigated using nite element modelling. Thus, showing a predictable and stable collapse behavior. This pattern can be stamped out of a thin sheet of material.

The results showed that a properly designed origami pattern can consistently trigger a extensional collapse mode which can significantly lower the peak values of crushing forces and deceleration without compromising on the mean values. Also, a comparison has been made with the behavior of proposed origami pattern for extensional mode verses origami pattern with diamond fold.

1. INTRODUCTION

1.1 Thin Walled Energy Absorbing Structures

Impact accidents are unfortunate but common occurrences. An astonishing increase in traffic accidents has been witnessed accompanying the rapid development of the transportation vehicle industry. A report from the World Health Organization [1] pointed out that around 1.2 million people were killed and up to 50 million injured in road accidents each year. In addition, it was predicted that road traffic injuries could be the third leading cause of disease and injury by 2020 due to the expansion of car markets especially in less developed countries. Apart from severe injuries to human beings, an impact, once happens, often leads to catastrophic damages to the structures of the vehicles involved and the surrounding environment.

A most common approach of minimizing the loss of life and property in an impact accident is to install energy absorption devices in the structures, which are designed to convert, totally or partially, kinetic energy into another form of energy during the accident so that damages to the important main structures are mitigated [2]. An ideal energy absorption device should meet the following requirements [3]:

1. Irreversible energy conversion to avoid a second impact caused by energy release.

2. Long stroke to allow space for plastic deformation

3. Stable and repeatable deformation mode to ensure predictable performance in each impact.

4. Restricted and constant reactive force so that no excessive force is transmitted to the main structure to be protected.

5. Light weight and high energy absorption to absorb as much energy as possible.

6. Low cost and easy installation as it is a one-shot device and needs replacement after an impact accident.

Practically, two parameters are extensively applied to evaluate the energy absorption performance of a device: the specific energy absorption (SEA), defined as the energy absorption per unit mass, and the load uniformity, defined as the ratio of the peak force to the mean crushing force [4]. Here the peak force is the highest reaction force during the crushing process and the mean crushing force is the total energy absorption dividing the final crushing distance.

Thin-walled tubes are among the most commonly used energy absorption devices due to their high manufacturability and low cost. The main deformation modes of thin walled tubes include axial compression [5], lateral compression [6], lateral indentation [7], inversion [8], and tube splitting [9]. Lateral compression and lateral indentation of tubes can lead to a smooth force vs displacement curve, but the SEA is relatively low because the stroke length is small. Tube inversion and tube splitting can generate a quite high SEA, but requires special dies for the deformation modes to be induced. Axial compression of tubes has the merits of a relatively long stroke length, high SEA, and mechanical simplicity, and is therefore widely applied in practice. The main energy dissipation mechanism of this type of device is material plastic deformation. In automobiles such devices, are also known as crashcans, are mounted between the bumper beam and the main frame of a vehicle. They are designed to absorb energy during a low speed collision. The primary energy absorbers in trains, are similar thin-walled tubes with a square cross section [10–12]. Tubular devices are also found in helicopter landing gears, except that they generally have a circular cross section [13]. Because different designs result in different performances, it remains a challenge to achieve both high SEA and low load uniformity while reducing cost.

Thin-walled tubes are another type of commonly used energy absorption device. It usually adopts a curved profile with a box cross section and is designed to absorb kinetic energy as well as to transmit the impact loading to the two crashcans in a frontal collision. Thin-walled beams are also seen in roadside guardrail systems [14],

designed to contain and re-direct out-of-control vehicles in order to reduce injuries to the occupants and damages to the vehicles themselves [15]. Unlike the axial compression of thin-walled tubes which generates extensive material plastic deformation, the lateral bending collapse of thin-walled beams features localized plastic deformation, leading to relatively low energy absorption efficiency. Therefore despite having practical applications, thin-walled beams have not received much attention from researchers and engineers.

1.2 Origami Design

Origami is an ancient Japanese art of producing intricate 2D or 3D models through folding paper or cards. In its traditional form, a piece of paper is formed into an endless variety of shapes following a pattern design. The basic technique of origami is folding with two types of folding creases, namely the valley and the mountain creases. A folding pattern is produced by combining and arranging those creases. An obvious yet significant application of origami is to use it to control the deformation process and final configuration of a thin sheet of material. This shape changing property of origami makes it possible to be applied in a variety of engineering fields in which configuration design and control are vital. Current applications of origami can be classified into two categories. One involves the design of arbitrary shapes. For instance, a technique known as DNA-Origami manages to fold long, single-stranded DNA molecules into arbitrary 2D shapes in order to create nanostructure shapes of high complexity [16]. The other is for packaging structures so that they can be conveniently stored or transported. Deployable cylinders, mainly used as inflatable deployable booms in aerospace engineering, fall into this category [17–22]. In both categories of applications, structures with origami patterns are required to be deployed and folded with minimum effort, implying a small variation in strain energy during the folding process. At the other end of the spectrum, some origami objects may

induce large deformation in thin-walled materials. This feature has never been fully explored.

1.3   Purpose of this Thesis

Comparison of the behavior of thin-walled tubular energy absorption devices and deployable cylinders clearly demonstrates the strong correlation between collapse mode and energy absorption capability. A normal tube requires a great deal of energy to be crushed axially because it follows a particular failure mode, whereas a tube with a type of origami pattern on the surface can be folded with ease if the pattern is carefully selected and its folding follows the given pattern. Therefore if we can use origami patterns to direct a thin-walled tube to collapse in a failure mode that involves extensive material plastic deformation, high energy absorption could be achieved. The aim of the work is to explore the possibility of designing high-performance thin walled tubular energy absorption devices by means of innovative application of origami patterns. Specifically, a novel origami pattern is developed to design thin-walled tube subjected to dynamic axial compression a, referred to as the origami tube, in the thesis due to the fact that they have origami patterns on the surface. This thesis concentrates on the structural design and analysis of the origami tube, in which numerical analysis approach is employed. Since the concepts developed here are purely structural, they can be applied to energy absorption devices with various dimensions and material types. The main contents of the thesis are as follows:

1. Numerical analysis of the dynamic axial crushing of the conventional square tube.

2. Structural design of the origami tube as an energy absorption device.

3. Numerical analysis of the dynamic axial crushing of the origami tube.

4. Parametric study on different parameters of origami pattern.

1.4 Thesis Layout

A brief review of previous work relevant to thin-walled tubular structures is provided in Chapter 2. Emphasis is placed on the static and dynamic axial crushing of circular and square tubes, i.e., thin-walled tubes with circular and square cross sections, as well as existing designs of thin-walled tubes and beams for the purpose of energy dissipation. A number of origami designs, specifically related to square and rectangular cross section are also reviewed in this chapter.

Since the entire work in this thesis relies heavily on Finite Element Methods (FEM), Chapter 3 discusses regarding finite element formulations for dynamic crash analysis. An overview of finite element methods is given followed by differences in linear and nonlinear analysis are pointed. Different nonlinear properties used in defining the FE model are discussed in detailed. Mesh sensitivity study and node point integration (NIP) sensitivity study has been performed and their effects on crash performance is discussed. And finally a benchmark formulation is created with conventional square tube, to compare the performance with that of the proposed origami design.

Chapter 4 address the design and analysis of the proposed origami pattern and focuses on the numerical study of the origami tube. Folding pattern in conventional square tube is analyzed first before developing the origami pattern. Then the design and geometric analysis of the novel origami pattern for origami tubes with square cross section is covered. Subsequently 37 origami tubes with varying configurations are designed and analyzed to investigate the failure mode and energy absorption properties of the origami tube subjected to dynamic axial crushing. Finally, several important factors influencing the performance of the origami tube as a practical energy absorption device, like the effect of different dihedral angle, different number of modules M and the effect of dimension b of hexagonal element is discussed.

Chapter 5 covers the main achievements of the current research and suggestions of work to be conducted in the future, which concludes the thesis.

2. REVIEW OF PREVIOUS WORK

2.1 Overview

Chapter 2 briefly covers concepts in crashworthiness, different types of collapse patterns and presents a survey of previous work. Section 2.2 and section 2.3 briefly covers crashworthiness basics. Section 2.4 describes different modes of crash and elaborates crash behavior in those modes. Section 2.5 and 2.6 focuses on various requirements in crash structure and about designing crash efficient structure Section 2.7 and 2.8 explains in detail different types of axial collapse in thin walled structures, and also listed their respective advantages and disadvantages. Further stability in axial crushing is also briefly covered. Section 2.9 discusses in detail, different types of energy absorption devices used in crash analysis and further explains individual advantages and shortcomings.

2.2 Crashworthiness

Crashworthiness is an engineering term which defines an ability of an structure to protect its occupants in an event of an crash [23]. In other words, its an measure of an ability of a vehicle structure to sacrifice itself to resist the effect of impact, to protect its occupants in the event of crash. It was seen to be initially used in 1950's in the aviation industry for evaluating the margins of tolerable damage human can sustain during crash. Application of crashworthiness covers all the vehicle forms from air, water and land transportation industries. Safety of the passenger is of utmost priority, hence developing structure with higher crashworthy efficiency is one of the important design consideration during design phase. We have seen an evolution in design goals from 1980's to present day because of increase in types of automobiles

we offer and due to advancement in manufacturing techniques. Currently vehicle structures are manufactured widely using welding of stamped steel panels leading to create a unibody structure as opposed to body on frame, as seen few decades ago. To provide safety to occupant cabin, the crash structures are designed in a way to absorb the maximum amount of crash energy so as to lower the deceleration to an acceptable level. Hence, the objective of crashworthiness is to have a structure capable of absorbing maximum impact loads while controlling its crash behavior in order to minimize the amount of residual energy getting transferred to the passenger cabin and in turn to the passenger. Lower the residual energy transfer to the cabin will result in lower deceleration forces on occupant. Therefore to design a crashworthy structure it is necessary to discern the key factors influencing the crash behavior. In the following section we will review the key characteristic features seen in crash.

2.3   Crash Characteristics

Galganski in his work in [24], performed extensive study on experimental crashworthiness in automobiles and have described general physical principles involved in the high speed crash. According to him, crashworthiness problems can be characterized by:

1. Crushing distance: With advancement in technology and time, the crushing distance of a crash structures are lowered but at the same time they need to absorb the same amount of crushing loads as required by the safety standards.

2. Crash pulse: When vehicle encounters an impact, which causes an sudden deceleration in the body of the vehicle and in turn deceleration is induced in occupant, which is called crash pulse. Head Impact Criteria (HIC) is the most commonly used criteria for measuring the injury prediction on brain due to crash [25].

3. Location of crash: The crash structure should be crashworthy enough to handle the crushing load occurring in different crash locations, may that be straight or oblige loading with all types of crash loading events described by safety standards.

4. Congruity: The crash structure should be able to handle the crushing load in case of crash involving vehicles with different models of different weight, size and shapes.

2.4   Accidents Types

In real life situations, the crash occurs in an arbitrary manner, involving vehicles with different shape, size and weight. The crash can happen involving various vehicles with traveling at different speeds or even an immobile objects like a tree, electricity pole, concrete road divider, etc. Also the crash can involve one or numerous impacts. Since there are various scenarios in which vehicle can crash, for the purpose of development of crash structures, vehicle crash are classified into four broad categories - front, rear, side and rollover crash With different scenarios in mind, crashworthy structures are developed based on the crash category. The crash effectiveness of a structure are independently judges for the above mentioned crash categories. The calculable data which is required such as crash pulse, impact load on passenger, occupant safety, etc. can not be obtained by crash reconstruction. Hence physical testing is needed to be conducted in labs for ground up evaluation for passenger safety. There are basically four types of impacts categorized broadly - Front, rear, side and roof impact. Figure 2.1 shows passenger car accidents by type of impacts. We will go through each of them one by one.
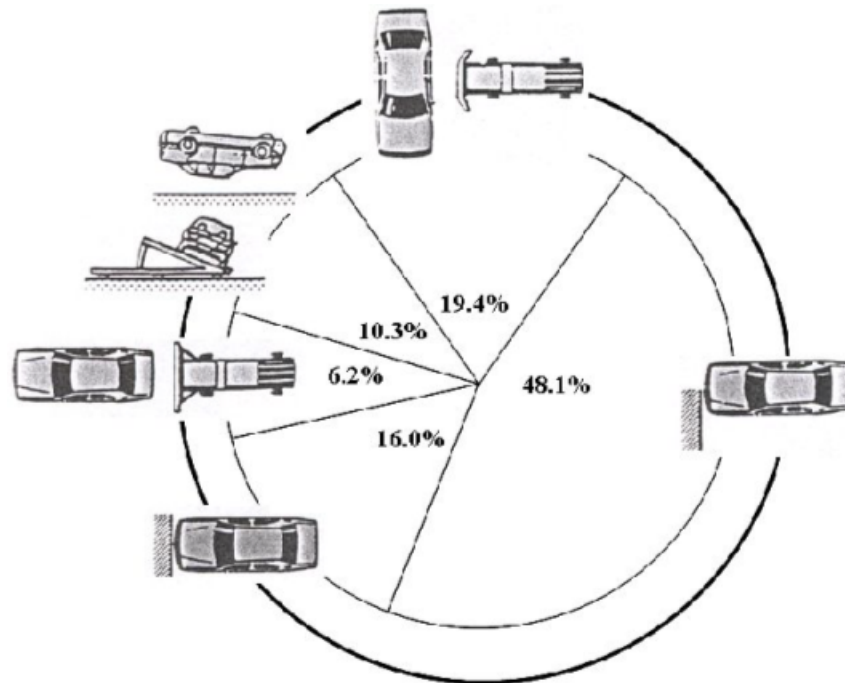
Fig. 2.1. Passenger car accidents by type of impacts [26]

2.4.1 Frontal Impact

The frontal impacts list first when we see the most common modes of crash. From Figure 2.1 we can say, almost 64% of crashes are seen with front impact [26]. Imagine a situation when vehicle impacts an stationary, as seen in Figure 2.2, or moving target from front, as seen in Figure 2.3. During front impact, at first, the vehicle structure absorbs the kinetic energy by undergoing plastic deformation. After the crash structure, the generated crash pulse is then transferred to the passenger cabin, which causes the passenger to move in the direction of inertial forces and against the restraint system. Now the residual energy is then transferred to the restrain system which leads to interior deformation and compression of passengers body. If the deceleration amount is higher than a certain amount, can injure the passenger. Hence, while developing crash structures focus is there on maximum energy absorption but it is made sure that the deceleration is happening gradually and its values are within

human acceptable tolerance limit. Besides developing the design of crash structure, different restraint methods are also used like seat belts, air bags, pretensioners etc. to lower the possibility of injury to passenger. The vehicle companies needs to prove safety of a vehicle to a certain acceptable level by showing their designs satisfying the safety standards created by government firms. For front impact, in USA the manufacturers need to follow FMVSS 208, in Canada the standard is CMVSS 208 and in Europe it is ECE R-12 [27–29].
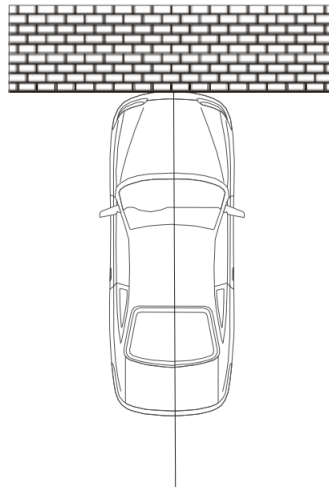
Fig. 2.2. Front Impact with Fixed Barrier [30]
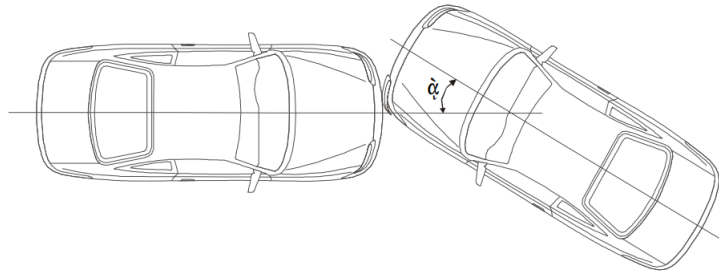
Fig. 2.3. Car to Car Frontal Crash [30]

2.4.2 Side Impact

After front impact, the second most common mode of crash is through sideways. Almost 19% of all the crashes are recorded with side impact, as seen in Figure 2.1. Imagine a situation when a car is impacting another car on one of its side pillars or even to an stationary electricity pole, tree or a barrier. Figure 2.4 shows an example of side impact from one vehicle to another.
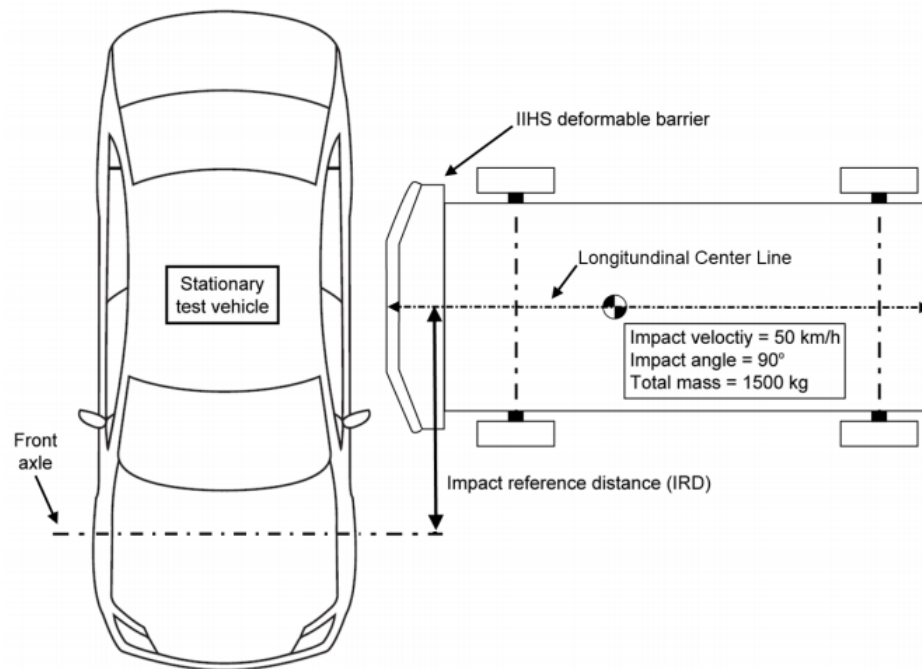
Fig. 2.4. Side Impact with Moving Barrier [31]

As discussed in front crash, in side crash also the crushing forces generated by the another vehicle are absorbed by the side pillars of the primary car by undergoing plastic deformation. This is the phase where the major amount of deformation happens. The crash pulse then travel through the passenger cabin which causes the passenger to experience sudden deceleration. The energy absorption due to restraint systems are very low in side crashes when compared with front crashes, as the distance between the pillars and the passenger is very low. Hence the major EA in side

crashes is done by the pillars, absorbing all the crushing forces and going under plastic deformation in turn lowering the deceleration pulse. Hence while development phase, a lot of emphasis is given to maximize the stiffness of A-pillar, B-pillar and C-pillar of a car chassis. If the deceleration amount is higher than the certain tolerance limit [27] can cause serious injuries to passenger. There are many systems which do contribute to energy absorption which are responsible for In USA for side crash, FMVSS 214 standard is followed, in Canada CMVSS 214 is followed and in Europe ECE R-59 standard is followed [27–29].

2.4.3 Rear Impact

Rear impacts are the lowest recorded impacts out of all the impacts. It accounts for about 6% of all the impacts seen [26]. Additional precautions are taken while designing the rear crash structures than that of the front crash structures because of two main reasons. First, although the number of rear crashes are few but the whiplash injuries are much severe and complex than that of the side and front impact [32]. Second, most of the family vehicles have gas tank and fuel systems placed at the back of the vehicle, hence there is a higher change of leaking them in the event of crash. Besides structural crash members, the interior systems like the head restraints, seatbelts and back seat also contributes in energy absorption in the event of crash. In USA for rear crash, FMVSS 224 standard is followed, in Canada CMVSS 224 is followed and in Europe ECE R-42 standard is followed [27–29].
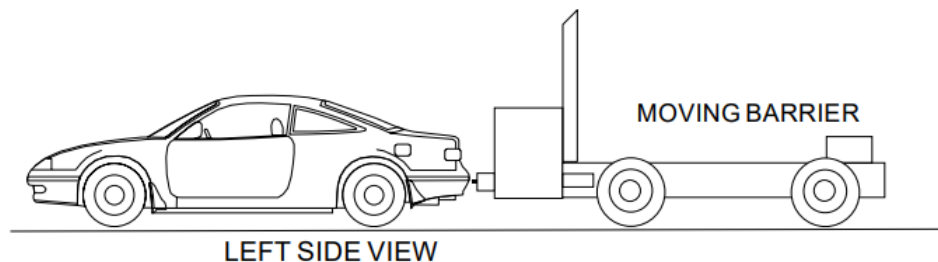
Fig. 2.5. Rear Impact [33]

2.4.4 Rollover Impact

Rollover impacts accounts for almost 10% of impacts recorded [26]. In rollover impacts there are two systems who play an important role parallelly. Firstly, the structure needs to absorb the impact but the structure should not deform more than a certain crushing distance or will cause injury to passenger. And secondly, the restraint seatbelt system plays a vital role here in minimizing the crash pulse transfer to the passenger While developing structure for rollover impact scenario, there are many things that needs to be considered like the door must remain closed during rollover. Also special care is taken for avoiding fuel spill like directing the fuel to coal base dump can to prevent fire [34]. The rollover impacts are more seen in bigger vehicles like buses because of their higher center of gravity. Hence rollover impacts are widely studied in them. Rollover impacts can be avoided by managing the dynamic parameters like braking performance, as described by El-Gindy in her work [35, 36]. In USA for rollover crash, FMVSS 201 and 208 standards are followed, in Canada CMVSS 201 and 208 are followed and in Europe ECE R-21 standard is followed [27–29].

2.5 Crash Structure Requirements

A crash structure to be crashworthy it is needed to satisfy some prerequisite conditions and requirements to bring down the deceleration pulse within acceptable limits, for range of impact velocities and impact masses. These requirements are elaborated below.

1. The crash structure should be able to collapse progressively rather than static buckling to maximize kinetic energy absorption so that restrain system has to handle minimum amount of kinetic energy which is transferred to cabin.

2. The front structure should be reasonably stiff and deformable enough to absorb the impact energies generated during frontal crash, by undergoing plastic defor-

mation without intruding the occupant cabin. Figure 2.6 shows an generic body in white structure of a car. From Figure 2.6 it can be seen, the bumper beam and the s rail will not allow for intrusion, due to deformation, in the engine bay and also in occupant cabin.

3. For side and rollover impact, cabin intrusion due to deformation needs to be within acceptable limits, as the amount of space available for deformation is pretty tight.

4. Rear structures needs to have extra structural integrity as it needs to protect the gas tank and fuel systems too besides occupant.

5. The restrains like seat belts, pretensioners, air bags, etc. needs to be appropriately developed for absorbing the residual energy transferred to the cabin.
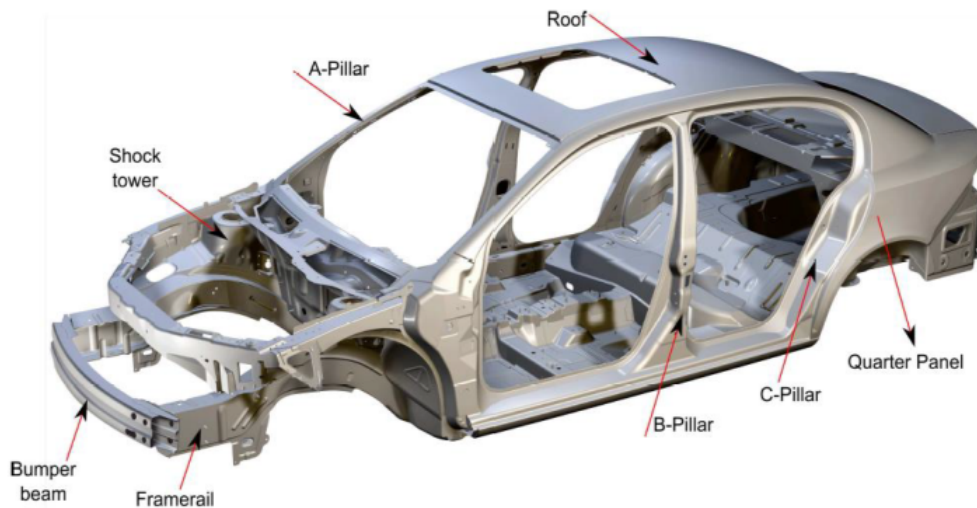
Fig. 2.6. Body In White Structure Of A Car [37]

An favorable design needs to satisfy these requirements and also needs to follow with other design goals like mass of the structure, which in turn affects the fuel economy. When developing a crash structure, there are many other goals that needs

to be addresses besides mass of the chassis. Hence the entire developing process is much more complex and challenging. Now, to have a clear understanding of these goals we need to understand the different collapse modes in which tubular structures collapse.

2.6   Crashworthiness Design

In 1950's, due to lack of technological development, physical testing of the crash structures was the best way of validating the design. But this prototyping method lead to higher validation time and also higher improvement price which inturn lead to evolution in computational based simulations using Finite Element Methods (FEM). Validating a design using finite element method was highly cost effective and also required small amount of validation time in order to develop a crashworthy design. FEM has made a lot of development in last few decades, and current algorithms can predict outcomes which are fairly accurate enough and can be compared with prototype validation results. Today component design validation is primarily done using computer simulations with FEM and only the final entire vehicle assembly is validated using prototyping method for making sure occupant cabin in not compromised. The vehicle chassis are getting complex as we are developing crashworthy structures with a goal to maximize the kinetic energy absorption and at the same time satisfy the safety standards with minimum amount of cost as possible. Hence higher the material used for manufacturing the structure, higher will be the manufacturing cost. The deceleration values and the crushing force values seen during crash are dependent on the amount of material used in the crash structure. Normally for running entire car crash simulation takes about 14 to 16 hours. The time is dependent on the model definition, its complexity and crashing scenario. Hence different ideas can be developed with sound engineering judgement and can we checked and validated upfront without significant computation time and cost. With this approach, the results are often not the best but it gives clarity in direction and the results can

be improved using optimization methods. Response surface method can be used to generate smooth approximation of functions to predict the design space. Design of experiments or parametric study can be performed to for finding optimal parameters. The final aim is to develop a best solution for a given design formulation. As day by day the safety regulations are getting tighter, with this approach, crash structures who are satisfying safety standards, can be quickly developed and validated without higher development time and money.

2.7 Axial Collapse in Square Tubular Structures

Square tubular structures broadly fall under two collapse mode. Firstly, the Eulerian Buckling collapse mode in which the structure collapses around the discrete plastic hinge line formed while crashing. And Second is a axial collapse mode or progressive, in which the formation of complete folds are seen around the length of the tube. The fold formation can be symmetric or asymmetric. Both the collapse modes are discussed in detail in the following sections

2.7.1 Static Buckling in Square Tubes

Buckling in thin walled structures has always been a challenge to overcome. Therefore, a lot work has been done in this field to overcome it. Buckling is normally seen in long tubes rather than short tubes, which is also known as Eulerian Buckling, as low energy path is formed in long tubes and thats difficult to form in short tubes. In 1960's Timoshenko derived an equation 2.1 [38], for finding a critical buckling force in an simply supported long tube.

$$P = \frac{\pi^2 EI}{L^2} \tag{2.1}$$

where E is the Youngs modulus, I is moment of inertia, and L is the length of the tube. He also developed an formulation for critical load for thin walled square structures as follows [38],

$$P = \frac{4\pi^2 E t^2}{3(1 - v^2)}\left(\frac{t}{b}\right) \tag{2.2}$$

where b will be the width.

Fig. 2.7. Euler Buckling [38]

An numerous amount of testing of were performed in the work [39, 40], leading to a conclusion that buckling only happens in thicker beam and the equation 2.1 aggrandize the critical buckling load. To account for this error, Yoshimura performed a set of experiments and detected a new type of buckling mode called as diamond collapse mode and later as Yoshimura pattern. This new pattern led to development of new critical load formulation, whose results were matching well with the exploratory results. In 1960's [41], various experimental data showed formation of equal amount of alternating folds on the sides on the tubular structure. Later in 1983 Meng [42] observed zero bending moment on the edges of these crushed tubes.

2.7.2   Static Axial Crushing in Square Tube

Highest amount of plastic deformation is noted during post buckling phase which leads to highest amount of energy absorption being recorded during this phase. In tubular structures, controlling this post buckling phase is very challenging, hence by just using analytical approach the collapse behavior can't be tracked back. Hence difficult to obtain the crushing distance vs crushing load plot. Normally just the mean crushing load can be calculated through theoretical approach, as described in the work done by Wierzbicki and Abramowicz [43]. Initially they identified an element in the entire collapse of an tubular structure which captures the most of the folding character. From this element the energy retention capacity is calculated by identifying the source of energy in the element. Then the total energy dissipation is the difference between the external work done by the axial collapse of the structural element and the energy dissipation by that element. Now the mean crushing force is the ratio of total energy dissipation to crushing length.
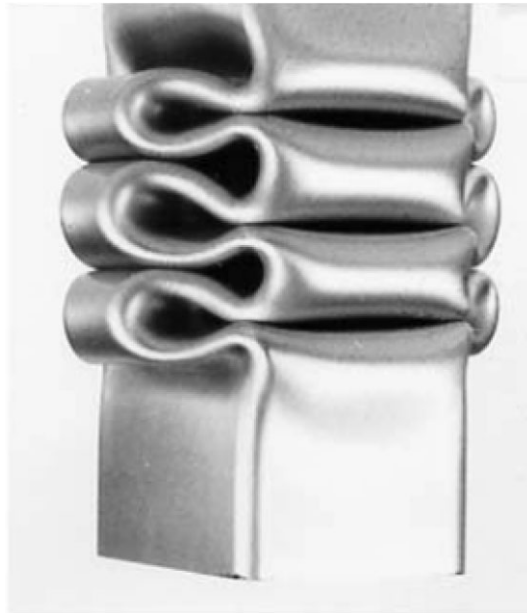
Fig. 2.8. Progressive Collapse in a Square Tube [44]

Many research has been done over attaining progressive collapse in tubular structures. And it seen that the collapse behavior pattern is proportional to width to thickness ratio, w/t, of the tube. If the thickness of the tube is very thin or the width to thickness ratio is high like, $w/t = 80$, then it will collapse with non compact mode, as seen in Figure [9]. But the collapse with this type is highly not favorable. First, because of thin thickness, the structure is more likely to buckle than progressive collapse. And second, the total energy absorption will be lower too.

Fig. 2.9. Non Compact Mode [9]

Now consider a square tube with dimensions of width as 60 mm, height as 100 mm and thickness as 2 mm. With such moderate w/t ratio, the tube will crush with symmetric collapse mode which can be seen in Figure 2.8. The collapse behavior in this mode is linear, starting form the point of impact and linearly travelling to the end. It can be stated that the major energy absorption are handled by the edges of the tubes, by under going plastic deformation, while the side surfaces of the tubes shows little deformations.

The superfolding elements was first developed by Wierzbicki and Abramowicz in their work in [5], where they determined the mean crushing load for symmetric

collapse mode as shown in equation 2.4 and concluded that about 70% of entire energy absorption in crash is due to plastic hinge line propagation.

$$P_m = 9.56\sigma_0 t^{5/3} b^{1/3} \tag{2.3}$$

Abramowicz later in his work in [5, 45] performed multiple crushing of tubular structures and found the tubes getting collapse in three different fashions: In-extensional mode, extensional mode and mixed mode. And later developed an equations for finding the mean crushing forces for inextensional and extensional mode, which are shown as follows,

$$P_m = 13.06\sigma_0 t^{5/3} b^{1/3} \tag{2.4}$$

$$P_m = 10.73\sigma_0 t^{5/3} b^{1/3} + 0.79\sigma_0 t^{4/3} b^{2/3} + 0.51\sigma_0 t^2 \tag{2.5}$$

In the work performed in [46], Weigang further simplified the equation 2.4, and got the following equation,

$$P_m = 6.68\sigma_0 t^{3/2} b^{1/2} \tag{2.6}$$

Now consider a tube with thicker dimensions like, width as 40 mm, height as 100 mm and thickness as 3 mm. Now with such lower width to thickness lower, the tubes normally crumple under extensional mode. This mode have higher EA capacity than the other two as in plane stretching takes places which needs higher amount of energy for initiating the stretch. The mean crushing force for this mode was calculated by Abramowicz in his work in [45]

$$P_m = 8.16\sigma_0 t^{3/2} b^{1/2} + 2.04\sigma_0 t^2 \tag{2.7}$$

2.7.3   Dynamic Axial Crushing in Square Tubes

In real world, crashes doesn't happen with ideal conditions like, 100% frontal impact. Hence the buckling behavior is not just dependent on the crushing force but also on the impact direction. To name a few factors, the dynamic effect are generated by the inertial forces of the crash structures and also form the dynamic behavior and

interaction between the materials involved in crash Many of these inertial loads and strain factors are kipped in the quasi-static analysis of the tubular structures.

For crash with low velocity like 5 m/s, the crash results are seen to be similar in dynamic crash and quasi-static crash analysis. This is because the inertial effects, strain rate effects, etc are not heavy enough to dominate the crushing pattern. For such low speed crash analysis, it can be performed with quasi static analysis by making some considerations for dynamic parameters. In the work in [5, 45, 47, 48], provided us with an equation for conversion between the dynamic and static flow stresses.

$$\frac{\sigma_0{}^d}{\sigma_0} = 1 + (\frac{\varepsilon}{C_r})^{\frac{1}{q}} \tag{2.8}$$

Now for crash with higher velocity like 15 m/s, the difference in collapse pattern can be seen between dynamic crash and quasi-static crash analysis [49, 50]. Since at such speed inertial forces are strong enough to dominate the collapse pattern. And even with considering dynamic scaling factors in quasi static analysis, the collapse results were different [49, 50]. Therefore for studying high speed crash behaviors, the dynamic crash analysis is a better approach.

During dynamic crash, the physical parameters of the tube, crushing speed, material definition, contact definition, etc plays an significant role in collapse behavior, whether it will collapse axially or buckle [51]. Hence dynamic problem definition is pretty complex and difficult to have analytical results. Therefore simple analytical models are created first and then numerical approaches are applied on that simplified model to identify the effects caused by different parameters.

In [49,50,52–54] Karagiozova studied buckling collapse modes in thin walled square tubes and identified inertia and strain rate sensitivity as the main causes for strain concentration during dynamic collapse of tubes which leads to buckling in the tube. He studied the tubes with emphasis on stress wave propagation through the structure and resulting fold generations. He also identified, in dynamic crash, the buckling is largely depended on the thickness of the tube and concluded the thicker tubes will

collapse with buckling mode due to generation of strain concentration. It was also found, stress wave traveled quicker in square tubes than that in circular tubes.

2.8   Stability of Axial collapse

Progressive collapse are highly desirable because of the their higher energy absorption efficiency but attaining progressive collapse is difficult. In lot of structures they start collapse in an progressive manner but suddenly undergo Euler buckling and completely changes the behavior of the structure. Hence it is very crucial to under what is causing this sudden change in the behavior of the structure, as it is significantly dropping its energy absorption capacity.
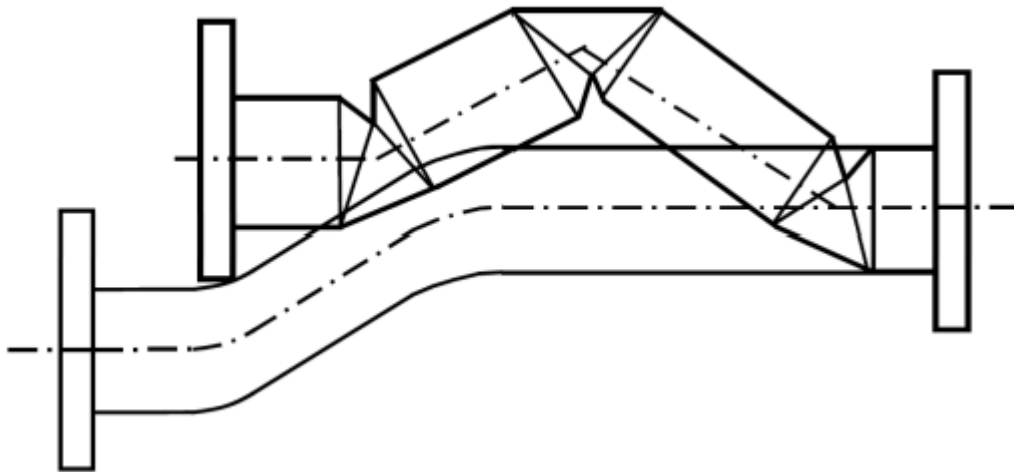
Fig. 2.10. Bending Collapse [55]

Even though this is an major problem in crashworthy structures, marginal amount of research have been done to study this behavior change. Abramowicz and Jones [56] performed various series of tests for studying the transition and were able link the sudden change in behavior to sudden drop in stiffness of the structure, which leads to Euler buckling in the tube. The drop in stiffness of the structure was seen on both static and dynamic crash testings. After testing the tubular structures extensively,

they developed a formula and stating a critical limit for square tube dimensions, as shown in eq x.x

$$\frac{L}{C} = 3.423 e^{\left(\frac{0.04C}{t}\right)} \tag{2.9}$$

Where L is the critical length of the tube, and t is the thickness of tube walls. If the length of tube to wide ratio is higher than critical value, the tube will see Euler buckling [56]

2.9 Energy Absorption in Thin-Walled Tubular Structures

For decades thin walled tubular structures have been widely used as energy absorption devices. A lot of decades of research have been done in improving them, with different objectives like increasing energy absorption capacity, lowering peak crushing force, attain progressive collapse mode, etc. Different types of tubular designs have been proposed to attain these goals. In this section we will go briefly over the different energy absorption devices available.

2.9.1 Square and Circular Tubes with Crush Initiators

These are the most common and widely adopted tubular energy absorbing structures in the automotive industry. Since they are widely used, a lot of research has been done with these structures to increase its specific energy absorption capacity and lower the peak crushing forces. For lowering the peak crushing force, a efficient but effective way was to introduce crush initiators through out the structure. These initiators not only help in lowering the peak crushing forces but help in stabilizing the collapse in order to attain a specific collapse mode.

Eren [57] studied and compared different types of crush initiators and showed the significant reduction in peak crushing force and also was able to see progressive axial folding. With the use of corner holes in an rectangular tubes as triggering method, Abah achieved control in crushing pattern and also seeing lower peak crushing loads [58]. Similar results were seen by Lee [59], where he have seen increase
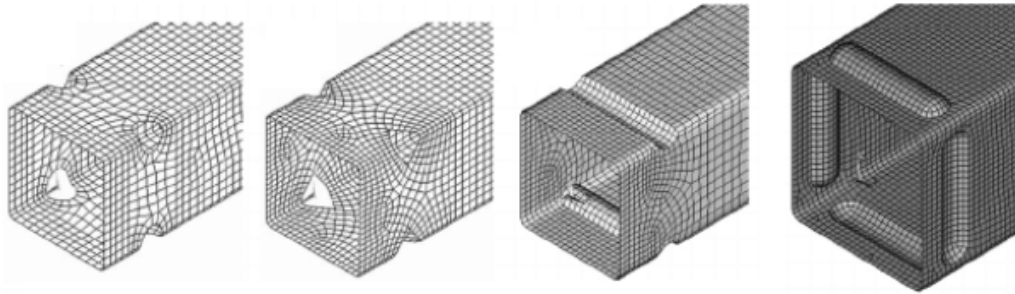
Fig. 2.11. Crush Initiators On Square Tube (a) Hole punch (b) Diamond punch (c) Corrugation (d) Bead [37]

in energy absorption capacity in aluminum square tubes due to control in collapse behavior. A series tests were conducted with axial loading on aluminum square tubes with chamfered edges and other mechanisms for controlling collapse behavior [60]. Chase studied different crush initiators in square and circular tubes to overcome the challenge of Euler buckling and attaining progressive collapse [61].

Dents are another type of crush initiating method widely studied, as they are easy to manufacture on any tubular structure. Initiating crush with inward and outward dents on the surface of the tubes were studied in [59, 62], and were able to create a symmetric collapse mode through out the length of the tube in a controlled fashion. Different types of corrugation design on rectangular surface were studied by Daneshi and Hosseinipour [63] and were able to see significant drop in peak crushing forces, but some of the design have seen decrease in energy absorption capacity. Singace and El-Sobky [64] also studied the corrugation design on circular tubes and were able to achieve stable crushing force behavior but in this study too, they saw reduction in energy absorption capacity. We can now definitely conclude, dent and corrugation helps in lowering the peak crushing force by avoiding initial buckling but such design lowers the energy absorption capacity too.

Zhang in [65] overcame the disadvantages of corrugation and dents with the introduction of surface patterns which helped in increasing specific energy absorption and

at the same time having an controlled collapse pattern [43] Plastic buckling mode or surface pattern proposed and studied by Shakeri [66] to trigger a crushing process and attain axial collapse in cylindrical tubes. Now for increasing energy absorption capacity in circular tubes, Adachi [67] created ribs inside the tubular structure, to collapse under concertina mode. In terms of energy absorption capacity, diamond mode was found to be inefficient when compared with concertina mode [68]. The energy absorption with diamond mode was about 60% of that of concertina mode. Lee was able to increase energy absorption capacity in square tubular structures by about 25% by using a controller in tube design [69].

Some crush initiator design were able to attain both the objectives of lowering the peak crushing force without compromising in energy absorption capacity. Zhang created pyramid elements and patterned it all over the surfaces of square tube and studied energy absorption behavior of the tube [70]. The pyramid element resulted in folding the tube under octagonal mode and with it lower peak crushing force and higher energy absorption was observed.

2.9.2   Polygon Tubes

Lu studied the energy absorption capacity in square and circular tubes and was able to conclude square tubes have smaller energy absorption capacity than the circular tubes with similar surface area [3]. But circular tubes are pretty difficult to control in crushing process and hence buckling is a major challenge with it. Hence polygons is a balance between the round and square tubes, as they are easier to control in crushing as compared to circular tubes and offer higher energy absorption than the square tubes.

Abramowicz [71] in his work, evaluated crash behavior of multi sided polygons and later derived an empirical formula for mean crushing force for polygon with six sides, which can be seen in equation 2.10.

$$P_m = 20.23\sigma_0 b^{0.4} t^{1.6} \tag{2.10}$$

While Mamalis studied crash behavior for octagonal tubes and new collapse mode called as square mode [72]. He even conducted experimental testing and was able to validate this new collapse mode. He was also able to conclude that octagonal tubes were able to absorb more energy than the square counterpart. The energy absorption during experimental testing of octagonal tubes was almost equal to that of the circular tubes but higher than the square tubes.

Yamashita [73] studied the effect of increasing polygon size on collapse pattern and energy absorption behavior. He noticed as the number of sides are increased the energy absorption too increases with it to an extent beyond which the polygon tube acts like a circular one. He concluded eleven sides as the end point beyond which the behavior of the polygon tube is completely similar to circular ones. Hence polygons with more than eleven sides were not consistent with collapse pattern.

2.9.3 Cellular Tubes

While studying the effect dimensions width and thickness on collapse behavior of square tube, Abramowicz observed the folding length in is directly proportional to the width of the tube [43]. Higher the width of the tube, higher will be the folding length. So now if we consider two tubes having same dimensions besides width. One with smaller width than other. We know energy absorption capacity in tube is directly proportional to the number of folds created, as higher the number of folds higher will be the travelling plastic hinge lines [43]. Hence the tube with smaller width will have greater number of fold resulting in higher energy absorption capacity. This observation led to the development of multi cellular tubes. Figure 2.12 and 2.13 shows some of the cross sectional patterns seen in cellular tubes.

Chen and Wierzbicki [46] empirically and mathematically studied the crushing behavior of multi cellular tubes and saw a significant increase in the energy absorption
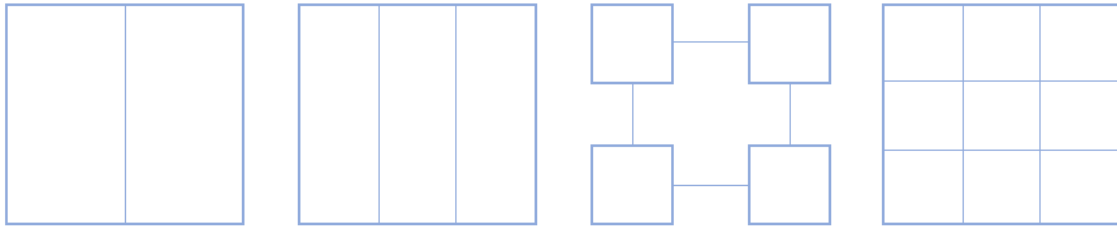
Fig. 2.12. Cellular Cross Section Pattern Types (a) Dual cell (b) Triple cell (c) Multi Cell (d) Multi Cell
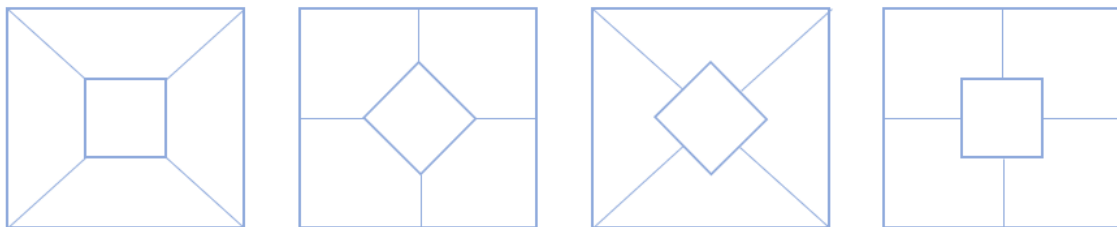
Fig. 2.13. Alternative Cross-section Models for Multi-cell Columns [74]

capacity than that of conventional square and circular tube. A similar observation was made by Kim [75], where he proposed a new type of cellular pattern, as seen in figure 2.12, which double folded the specific energy absorption capacity than that of conventional square tube, but at the same time peak crushing force was also raised by considerable margin. Zhang [76] specifically studied energy absorption behavior in cellular tubes with 3 x 3 compartments. It was seen the energy absorption capacity increased by 1.5 times the square tubes. With all the proposed multi cellular design and their results, it can be concluded that they do offer a higher energy absorption capacity but at the same time increases peak crushing force considerably. Also besides this, manufacturing these tubes is difficult. Because of these flaws multi cellular designs are not widely used.

2.9.4 Tapered Tubes

In past decade a lot of research have been done in developing tapered tubular designs, because of its advantages like, higher crushing distance available for axial loading, lower introductory buckling loads, and efficient energy absorption behavior under oblique loading. Nagel and Thambiratnam [77, 78] performed an extensively studied the dynamic crash behavior of the tapered tube for axial and oblique loading. It was seen, in both the loading conditions there was lower initial buckling resistance. Also for oblique loading the tapered tube showed better energy absorption capability than the square tube with oblique loading. Mamalis and Reid [9, 79] studied tapered tubes, as seen in Figure 2.14, for collapse behavior and for crushing force efficiency.

They observed stable crushing load displacement graph for axial loading, but the stability and the collapse mode was seen to be depend on the dimensions of the tubes, especially the tapered angle. They were able to see both inextensional and extensional collapse modes by varying the tapered angle. The energy absorption capacity was also seen to be higher than that seen in straight tubes, which makes them a good alternative for conventional straight tubes. In automotive industry, for joining two crash structures with different cutaway areas, tapered tubes are used as a connector which is having energy absorption capability.

Fig. 2.14. Four Sided Tapered Tube [79]

Mamalis also studied the tapered circular tubes for their crash behavior in series of his work [62, 79] He was able to conclude, the geometry of the tube plays a very important role in deciding the collapse mode. Of the number of tests he performed he was able to get concertina and diamond mode for different tapered designs.

It can seen there are lot of similarities between the tapered and square tubes behavior like the inextensional and extensional collapse modes, stable crushing force plots with certain design. Hence many of the analytical methods used in studying straight tubes can be used for studying and calculating empirical formulas for crushing forces and energy absorption capacity.

2.9.5   Foam Filled Tubes

In the past decade with the development in new manufacturing techniques, manufacturing complex parts and materials are made possible. This lead to a increase in research and development in creating filler materials with higher energy absorption capacity. The objective of addition of filler materials in tubular structures, is having increased the energy absorption capacity by adding stiffness to the tube. And also targeting for minimum weight design. Figure 2.15 shows some of the widely researched foam fillers.

From 1990's researchers have been trying to develop stiffer tubular structures by adding naturally available filler materials from the nature, like wood. In 1998, Santosa and Tomasz [81] studied the effect of aluminum honeycomb on axial crushing in straight tubes. Significant rise in energy absorption was seen with moderate strength aluminum honeycomb. He also developed an formula showing relation between the strength of foam and the mean crushing force. Later in his work he also studied the effect of filler material adhesive on crushing behavior. In 2002, Kim and Chen [82] studied the S frames filled with three dimensional aluminum foam and studied the crash behavior by varying the thickness and relative foam density. They observed about 75% increase in energy absorption capacity both in analytical and simulation
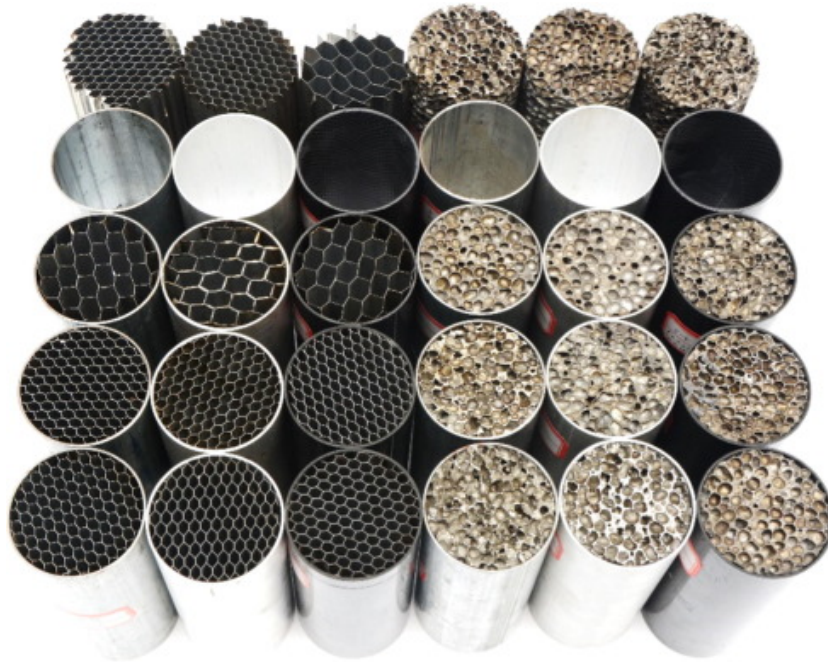
Fig. 2.15. Types of Foam Fillers [80]

results. In [83], aluminum tube filled with polystyrene filler material was studied for dynamic crash and was able to see three different collapse modes: compound diamond asymmetric, concertina axisymmetric and mixed mode folds. Figure 2.16 shows crushing pattern in foam filled square tubes.

In 2000, Hanssen and Langseth [84], performed 96 tests for studying the crash behavior for aluminum foam filled straight tubes for dynamic loading. For different foam density he studied the behavior of peak and mean crushing forces besides energy absorption capacity. He also derived formulas relating the foam density with peak and mean crushing forces. In 2007, Zhang and Cheng [85] studied the behavior pattern between foam filled and multi cellular aluminum tubes for dynamic crash. It was noted that multi celled tubes showed 50% to 100% higher energy absorption than that of the foam filled tubes. In 2008, Mirfendereski [86] performed parametric study and numerical analysis to compare the straight tubes with foam filled tubes in detail for dynamic and static crash. Zarei and Kroger [87, 88] also studied the bending
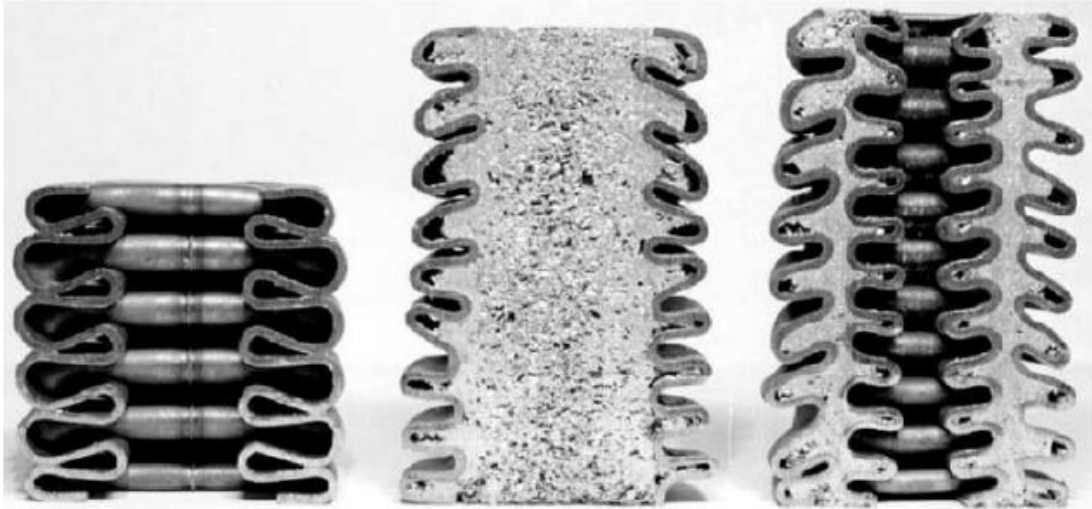
Fig. 2.16. Crushing Pattern In Foam Filled Square Tubes [83]

behavior of straight and foam filled tubes and later proposed an honeycomb filled crash box design. In 2010, Ahmad [89] studied the energy absorption capacity for oblique impact in conical tubes filled with foam. He studied the crash responses by varying the impact angle and tube dimensions. He was also able to conclude, the foam filled conical tubes can handle greater oblique loads than the empty one. Hence it can be stated, for axial loading, the behavior of foam filled tubes are more similar to that of cellular tubes, offering higher stiffness to the tube in turn resisting the initial buckling. This causes peak crushing force to peak up. At the same time significantly increases the energy absorption capacity of the tube. Foam filled tubes are also seen to be insensitive to changes in the dimensions of the tube and can always predict stable crushing behavior.

2.9.6 Composite Tubes

In the past decade, we have seen a lot of research and developments with composite materials because of their light weight and significant higher strength. Due to this the strength to weight ratio is significantly higher than that of the metals widely used in

automotive industry. Higher strength to weight ratio leads to higher specific energy absorption capacity.

In 1990's Farley and Jones [90] developed and studied continuous fibers reinforced composite tube, where they described complicated crushing behavior and the controlling points for controlling the crash. Later in their work in 1992 [91], they proposed a method for calculating the energy absorption in Kevlar-epoxy and graphite-epoxy tubes. While in [92], effect of tube geometrical parameters on energy absorption behavior of composite tubes was studied.

Mamalis in [93] performed an theoretical and experimental analysis for studying fiberglass conical tubes under static an dynamic crash and showed significant rise in energy absorption capacity. He also studied different failure collapse modes [94] observed in axial crushing of square tubes made with fiberglass and proposed a method for calculating crushing loads and energy absorption. The fiberglass tubes basically failed with cracking fail mode as they are too brittle in nature. Hence the collapse mode was unstable and was found difficult to control. Figure 2.17 shows fiberglass failure.
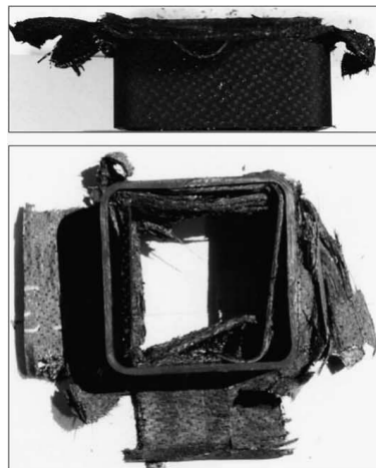
Fig. 2.17. Fiber Glass Reinforced Plastic Tube Under Dynamic Axial Crash [95]

In 2005, he studied carbon fiber reinforced plastic tube for high speed dynamic crash and evaluated the effects of tube dimensions and material property on crash

performance [96]. Fig x.x shows the axial high speed dynamic crushing of carbon fiber reinforced plastic tube. Energy absorption was seen to be doubled than that of the metal tubes.

Through all his research with fiberglass tube crash, it can be seen, fiberglass do provide significantly higher energy absorption but they never fail in progressive collapse instead they are very breakable. As from Figure 2.18 it can be seen their collapse pattern is highly uncertain, which is their biggest drawback.

Many research have been undertaken [95, 97] to remove the uncertain collapse behavior of fiberglass and carbon fiber tubes by binding these tubes with metal tubes. Thus take advantage of high energy absorption capacity of fiberglass and carbon fiber tubes and progressive buckling behavior of metal tubes. The tube was seen to collapse in a stable manner without cracking and still achieved additional 40% energy absorption. Lower amount of unbinding was seen in certain folds.
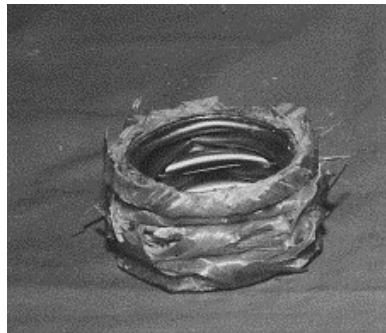
Fig. 2.18. Fiber Glass Tube Reinforced With Metal Tubes [95]

Similarly, [98, 98, 99] these researches were performed by binding the carbon fiber tube with metal tube. The tube was seen to be collapse in symmetric mode, creating alternating fold patterns, which can be seen in Figure 2.19. Addition in energy absorption was seen to be more than 55% but significant amount of unbinding between the two materials were seen.

So it can be concluded, composite tubes do offer a increase in specific energy absorption capacity but their collapse mode is highly unreliable Although, increase
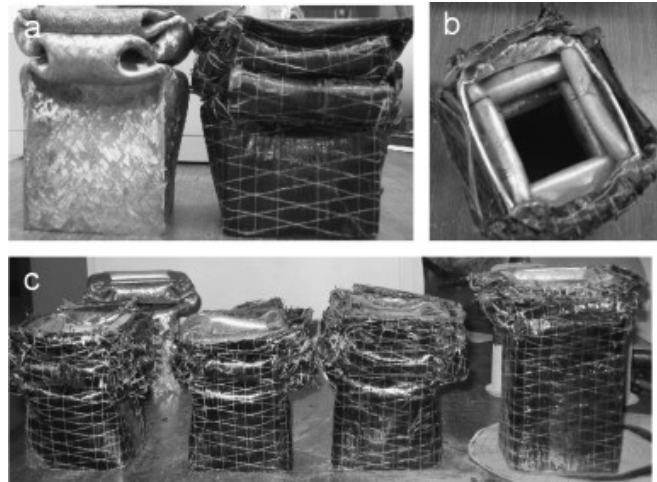
Fig. 2.19. Crushing Of Carbon Fiber Tube Reinforced With Metal Tube [98]

in specific absorption of energy was seen even with stable collapse manner like, in fiberglass reinforced metal tubes, manufacturing these tube is both time consuming and costly. Hence they are not used for mass production of family cars but instead used specifically just for certain applications like in airplanes, where higher specific energy absorption and light weight both features are needed.

2.10 Origami Tubes

Ideally an energy absorbing device should be able to have high energy absorption and at the same time low peak forces. But with conventional designs it was seen, with increase in the energy absorption a resultant increase in peak crushing force, which is not desirable. To address this drawback various methods were proposed. One way was to create a variable thickness [100–102] in the tubular structure so the peak crushing forces will be lower and energy absorption will be gradually increasing as the collapse progresses. But creating variable thickness tube is much more expensive approach, hence cost per specific energy absorption ratio is higher. Another way was to create tubes with prefolded origami designs to force the tube to collapse in a specific mode. The prefolds helps in lowering the initial peak crushing force, while the purposefully

designed plastic folds lines are responsible for higher energy absorption. The another advantage with this approach is its packaging efficiency. Tubes with certain origami designs can be folds to almost zero position i.e., the crushing distance achieved is maximum. Which in turn leads to higher energy absorption.

The origami approach of energy absorption has been widely studied in the past decade. Song [103], numerically and experimentally studied origami tubes of square, hexagonal and octagonal sections for their crushing behavior. The force displacement plot showed peak crushing force to be significantly lower when compared with the conventional design. Also, the tube collapse was also seen to be in a progressive manner.

Ma and You [4] also proposed a novel origami pattern acting as an geometric trigger to create diamond fold pattern when collapsed, followed with extensive numerical analysis. They were able to lower the peak crushing force by about 25% and at the same time achieved increased mean crushing force by about 70%. They also proposed a kite shaped origami design [104] as energy absorption device and performed numerical analysis on that pattern with quasi static analysis. They were able to lower the peak crushing force by 29.2% and increased mean crushing forces by 56.5% when compared with the conventional square tube design. Both the origami patterns developed can be seen in Figure 2.20.
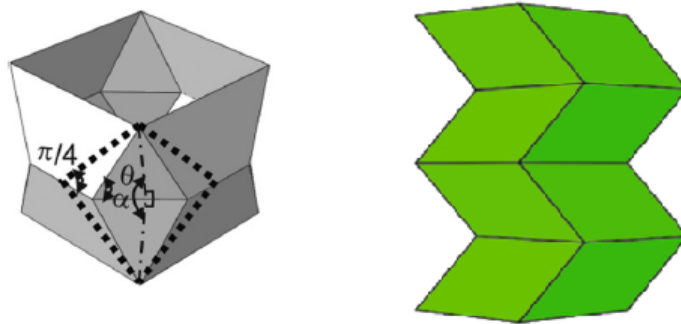
Fig. 2.20. Diamond Fold Pattern (left) and Kite Pattern (right) by Ma and You [4]

Yang [105], introduced two origami patterns for circular tube to create diamond
and full diamond mode when collapsed, which can be seen in Figure 2.21. In both
the designs there was a noticeable difference in peak crushing forces, while origami
with diamond fold showed higher energy absorption than the diamond fold pattern.
In both the designs energy absorption was adequately higher than the conventional
design.

Fig. 2.21. Diamond (left) and Full Diamond (right) patterns by Yang [105]
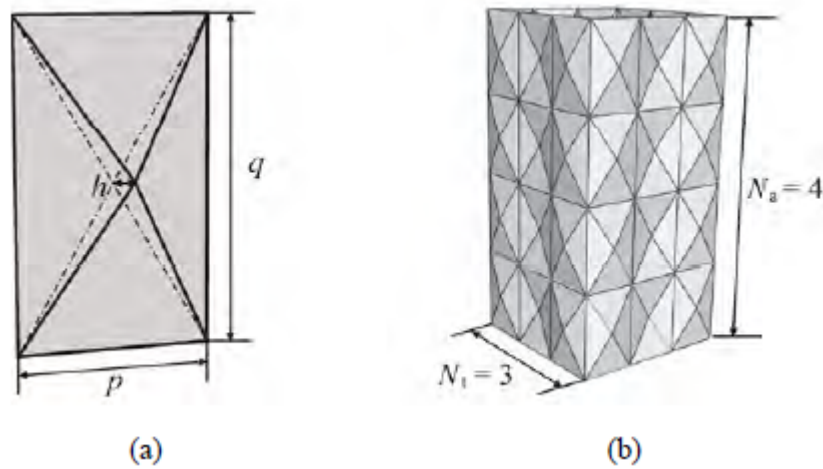
Fig. 2.22. Basic Pyramid Element (left) and Square Tube with Pyra-
mid Element (right) by Zhang [70]

Zhang [70] introduced an two pyramid shape origami patterns for conventional square tubes for quasi-static crushing and performed 30 simulations on them. Figure 2.22 shows the basic pyramid element and the tube with pyramid pattern. In one pattern he obtained an extensional collapse mode, while in another symmetric collapse mode was achieved. Both the designs were able to achieve about 15 to 30% additional energy absorption than the conventional square tube design.

3. FINITE ELEMENT FORMULATION FOR NONLINEAR CRASH

3.1 Introduction

The origami pattern developed in this thesis relies heavily on the FE methods for developing the origami design for nonlinear analysis. Hence this chapter is focused on creating the right finite element formulation definitions for nonlinear crash analysis and developing a benchmark problem. Section 3.2 gives a brief overview of Finite Element Methods, followed by differences in linear and nonlinear analysis. Section 3.3 gives brief idea on nonlinear FEA in crashworthiness and focuses on theoretical aspect of finite element formulation for explicit nonlinear analysis and selecting right parameters for creating benchmark formulation. Section 3.4 lists and summarizes effects due to imperfections in finite element analysis. Since experimental validation is out of scope, sensitivity studies are of paramount in this study. Therefore, section 3.5 focuses on crash analysis of conventional square tube and performing different sensitivity studies for mesh size, through point integration's (NIP) and tube length. via FEA simulation and measuring its effect on different crash indicators like Von-Mises stress, crushing force and deceleration. And finally, summary is given in section 3.6.

3.2 Finite Element Methods

3.2.1 Overview

Finite element method is a numerical method for solving complex engineering and mathematical problems. The numerical method helps in detailed understanding and quantifying a physical phenomenon like wave propagation in a structure, etc. FEM

can be said to have its origins in the works of Euler, in sixteenth century. However, the earliest mathematical papers on FEM can be found in the works of Shellback and Courant [106]. FEM was independently developed by engineers in 1950's to address the structural mechanics problem in the aerospace industry [107].

The finite element formulation basically consists of set of partial differential equations for the entire domain. Now the entire domain is subdivided into subdomains, representing set of equations to the original problem. These subdomains are called as finite elements. The FEM divides the entire domain in to smaller sized subdomains, called as finite element. Each of these subdomains represents simpler set of algebraic equations. These simpler set of algebraic equations are then assembled into a larger system of equation, representing the original problem formulation. These equations are then solved by using different numerical techniques. Variational methods are then used to approximate the solution based on the minimization of the error function. There are various types of finite element methods like AEM, Generalized finite element method, Mixed finite element method, hp-FEM, hpk-FEM, XFEM, Scaled boundary finite element method (SBFEM), S-FEM, Spectral element method, Meshfree methods, Discontinuous Galerkin methods, Finite element limit analysis, Stretched grid method and Loubignac iteration [108].

3.2.2   Linear versus Nonlinear Analysis

Finite Element Analyses are basically divided into linear and nonlinear analysis. Linear analysis, as the name implies, holds linear relation between the input and the output, since the model stiffness matrix is constant. Hence are applied to problems where the stress remains in elastic range. The displacements seen in the system are generally very small. The linear analysis is computationally efficient and easier to compute when compared with nonlinear analysis, hence are used to get an idea before executing the nonlinear run. The principle of superposition can be applied here hence solutions can be combined with each other. In Nonlinear analysis, holds nonlinear

relation between the input and the output because of the introduction of nonlinearities. Nonlinearity in the problem can be introduced through different definitions like contacts interactions between the models, plasticity behavior of the material, large geometry deformations throughout the analysis, the way the models are constrained in the formulation, etc [106]. Hence an extra care needs to be taken while developing a finite element formulation for nonlinear analysis. These analyses are generally complex and computationally expensive, and the principle of superposition can't be applied here.

3.2.3 Nonlinearities in Solid Mechanics

Nonlinearity are basically of three types: Geometric nonlinearities, material nonlinearities and contact nonlinearities. Geometric nonlinearities cover the nonlinearities such as strain displacement relationships which occur due to large displacement or large strains. Material nonlinearities occurs when the stress strain behavior is not linear i.e elasto plastic material introduction.

3.3 Finite Element Formulation in Crashworthiness

Vehicle crash transfers its kinetic energy into strain energy stored in the structure via a sequential deformation wall crushing process. These structures experience a large amount of crushing load in a relatively small amount of time, introducing Nonlinearity. To properly simulate the crash process, nonlinearity is needed to be considered, which makes this problem formulation very complex. Solving these complex equations using analytical approach is not possible, which opens door for using numerical approach. There are various numerical software's available in the market like Abaqus, Radioss, Ls-Dyna, Pam-Crash, etc. For the study performed in this dissertation commercial software package Radioss was used. For CAD modelling of the tubes throughout the study, Solidworks modelling package was used meshing of those models were done using pre-processor package Hypermesh.

3.3.1 Material Property

The square tube was made from material DP600 (Dual phase steel), which is widely used in automotive industry for thin walled tubular structures because of good energy absorption capacity. Mechanical properties for DP600 material were obtained from [109] which are listed in the Table 3.1 and Figure 3.1 shows stress vs strain plot for DP600 [109].

Table 3.1.
DP600 Material Properties.

Property	Values
Young's Modulus (E)	210 GPa
Density (r)	7800 kg/m^3
Yield Stress	335 MPa
Poissons Ratio (n)	0.3
Plastic Hardening Parameter	0.5
Plastic Hardening Exponent	0.5
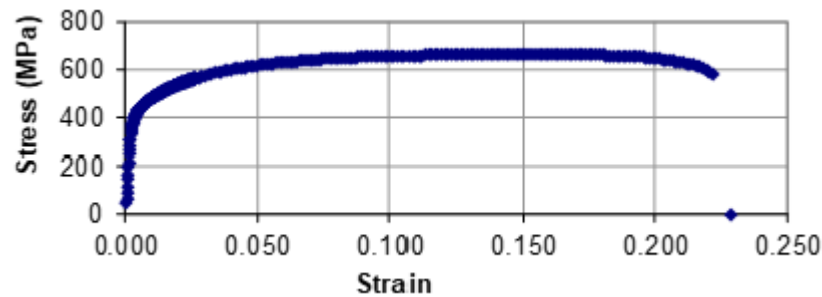
Fig. 3.1. Stress Strain Plot for DP600

To define material in Hyperworks, elasto-plastic material Johnson Cook (LAW 2) was used. This law was selected as the material behaves as linear elastic when the equivalent stress is lower than the yield stress. For higher stress values the material behavior is plastic. The stress strain measure is the distinguishing factor between

the linear static and the nonlinear FEA. In nonlinear analysis true stress strain is typically used. In Johnson Cook (LAW 2) the yield stress is also converted into true stress.

3.3.2 Shell Property

The thin walled tubular structures are widely used in the auto industry. If a surface is having relatively small thickness value when compared with its other two values, we can call it as shell. Consider a solid with length as L and thickness as t. If L/t ratio is greater than 20 [110] then thin shell elements are considered to capture better results in simulation. Therefore almost 90% of car model is made up with using shell formulations [110]. The work presented here, summarizes and describes the important literature's on shell elements over last 15 years [111]. Radioss element library contains 6 shell element formulations, which are based on Mindlin-Reissner shell theory. Table 3.2 lists all the shell formulations available in Radioss library.

Table 3.2.
Shell Formulations in Radioss Library

Element Name	Number of Integration points	Hourglass Formulation
BT (Classical Q4)	1	Four types based on Penalty method
QEPH	1	Physical Stabilization
QBAT	2x2	Fully Integrated Element
C0	1	-
DKT18	3	-
S3N6	1	-

BT (Classical Q4) Element

BT is an under integrated element which is non-sensitive to mesh size. The formulation is simple and efficient do not demand high computational resources

QEPH

The results obtained from the QEPH formulations falls close to QBAT formulation, without high computation cost. Hence for explicit structural analysis QEPH is taken due to its balance in accuracy and computation cost and controls hourglass energies. Computation time is marginally higher than that of BT formulation.

QBAT

QBAT is a fully integrated element and the most precise element in Radioss. Hence it makes a good choice for finding accurate results, especially in nonlinear crash simulations. The fully integrated QBAT elements eliminate hourglassing. But it uses a lot of computational resources, almost thrice that of BT formulation.

C0 and DKT18

These are triangle elements. C0 tria element is too stiff and DKT18 has a good bending behavior but it is computationally expensive. Hence these are normally kept to minimum during meshing of model.

S3N6

S3N6 element is less used one, mostly used in special applications like simulating stamping because of its good bending behavior.

During highly nonlinear crash analysis, when under integrated elements are used, hourglass modes are generated due to a smaller number of node point integration's

available [110]. Hourglass mode is an element distortion having zero strain energy. Radioss employs two methods for correcting hourglass modes. First will be Penalty Method where hourglass is controlled by applying anti-hourglass forces to maintain stability. Second will be Physical Stabilization Method where internal energies are corrected in an analytical way.

For crash simulations in this research, 4 node shell elements with QEPH formulation were selected as it proved to be good enough to capture all the details in the high speed collapse behavior without high computation cost of QBAT shell formulation. QEPH elements correct hourglass energies by using physical stabilization method. To ensure the solution accuracy of crash results, the zero energy modes were checked throughout so as the structure's true response is not affected. According to the recommendations by Radioss User's Guide [112], to check the hourglassing effect the hourglass energy was compared to the internal energy and was made sure the hourglass energy was below 5% throughout the crash simulation. The thickness of the shell elements was taken to be 2 mm throughout the work.

3.3.3   Contact Interface

One of the distinctive characteristics of a crash is that, a large amount of energy is dissipated in a relatively short amount of time. Nonlinear crash simulations are very dependent on contact definitions and can have a sever affect if not done correctly [113]. An algorithm is required to capture the transition in elemental forces to get simulation results close to experimental ones. Hence modelling a proper contact definition was an important factor here, in achieving lateral strengthening effect. In nonlinear explicit solver, Radioss, there are two approaches [110] that deals with contact definitions which are listed as below.

1. **Lagrange Multiplier Method**

   Lagrange Multiplier method is completely mathematical method hence doesn't require any physical elements incorporated into the model. A nonlinear system

of equations is solved to account for contact conditions. This method takes more computational time for each iteration, since it must solve all these complex equations using nonlinear solver. Also, contact friction can't be calculated using this method.

2. **Penalty Method**

   Contact interfaces using penalty method depends on the treatment given to the master and slave entities. Here contact is only defined between a slave nodes and master segments, which are dependent on the type of element they lie on. In case of four node shell element, the segment is the surface of the element. A minimum contact activation gap is defined to determine whether a node is in contact with a segment. As soon as a node penetrates the gap, an elastic spring is added between the slave node and the master segment. Contact ends when the penetrated node is completely pushed out of the gap. Since the penalty method is widely used in crash analysis [114], we are defining the contact definition for this these formulations using penalty method.

For defining contact interactions between the folded lobes of collapsed tube during high speed crash, contact interface Type 7 using a penalty algorithm was used. Tube walls were used for self-impact contact definition as only one surface is required. The main advantage of Type 7 contact is that the stiffness is not fixed and increases with penetration preventing the node from going through the shell mid-surface because of its penalty algorithm. Contact gap is used on both sides of the mid surface, to ensure that no penetration occurs before the intended contact, which can be seen in Figure 3.2. In Radioss for shell elements, the minimum contact activation gap for type 7 contact is defines as $t/2$, where t is thickness of the master segment [110]. Hence, contact activation gap of 1 mm was used throughout the work.

Geometric boundary conditions include displacement constraints given on the tube model. In the model definitions, the rigid wall is kept fixed and the model is impacted axially on the rigid wall. The tube has a rigid mass of 500 kg attached to the very
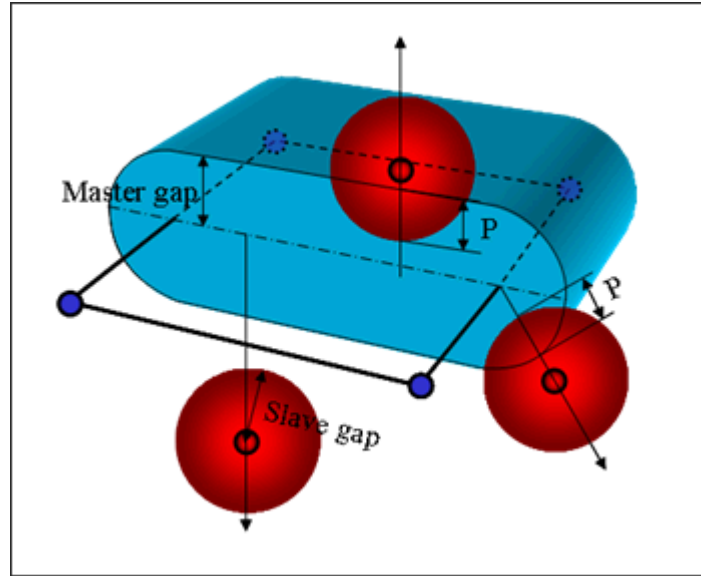
Fig. 3.2. Offset Gap in Type 7 Contacts [110]

end. The rigid mass is constrained to move only along the axis of tube travel i.e., along Z direction only. Remaining all the transnational and rotational degrees of freedom are constrained. Besides rigid mass constrained, the tube is not constrained by any other way, and is free to deform as the forces gets applied.

3.3.4   Friction

Friction plays an important role in the sliding of the folded surfaces during crash. Estimating values high or low will significantly deviate results from real run values. Hence it was necessary to estimate a right one. Static Coulombs friction was taken to be 0.25 [65] for contact between the lobes. To allow for sliding movement between the tube and the rigid wall sliding friction of 0.3 [115] was taken.

3.3.5   Velocity Boundary Conditions

In this dissertation, the origami creasing pattern are developed for high speed impact. Therefore, velocity conditions are applied as close as possible from FMVSS

208 standard for frontal crash in a vehicle [27]. On the extreme end of the tube a 500kg rigid mass is attached [27]. To obtain crushing in the tube, an initial velocity of 13.33 meters per second i.e., 30 miles per hour was given to the tube and the rigid mass. The crushing is allowed to happen under the influence of the inertial forces taking place due to the rigid weight and the tube's own weight, so as to replicate real time crash. The tube is not limited to stop after a certain limit, instead its allowed collapse fully under the impact load.

3.3.6 Time Step and Simulation Time

For computational stability of the crash simulation the time step increment must be smaller than the highest frequency of the system [61]. In Radioss, the elemental time step increment is calculated from smallest element in the structure, besides the rigid elements that do not deform. The time step increment can be determined using the following formulation,

$$\triangle t = 0.9 \frac{l}{\sqrt{\frac{E}{\rho}}} \tag{3.1}$$

where, l is the critical length of the element, E is Young's Modulus and ρ is material density. A scale factor on time step value was used as 0.9 [110].

Considering the simulation time was an important factor. The simulation time need to be long enough to capture entire crushing behavior but at the same not being computationally expensive. After multiple simulation runs, the simulation time was taken to be 5 milliseconds. Since the length of the tube is small and dynamic loading conditions were applied, this small duration proved good enough to capture all the crushing details while being computationally fair with fine mesh.

3.4   Effects of Imperfections in FEA

Crash simulations are performed with the assumptions of ideal behavior. And in many cases the parameters are assumed due to unavailability of the real values. For example, the real dimensions of the tube won't be the same as that on the paper. Similarly, the exact yielding behavior is not known. These differences add up and causes the difference in the results of FEA simulations and experimental validations. There are basically 4 types of imperfections described one by one below.

1. **Material Imperfections**: In crash analysis, one might select a material with homogeneous properties. But there are many reasons which might arise non-homogeneous properties in the material, like internal crack or void being present in the material.

2. **Geometry Imperfections**: Take a simple example of crash box here. In crash simulations we are defining a tube with dimension of the tube 60 mm x 60 mm x 120 mm with 2 mm thickness throughout. But in reality, we won't be getting the same tube dimensions throughout. Many factors affect this tolerance in the manufacturing process or defects in manufacturing processes causing nonuniform thickness and dimensions.

3. **Loading condition Imperfections**: In this crash box example, we are defining the tube to be placed horizontally and the impacting rigid wall to be perpendicular to the crash box direction of travel. But this can't be completely controlled in real life.

4. **Measurement Imperfections**: The values measured on the test setup are limited to the minimum unit of the measuring scale and the tolerance of the measuring devices. Hence one can see a difference between the real values and the measured values.

3.5 Sensitivity Studies and Benchmark Formulation

In this section, two sensitivity studies are conducted for formulating benchmark problem. First sensitivity study is done on mesh size, focusing on finding optimum mesh size for accuracy and computation cost. The mesh size sufficiency is decided based on the performance of crash indicators - crushing force, deceleration, and von mises stress. In nonlinear crash simulations involving shell elements, internal energies predictions rely heavily on through point integration, called as NIP throughout the study. Therefore, a second sensitivity study is focused to find a right NIP value for this study. And finally, benchmark formulation is created and the dynamic axial crushing of square tube is discussed.

3.5.1 Mesh Sensitivity Study

In crash analysis, the accuracy for the FEA results and the computation time required relies heavily on the mesh size. The models with coarse mesh will take less computational time but the accuracy will be punished. On the contrary, models with fine mesh, have high computation time but the accuracy will be good. But fine mesh do create a complexity in the model, hence they are offen preferred when high accuracy is need. Since crash analysis is highly non linear, there needs to be proper balance in accuracy and the computational time.

To achieve this goal, an sensitivity study was performed to reveal the effects of mesh size on crash indicators. Conventional square tube was considered with dimensions of 60 mm x 60 mm x 240 mm, meshed fully with 4 node shell element formulation with 2 mm thickness. Numerical simulations were performed on four created mesh models with 5 mm, 3 mm, 2.5 mm and 2 mm mesh sizes. All the models were analyzed under same simulation formulation. The following equation was used to calculate the mean crushing force and mean deceleration values.

$$P_m = \frac{\int_0^\delta P(x)dx}{\delta} \tag{3.2}$$

where δ is the final crushing distance. Table 3.3 tabulates the computation time simulation results for all mesh sizes.

Table 3.3.
Simulation Results for Different Mesh Sizes

Property	5mm	3mm	2.5mm	2mm
Number of Elements	3072	8560	12288	19200
Simulation Time (sec)	119	486	1058	2351
P_max (kN)	320.7	323.9	323.2	322.9
P_mean (kN)	121	116.3	115.3	114.9
A_max (mm/ms^2)	-0.720	-0.721	-0.725	-0.726
A_mean (mm/ms^2)	-0.239	-0.229	-0.224	-0.225

It can be seen that 5 mm mesh model, representing the coarse mesh density with 3072 elements, took 119 seconds to complete the simulation. The 3 mm and 2.5 mm mesh models, representing medium mesh density with 8560 and 12288 elements respectively, took 486 seconds and 1058 seconds respectively. And 2 mm mesh model having 19200 elements, took 2351 seconds to complete the simulation. It can be clearly stated that the time exponentially arises as the mesh size is reduced from 5 mm to 2 mm.
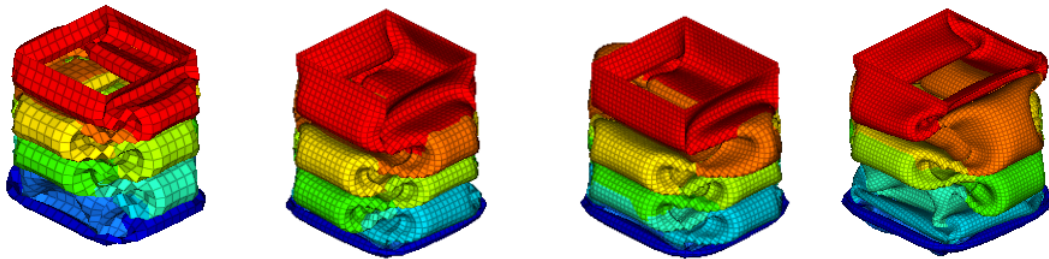
Fig. 3.3. Fold patterns with different mesh size
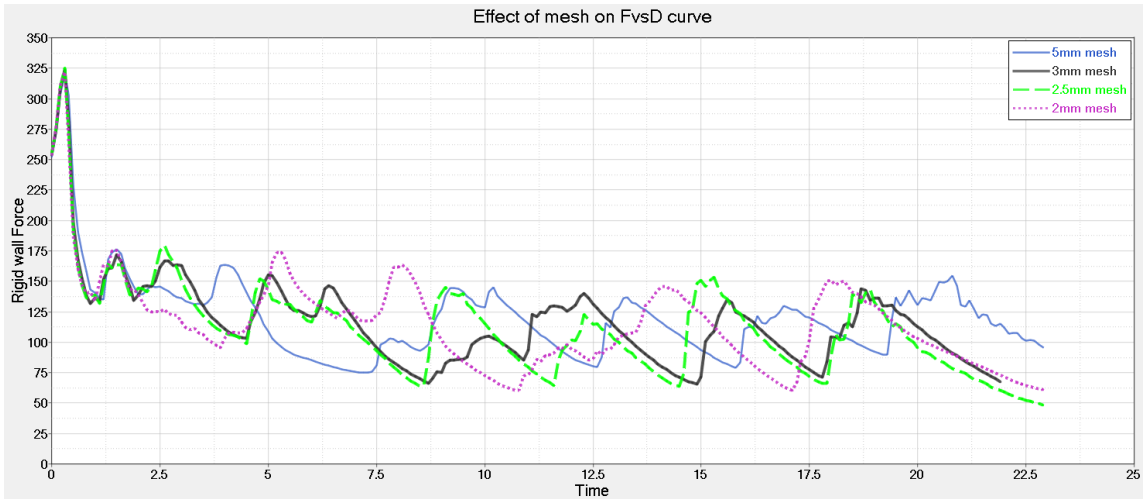
Fig. 3.4. Effect of Mesh Size on Crushing Force
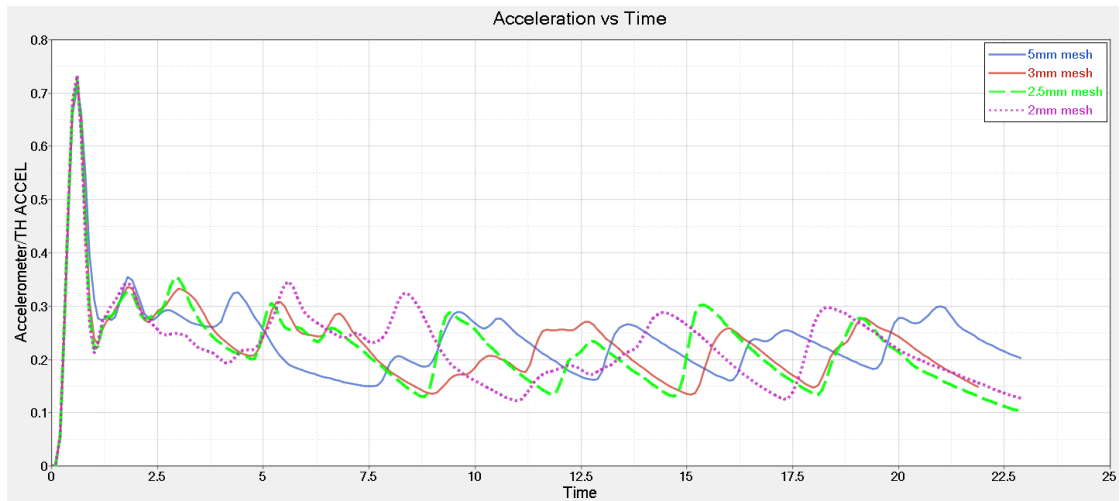
Fig. 3.5. Effect of Mesh Size on Deceleration

With different mesh sizes, the collapse pattern can be seen to be triggered at different time. Hence it can be said that mesh size affects the collapse pattern, which can be seen in Figure 3.4, showing a variation in mean crushing force values. With 5mm mesh size model, the mean crushing force values are seen to be under predicted showing an deviation of around 6 kN in values from 2 mm model. But as the mesh size is refined we are seeing a congruence in results. Similar trend can be seen in

mean deceleration values, showing an 0.014 mm/ms^2 variation in values, as seen in Figure 3.5. The peak crushing force and peak deceleration values are showing small variations but overall do not looked to be affected by changes in mesh size. Figure 3.3, shows the folding pattern for different mesh sizes. It can be seen that, the total number of folds remains the same, but as the mesh size are getting refined, change in fold lobe can be noticed. Mesh model with 2 mm size, should a significant larger lobe than that seen in other mesh models.

It can be concluded 5mm mesh model offers very low computation time but high variation in mean values are seen. 2mm mesh model offer refined results but at very high computation time. 2.5 mm mesh model results are within 5% range of 2 mm mesh model. And also computation time is half of it. Therefore, mesh size of 2.5 mm looks to be an better choice in terms of efficiency, but mesh size of 2 mm was selected for having higher accuracy for getting accurate fold patterns, since we are dealing with highly nonlinear buckling in the post buckling phase.

3.5.2   Node Point Integration Sensitivity Study

In elastic behavior, the stress variation is linear with respect to the thickness and hence internal energy can be easily calculated using integration. In plastic behavior, as we can see in Figure 2.7 , the stress distribution through the thickness in not linear hence needs at least 3 through thickness points, to account for nonlinearity, in order to calculate internal energy. The internal energy estimations depend on the number of through point integrations. Higher the node points, accurate will be the energy predictions. Also, using higher through node integrations (NIP) have seen to control hourglassing [116]. Several researchers have reported that through thickness integration points between 7-9 are optimal without reduced accuracy in integration points [116]. In crashworthiness internal energy plays an important role. Therefore, finding right NIP is crucial.
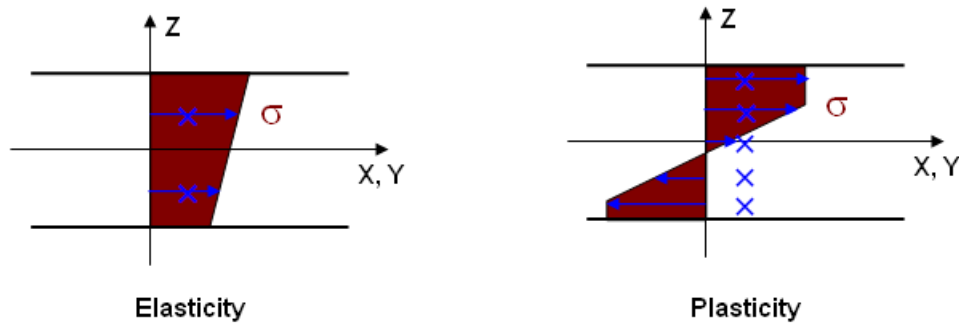
Fig. 3.6. Integration through Thickness [116]

Table 3.4.
Simulation Results for Different NIP

NIP	NIP 3	NIP 5	NIP 7	NIP 9
Simulation Time (sec)	119	486	1058	2351
P_max (kN)	320.7	323.9	323.2	322.9
P_mean (kN)	121	116.3	115.3	114.9

Four simulation models were created with NIP from 3, 5, 7, and 9. All the FE formulations were kept same as defined in earlier sections. Table below summarizes the simulation results for the sensitivity study and the crushing force variation with respect to change in NIP can be seen in Figure 3.7. A big variation can be seen between the mean crushing force values. With nip 3 model, the crushing force values are seen to be under calculated to 103.4 kN, showing a total of 17 kN of variation with value of nip 9 model. A negligible variation was seen in the between the peak crushing values of all the models, having a maximum variation of around 2 kN. Increasing trend can be seen for simulation time with increase in nip values.

It can be concluded, nip 3 model under calculates the crushing force values by almost 15%, hence can't be considered. With nip 5 model, the improvements in mean crushing force value looked to be more promising. The results of nip 7 model and nip 9 model are less than 3% off, showing congruence. Furthermore, there is only

120 seconds increase in simulation time. Hence 9 through point integrations were selected.
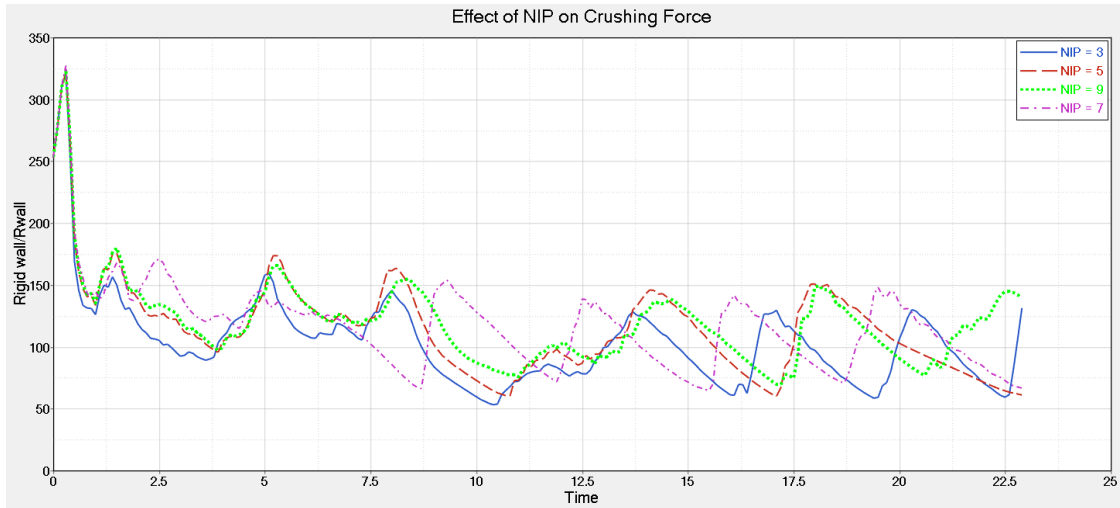
Fig. 3.7. Effect of NIP on Crushing Force

3.5.3 Benchmark Problem

A conventional square tube is considered for creating a benchmark formulation. No triggering points are introduced in the model. Numerical simulation of dynamic axial crushing is conducted on the tube and named as square tube throughout the work. The overall dimension of the tube was kept as 60 mm x 60 mm x 120 mm, with 2mm thickness throughout. The model was meshed with 4 node shell elements with 24 QEPH shell formulation. The QBAT shell formulation is the most accurate element, but the computation time is about two or three times the QEPH formulation, hence not considered. It was made sure the mesh is good enough by checking the aspect ratios for the shell elements. Since all the elements are 4 node shell, 0% elements were having aspect ratio greater than 1.5, indicating good mesh quality for nonlinear crash simulations. The scenario was modelled with rigid wall remaining fixed and one end of the tube 1mm away from the rigid wall, so as to avoid infinite contact force interaction at the initial numerical simulation. All the simulation setup remains

same, as discussed in detail through section 2.3. Figure 2.3 shows the finite element model of square tube.

The conventional square tube, named as SqTu, was analyzed first to validate the finite element model and create benchmark results for evaluating the performance improvement seen in origami tubes. The crushing process of conventional square tube and a plastic strain contour map (PEEQ) over undeformed shape is shown in Figure 3.8 for better understanding of crushing process and plastic strain propagation in hinge lines.
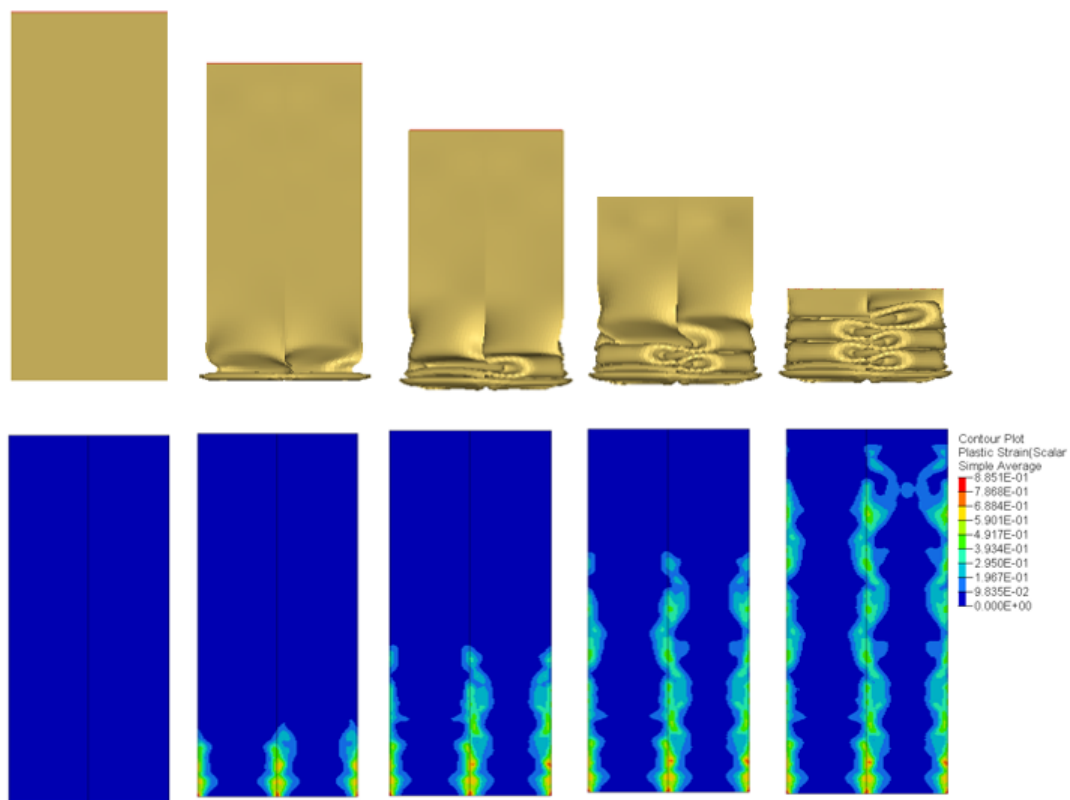
Fig. 3.8. Crushing Process and PEEQ Plot of Square Tube

It can be seen that the conventional square tube collapses, starting from the start of the tube, where rigid wall is present, and progressively collapsing axially towards the other end. In the deformation of conventional square tubes, the stress concentrations are seen on the corners of the tube, while negligible stress is seen

on the tube surfaces. Similarly, large plastic strain concentrations are seen on the plastic hinge lines on these corners, which can be confirmed in PEEQ map in Figure 3.8. These stationary hinge lines get created as the fold lobes are formed and travel from the start of the tube to the end. The propagation of horizontal stationary and inclined traveling plastic hinge lines forms the symmetric collapse mode. All the folds are in symmetric manner, and the folding pattern aligns with the experimental fold patterns seen in work [117] by Abramowicz.
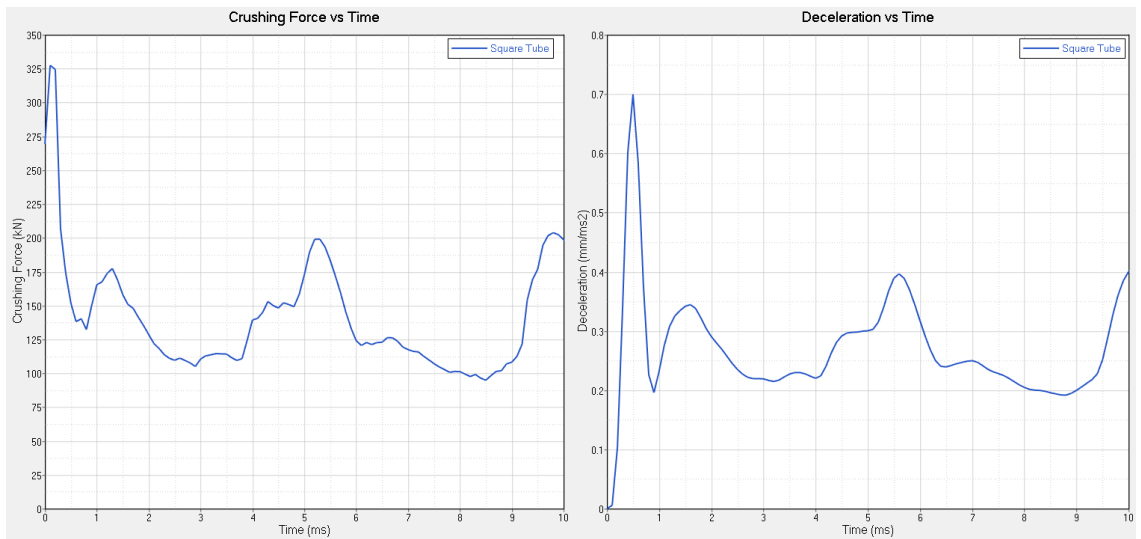
Fig. 3.9. Crushing Force and Deceleration Plot of Square Tube Crash

Force verses time and deceleration verses time plot for the square tube, is shown in Figure 3.9. In both the plots, a very high peak is observed at the start of the crushing, which shows a significant amount of energy is needed to initiate the buckling in conventional square tubes design. This can be confirmed form the higher peak crushing forces value of 327 kN and peak deceleration of 0.7 mm/ms^2 seen. Later, the crushing is followed by number of hills and valleys in the curve with a steady collapse behavior. The mean crushing force of 155 kN and mean deceleration of 0.29 mm/ms^2 was observed.

4. PROPOSED ORIGAMI DESIGN

4.1 Overview

A conventional square tube crash has been investigated in section 4.2 to understand the collapse mode occurring with predefined width to thickness ratio, to have a clarity before developing the origami collapse pattern. Section 4.3 discusses the about the design and geometric analysis of the proposed origami pattern. While section 4.4 focuses on developing origami tubular structure for conducting parametric study. Section 4.5 briefly jots down the finite element formulation used for origami tube. And Section 4.6 discusses in detail about the crushing of proposed origami tube. It also covers effect of different geometric parameters, like dihedral angle, number of modules, and hexagonal dimension b, on origami tube crash performance using crush indicators, like crushing force and deceleration. And finally a summary is given is section 4.7.

4.2 Basic Folding Pattern in Square Tubes

Before developing a fold pattern for an origami structure, it is very important to understand how the conventional square tube design collapse's. There has been a lot of studies done in understanding the collapse behavior to achieve progressive collapse. Wierzbicki and Abramowicz, in their work in [43,71], they proposed a theory describing the folding mechanism in thin walled structures and were the first ones to identify two basic forms of fold elements in square tube [43]. These elements are called as Type I and Type II fold elements, which can be seen in Figure 4.1, representing quarter of a square tube fold. Type I elements are the ones with opposite sides of the fold move in same direction, and the adjacent ones moves in opposite directions.

Type II elements are having all the folds moving in same direction, either inward or outward. And based on different combinations of the Type I and Type II elements, different types of collapse modes are seen.
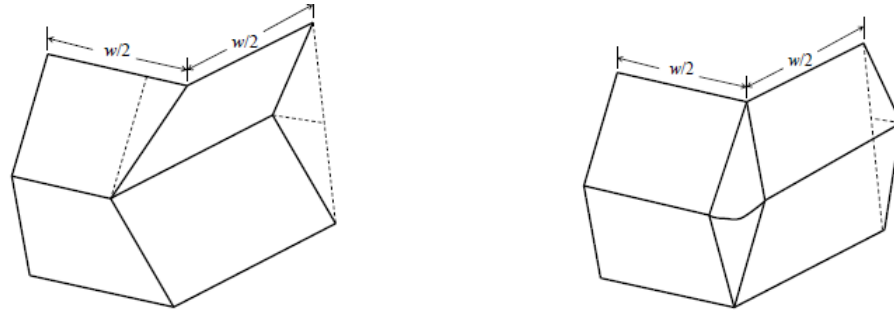
Fig. 4.1. Type I and Type II Fold Elements in Square Tube Fold [43]

Progressive collapse in tubes is achieved when a fold is generated in the successive layers. And for understanding the progressive collapse behavior in details, these Type I and Type II elements have been used extensively. There are three ways in which the crushing can happen in dynamic axial crushing of thin walled tubular structures with square cross section: symmetric crushing mode, extensional crushing mode and general mixed crushing mode, which can be seen in Figure 4.2. Of all the collapse modes, extensional collapse mode is having the highest energy absorption capacity due to its in plane stretching [118]. But, extensional modes are dominant in low width to thickness ratio, hence it is not possible to trigger naturally in square tubes with higher width to thickness ratio, as we are having in our benchmark problem. Also, controlling the natural collapse pattern of extensional mode is difficult. Hence to tigger the extensional mode in tubes with higher width to thickness ratio and to control their collapse, we need to force the collapse pattern in the square tube geometry.
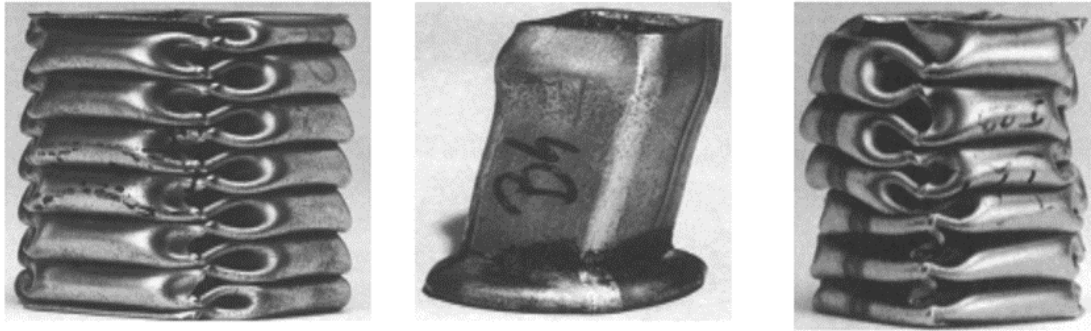
Fig. 4.2. Types of Collapse Modes in Square Tube [118]

4.3 Design and Geometrical Analysis of Origami Pattern

As we know from the previous sections that there are three collapse modes in which a folding happen in a thin walled tubular structures with square cross section: symmetric crushing mode, extensional crushing mode and general mixed crushing mode [118]. Extensional modes are very efficient in EA capacity but triggering them is difficult because a thin walled structure is more prone to buckle, due to lower resistance, than to stretch. Extensional collapse mode can be generating during crash by generating cylindrical or episoidal domes on the surfaces of the tubes, in a similar way the corrugation in tubes and episoidal domes were created in tubes to create an forced extensional collapse in these [64, 119] studies. Thus with indentation extensional mode can be achieved in an origami tubular structure which can be created from an flat surface. But the structure they developed were nondevelopable.

In conventional square tube, about seventy percent of EA is achieved due to the creasing lines And the energy absorption capacity is directly proportional to the length of the plastic creasing lines in tubular structure. Therefore with the increased creasing line, we can see higher EA capacity in origami structures than the conventional design square tube with equal surface area. This principle is applied with origami design in this study, where plastic creasing line length are increased with proper triggering point to start the extensional collapse in a desired way. The origami pattern developed in

this way is also seen to be developable from a flat sheet by folding at the creasing, as the end surfaces are seen to coincide, making it an developable from a flat sheet.

For developing pattern for extensional collapse mode, it was necessary to understand the extensional collapse behavior. Hence, a set of simulations were performed on square tube with different width to thickness ratios from 60, 40, 30, 24, 20,and 15. Exterior dimensions were kept constant to that of our benchmark problem i.e., 60 mm x 60 mm x 120 mm. Hence to achieve varying w/t ratio, thickness was varied. In all the simulations only symmetric mode was seen, besides one model with w/t ratio of 15. Figure 4.3 shows the crushing process for 4 mm thick tube with w/t ratio of 15.
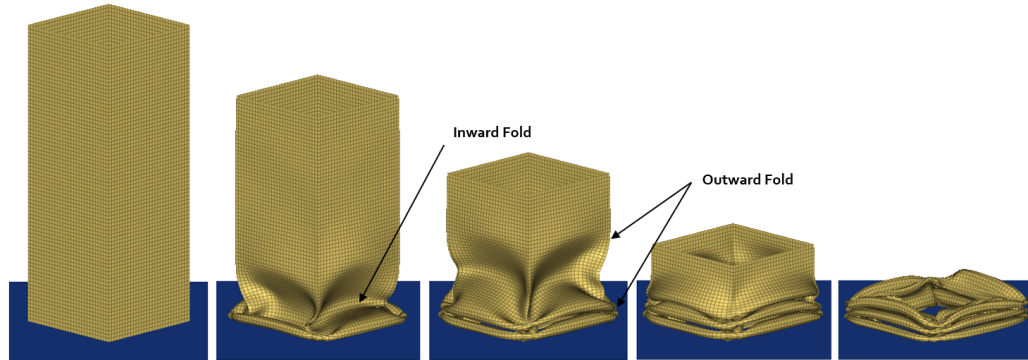
Fig. 4.3. Extensional Collapse in Conventional Square Tube with w/t ratio of 15
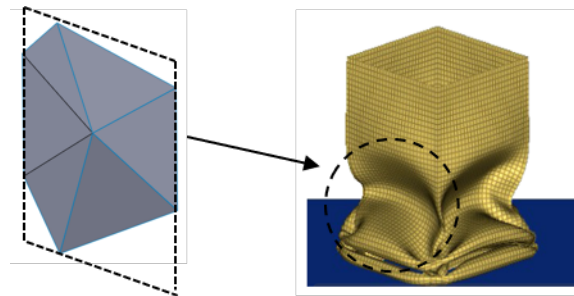
Fig. 4.4. Origami Hexagonal Dimple

This extensional collapse mode was studied for how the folding is initiated and gets propagated throughout the tube. It was seen, all the sides of the tubes either folds inwards or outwards to create one extensional fold. Also another thing that was

noticed, if one fold is acting inwards, then the subsequent fold will act outwards. This alternating pattern is throughout the crushing process, which can be seen in Figure 4.3. To replicate this alternating fold behavior on each face of the square tube, an hexagonal indentation (also called as origami element) was created on each face of the square tube to have folds generating in same direction i.e., either all faces folds in inward direction or all faces folds in outward direction, which can be seen in Figure 4.4. Hexagonal indentation was only available option to accommodate indentation and to have equal unfolded surface area as that of the square tube. Because of this hexagonal indentation, an inward folding will be generated at the center of the hexagon. And outward fold will get generated at the top and bottom edges of the hexagon. as the top ans This indentation is patterned on all the four sides of square tube to create a origami module. And by axially joining the modules we will get an origami tube.
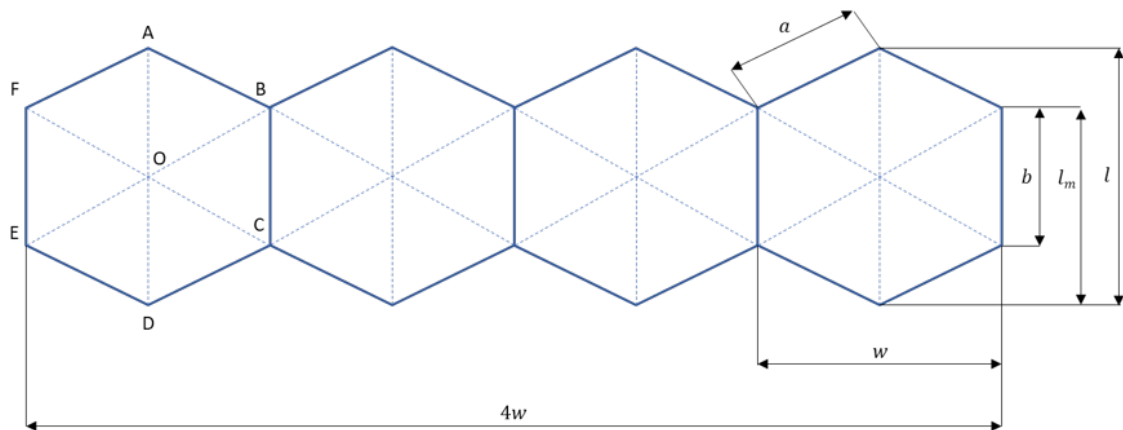
Fig. 4.5. Unfolded Origami Pattern on a flat sheet

Figure 4.5 shows a flat sheet with origami creasing design to form hexagonal dimpled pattern on each face of tube, where the solid and the dashed lines on the pattern forms hill and valley folds respectively. When the flat sheet of material is pre-folded according to the creasing defined and when the two extreme ends are connected, we will get a module for an origami tube, which can be seen in Figure
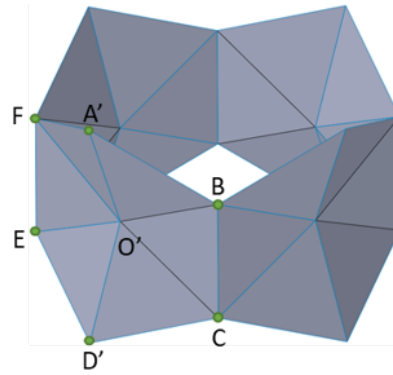
Fig. 4.6. Module created after folding
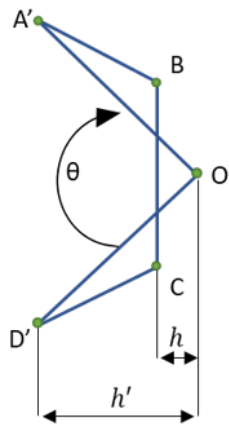
Fig. 4.7. 2D Side View of the Hexagonal Dimple

4.6. In Figure 4.5, A,B,C,D,E,F, and O shows the vertex positions of the unfolded hexagon. While in Figure 4.6 A',B,C,D',E,F, and O' shows the vertex position of the hexagon after folding. The pattern is designed in a way that throughout the folding, the edge BC and FE don't change the position, as they are the corner edges of the square tube. In the prefolded hexagon module, A'O' and D'O' will have hill fold, while FO', BO', EO', and CO' will have valley fold. Figure 4.7 shows an side view of the prefolded hexagonal dimple on the surface of the square tube. This figure helps to understand the folding process. As the crushing is started, A' and D' will come closer to each other, resulting in O' to pushed further inside the tube. Thus in a way acting like a compliant mechanism.

The origami prefold pattern showed in Figure 4.6 is primarily controlled by the four parameters: unfolded height of the module l, width of the tube w, vertical edge of the hexagon b, and the indentation depth h. Another geometrical parameter to define a origami tube of multiple units is the number of modules in the axial direction, M. Hence the total number of dependent parameters is five. The mathematical relationship between them are shown in equation 4.1 and 4.2.

$$l = 2\sqrt{a^2 - \frac{w^2}{4}} + b \tag{4.1}$$

$$h' = OO' = \frac{(\sqrt{2} - 1)w}{2} + h \tag{4.2}$$

where h' is the horizontal distance between the A' and O'. Theta is a dihedral angle θ formed between the vertical edges A'O' and D'O', which can be seen in Figure 4.7. The Dihedral angle θ depends on the l and h through the equation 4.3.

$$\theta = 2cos^{-1}(\frac{2h - 24.86}{l}) \tag{4.3}$$

The inward hexagonal dimple on each face of the tube is the characteristic feature of the structure, acting like an compliant mechanism during compression of the tube and diverting the longitudinal crushing forces into lateral direction. This hexagonal crush initiator is satisfying two objectives. Firstly, guiding the tube throughout the crushing process to collapse in a specific extensional deformation mode. And secondly, the angle in the hexagonal dimple is responsible for lowering the peak crushing forces observed during the initial crushing. And thirdly the vertical sides BC and EF, as seen in Figure 4.6, absorb the crushing forces by undergoing buckling, after the initial peak forces have been subsided.

This origami creasing pattern is desirable due to its properties as discussed below. The basic origami module shown in Figure 4.6 can be arrayed together along the longitudinal axis and the tubular structure can be tailored to required length. The same design with some modifications to the hexagon geometry can also be tailored for tapered tube designs for oblique loading. Different cross sectional tubes, like hexagonal

and octagonal cross section shaped, can be used with this origami creasing pattern. Rectangular cross section is widely used in the automotive industry, and the current pattern can be used with rectangular cross section tubes with little modifications.

4.4   Developing Origami Tube

Different configurations of the origami tubes were created and studied extensively to find the effect of different origami configurations on the crushing force and deceleration. The parametric study was done on two groups, A and B.

A total of 28 origami tubes configurations were created under group A to study the effect of number of modules M and variation in θ on crash performance. All the configurations were created under group A by varying geometric parameter h to change theta, and longitudinal axis of hexagon l, to change number of module M. All the configuration are listed in detail in Figure 4.8. The parameters in each configuration are varied in increments. The performance of all these 28 origami configurations was compared against the square tube performance.

The surface area and the thickness of all the origami tubes and the conventional square tube were kept same. Throughout all the configurations under group A, the dimension b was kept half to that of the dimension l. The model name stated the number of modules and the theta used in that config. For example, 2M_TH155 states that configuration is having 2 modules and the θ as 155°. The dimensions of the conventional tube were kept as, Length = 120 mm, width = 60 mm and thickness = 2 mm. The uncompressed length of the origami tube for all the configurations is kept equal to the length of the square tube i.e., 120 mm. Hence the compressed length of the origami tube will differ in each configuration based on the geometric parameters considered. Also the wall thickness in all the configurations are kept at 2 mm. The tubes were placed vertically and crashed dynamically along the length of the tube. And studied for two things, firstly, if progressive buckling was achieved with extensional collapse and secondly, for efficiency in crushing and deceleration.

The configuration table shown in Figure 4.8 also contains the numerical values from FE analysis for peak crushing forces, mean crushing forces, peak deceleration and mean deceleration, which will be discussed in the upcoming sections.

Model Name	l	M	θ°	h	t	P_{max}	P_{max} Reduction	P_{mean}	P_{mean} Reduction	A_{max}	A_{max} Reduction	A_{mean}	A_{mean} Reduction
	mm		°	mm	mm	(kN)	%	(kN)	%	(mm/ms²)	%	(mm/ms²)	%
Sq Tu	-		-	-	2.00	327	-	155	-	-0.699	-	-0.287	-
2M_TH140	60	2	140	-2.17	2.00	116	64.5%	94	39.4%	-0.251	64.1%	-0.171	40.5%
2M_TH145	60	2	145	-3.41	2.00	123	62.4%	96	38.1%	-0.265	62.1%	-0.186	35.3%
2M_TH150	60	2	150	-4.66	2.00	129	60.6%	101	34.8%	-0.279	60.1%	-0.189	34.2%
2M_TH155	60	2	155	-5.93	2.00	143	56.3%	105	32.3%	-0.294	57.9%	-0.197	31.5%
2M_TH160	60	2	160	-7.22	2.00	166	49.2%	110	29.0%	-0.319	54.4%	-0.207	28.0%
2M_TH165	60	2	165	-8.51	2.00	207	36.7%	117	24.5%	-0.361	48.4%	-0.217	24.5%
2M_TH170	60	2	170	-9.81	3.00	249	23.9%	123	20.6%	-0.429	38.6%	-0.226	21.4%
3M_TH140	40	3	140	-5.59	2.00	109	66.7%	97	37.4%	-0.231	67.0%	-0.173	39.8%
3M_TH145	40	3	145	-6.41	2.00	119	63.6%	101	34.8%	-0.249	64.4%	-0.183	36.3%
3M_TH150	40	3	150	-7.25	2.00	132	59.6%	106	31.6%	-0.276	60.5%	-0.192	33.2%
3M_TH155	40	3	155	-8.10	2.00	152	53.5%	112	27.7%	-0.308	55.9%	-0.204	29.0%
3M_TH160	40	3	160	-8.95	2.00	181	44.6%	122	21.3%	0.346	149.5%	-0.231	19.6%
3M_TH165	40	3	165	-9.82	2.00	217	33.6%	134	13.5%	-0.394	43.6%	-0.25	13.0%
3M_TH170	40	3	170	-10.68	2.00	261	20.2%	142	8.4%	-0.468	33.0%	-0.267	7.1%
4M_TH140	30	4	140	-7.30	2.00	128	60.9%	113	27.1%	-0.274	60.8%	-0.208	27.6%
4M_TH145	30	4	145	-7.92	2.00	143	56.3%	120	22.6%	-0.298	57.4%	-0.219	23.8%
4M_TH150	30	4	150	-8.54	2.00	161	50.8%	126	18.7%	-0.33	52.8%	-0.23	20.0%
4M_TH155	30	4	155	-9.18	2.00	182	44.3%	132	14.8%	-0.368	47.4%	-0.244	15.1%
4M_TH160	30	4	160	-9.82	2.00	208	36.4%	136	12.3%	-0.413	40.9%	-0.26	9.5%
4M_TH165	30	4	165	-10.47	2.00	242	26.0%	143	7.7%	-0.47	32.8%	-0.27	6.1%
4M_TH170	30	4	170	-11.12	2.00	282	13.8%	146	5.8%	-0.549	21.5%	-0.278	3.3%
5M_TH140	24	5	140	-8.32	2.00	159	51.4%	139	10.3%	-0.345	50.6%	-0.255	11.3%
5M_TH145	24	5	145	-8.82	2.00	177	45.9%	146	5.8%	-0.371	46.9%	-0.269	6.4%
5M_TH150	24	5	150	-9.32	2.00	197	39.8%	149	3.9%	-0.405	42.1%	-0.273	5.0%
5M_TH155	24	5	155	-9.83	2.00	220	32.7%	152	1.9%	-0.449	35.8%	-0.279	2.9%
5M_TH160	24	5	160	-10.34	2.00	247	24.5%	155	0.0%	-0.511	26.9%	-0.282	1.9%
5M_TH165	24	5	165	-10.86	2.00	279	14.7%	163	-5.2%	-0.576	17.6%	-0.308	-7.2%
5M_TH170	24	5	170	-11.38	2.00	310	5.2%	176	-13.5%	-0.61	12.7%	-0.332	-15.5%

Fig. 4.8. Configurations of Tube in Group A for Parametric Study for θ and M

Configurations shown in Figure 4.8 are arranged based on the values of the geometric parameters: number of modules M and dihedral angle θ. Number of modules are dependent on the ratio l/b, where l is the vertical diagonal of the unfolded hexagon and b is the vertical length of one of the side of hexagon. M is inversely proportional to the l/b ratio. Higher the l/b ratio, lower will be the number of modules. Figure 4.9 shows the modules arrangement in origami tube.

Another group B was built with 7 origami tubes to study the effect of the parameter b on crushing behavior. 'b' is the vertical dimension of one of the sides of
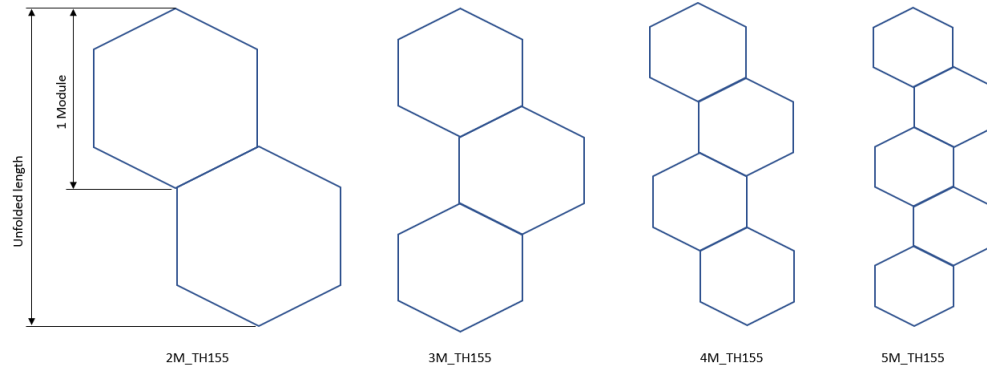
Fig. 4.9. Modules Arrangement in Origami Tube

Model Name	l	M	θ º	b	h	t	P_{max}	P_{max} Reduction	P_{mean}	P_{mean} Reduction	A_{max}	A_{max} Reduction	A_{mean}	A_{mean} Reduction
	mm		º	mm	mm	mm	(kN)	%	(kN)	%	(mm/ms²)	%	(mm/ms²)	%
SqTu	-		-	-			327	-	155	-	-0.699	-	-0.287	-
2M_TH155_b10	60	2	155	10	-5.93	2.00	128	60.86%	114	26.45%	-0.282	59.66%	-0.21	26.83%
2M_TH155_b15	60	2	155	15	-5.93	2.00	134	59.02%	114	26.45%	-0.298	57.37%	-0.215	25.09%
2M_TH155_b20	60	2	155	20	-5.93	2.00	134	59.02%	112	27.74%	-0.291	58.37%	-0.201	29.97%
2M_TH155_b25	60	2	155	25	-5.93	2.00	137	58.10%	109	29.68%	-0.293	58.08%	-0.202	29.62%
2M_TH155_b30	60	2	155	30	-5.93	2.00	143	56.27%	105	32.26%	-0.294	57.94%	-0.197	31.36%
2M_TH155_b35	60	2	155	35	-5.93	2.00	150	54.13%	105	32.26%	-0.309	55.79%	-0.198	31.01%
2M_TH155_b40	60	2	155	40	-5.93	2.00	160	51.07%	110	29.03%	-0.325	53.51%	-0.201	29.97%
2M_TH155_b45	60	2	155	45	-5.93	2.00	156	52.29%	108	30.32%	-0.326	53.36%	-0.199	30.66%
2M_TH155_b50	60	2	155	50	-5.93	2.00	170	48.01%	109	29.68%	-0.329	52.93%	-0.203	29.27%

Fig. 4.10. Configurations of Tube in Group A for Parametric Study for dimension b

hexagon, as seen in Figure 4.5. In this study only the parameter b war varied while all other geometric parameters were kept constant. Configuration 2M_TH155 was considered as an benchmark and different configuration in group B were created on this model, which can be seen in Figure 4.10. The uncompressed length and the thickness of all the origami tubes are kept constant to the conventional square tube. The model name nomenclature in this group is similar to one adopted earlier with addition of value of b at the end. For example, 2M_TH155_b25 states, there are 2 modules used in the configuration with θ of 155° and the length of b is 25 mm. The Figure 4.10 lists all the created configurations and tabulates the FE analysis result

values for peak crushing forces, mean crushing forces, peak deceleration and mean deceleration, all of which will be discussed in the upcoming sections.

4.5 Manufacturing of Origami Tubes

Origami tubes are developable structures, hence can be made out of flat sheet of material with little distortion. It is difficult to fold an entire tube out of a single sheet, hence a common approach in building tubular structures to create two half tubes which can be spot welded to create a complete tubular structure. This can be achieved by stamping the flat metal sheet to create a pair of male and female. Then folding the stamped sheet to create the half origami structure and then followed by spot welding both the parts. The indentation causing geometric imperfection can be achieved with stamping the indentation. This simple manufacturing approach is cost effective but do have its own limitations. Only thin walled tubes can be manufactured with this approach and the quality of the tubes will be crude too. Alternative to this method will be hydro forming and casting, both of which are costly options, especially, when the amount of units to manufacture are less.
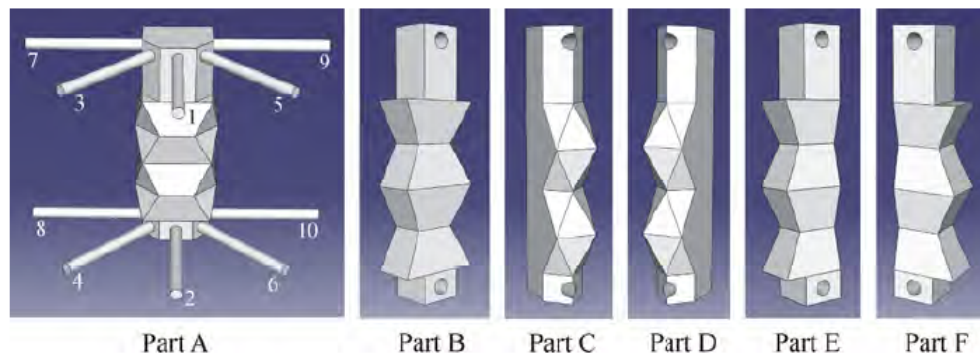

Fig. 4.11. Mould for creating Origami Tubes [4]

An cost efficient method of developing the origami tubes is proposed by Jiayao Ma [4]. In that approach, to keep the operations cost less, stamping process to create half tubes is kept same. But to improve the accuracy, new way of stamping was

suggested. Since its difficult to create origami tubes in with one single punch, s set of moulds were designed, which can be seen in Figure 4.11. The origami pattern will be developed by placing the steel sheet on the part A and then placing remaining parts on top of the sheet and compressing it to achieve the origami structure. The mould dimensions will be decided based on dimensions of the tube to manufacture. This approach is cost efficient and also moderately accurate. Also the manufacturing cost is similar to the manufacturing approach involving dents, as this method is similar to the manufacturing method used in industry.

4.6   Results and Discussion

4.6.1   Origami Tube Crash

For studying the crushing in origami designed tube, 3M_TH155 was considered as on representative model for all the origami configurations demonstrating predefined extensional collapse mode. The crushing process of the origami tube and its equivalent plastic strain (PEEQ) plot can be seen in Figure 4.17. All the three modules are named as 1-3 with 1 being the module close to the rigid wall i.e., the lowermost module in Figure 4.17, and the other two are the consecutive modules to it.

The folding starts with module 2, taking all the initial crushing load. As the tube is compressed further, pairs of plastic hinge lines are generated along the edges and the diagonals of each hexagon element and travels to the adjacent module as the compression advances. Followed by the compression of module 1 and 3 and progressing towards the end of the tube. During the collapse of the module, the center of the hexagon pyramid element moves inward, acting like a compliant mechanism by taking the longitudinal crushing load which results in movement in lateral direction.

In benchmark square tube PEEQ plot, seen in Figure 3.8, all the stress and strain concentrations were seen on the corner edges. And the plastic hinge line was seen to be traveling along the corner edges only. Therefore corner edges were the only one responsible for all the energy and the crushing force absorption in square tube.

While in origami tube PEEQ plot it can be seen, the plastic deformations started in module 2, can be seen all around the edges and the diagonals of the hexagon. When the corner of square tube and origami tube is compared, it can be seen, a square tube just has a single pair of plastic hinge lines, while a origami has two pair. Hence leading to a longer plastic hinge line, which results in increased energy absorption, dispersed stress and strain concentrations, and efficient extensional collapse in inward direction.
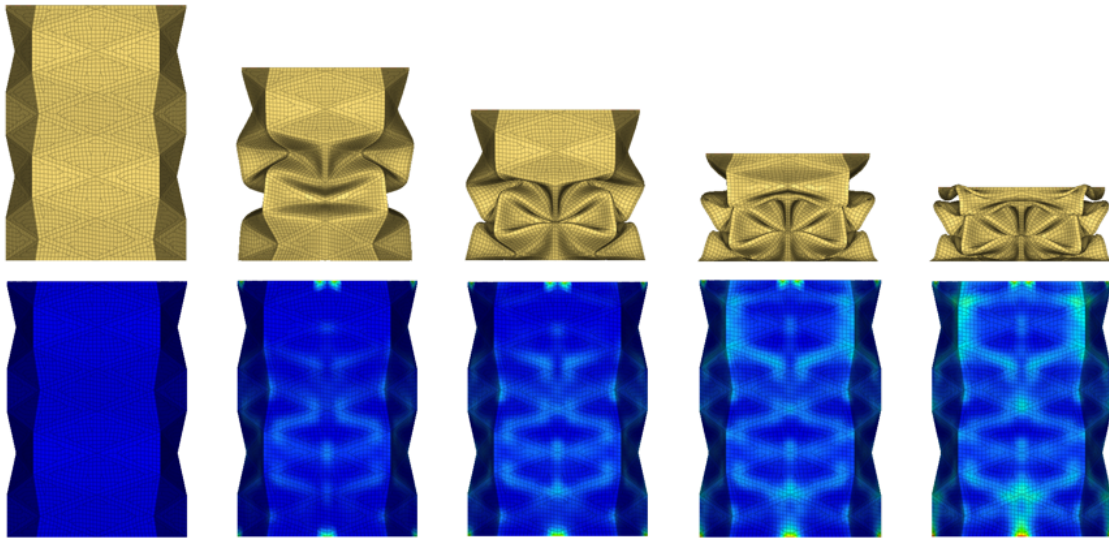
Fig. 4.12. Crushing Process and PEEQ Plot of 3MTH155 Origami Tube

Figure 4.13 shows the crushing force and deceleration plot for origami tube 3M_TH155 and conventional square tube for comparison. As we have seen in conventional tube, a significant amount of energy was needed to initiate the buckling, leading to a initial spike in crushing force and deceleration plots. In origami tube, the crushing behavior is seen to be almost linear. Even though there are three modules in the tube, the graph do not show any major excitement or transition in the crushing and deceleration behavior, instead showing a stable collapse. With this we can conclude the predefined origami pattern are efficiently absorbing the initial peak loads and having an stable collapse In origami tube with predefined pattern, we are able to see a 52% drop in
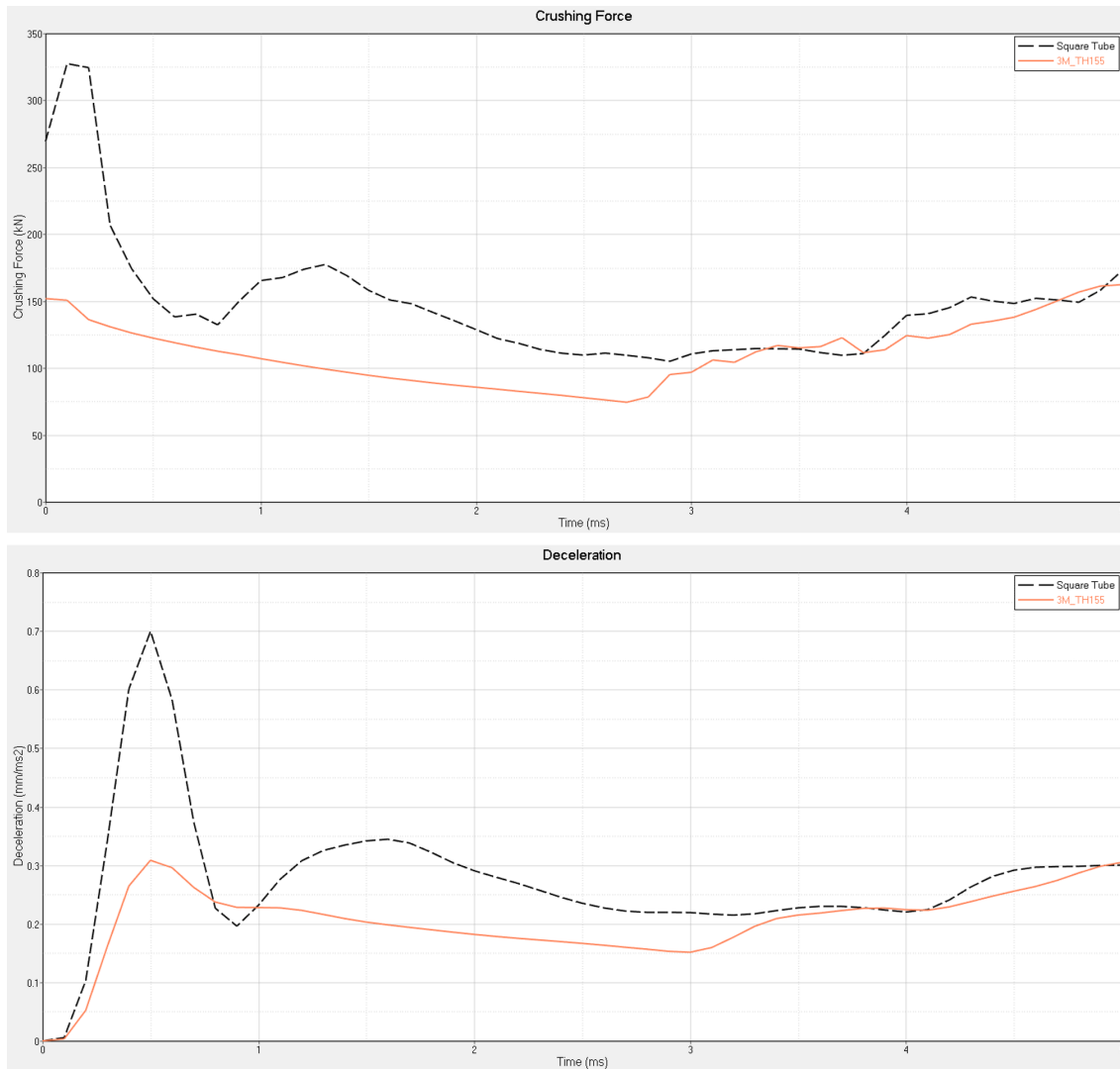
Fig. 4.13. Crushing Force and Deceleration plot for 3MTH155 and SqTu

the peak crushing force, from 327 kN in square tube while 152 kN in origami tube. Also 27% reduction is seen in mean crushing force values, with 155 kN in square tube and 112 kN in origami tube.

Similar pattern is seen with deceleration plots too. A 55% drop can be seen in the peak deceleration value also, with 0.7 mm/ms^2 for square tube and 0.31 mm/ms^2 for origami tube. Also a 29% reduction in mean deceleration is seen, from 0.29 mm/ms^2 to 0.2 mm/ms^2

4.6.2   Effect of Dihedral Angle θ and Number of Modules M on Crash

It can be seen from collapse of origami tube 3M_TH155 and conventional square tube, the extensional collapse mode is more efficient than the symmetric mode. Hence, now the next step in designing the origami tube will be to evaluate the range of the parameters with which we can see a stable collapse behavior with extensional mode.

The dihedral angle is following the equation 4.3, and plays an very important role in achieving the desired extensional collapse mode and how the plastic hinge lines propagates. When the dihedral angle is $180°$ then, it will form a vertical side of a tube, without any indentations. Hence, if the dihedral angle is very high, close to $180°$, then it can be stated that the desired collapse pattern is not completely followed leading to high crushing forces and deceleration values. Where as, if the dihedral angle is very low, then the desired collapse mode is achieved with lower crushing forces and deceleration values but the energy absorption efficiency will be low, as less amount of work will be needed in overcoming the buckling forces to initiate folds. In addition, the amount of rotation in plastic hinge lines will also be reduced.

The number of modules in an origami tube are inversely proportional with the ratio of length of module to width of module l/w. Throughout the study, the width is kept constant at 60 mm. And the total unfolded length of the sheet is kept at 120 mm. We can say that as the ratio l/w is smaller, we will be having more number of modules. Higher the number of modules will lead to increased in length of plastic hinge lines, which will lead to increased energy absorption. And similarly, lower the number of modules will lead to smaller length of plastic hinge lines and hence lower energy absorption. Having a very low number of modules will create complications in the collapse and will override the collapse pattern.

A total of twenty eight origami configurations are evaluated with different combinations of dihedral angle and number of modules. All other parameters like uncompressed length of the tube, surface area and hence mass of the tube are all kept

constant. Figure 4.8 lists all the twenty eight configurations from 2M_TH140 to 5M_TH170.

Origami Tubes with 2 Modules

The collapse mode were studied starting with tubes with $M = 2$ with dihedral angle theta increased in increments of five degree from $140°$ to $170°$, leading to 7 different configurations. From the simulation results it can be seen, desired collapse mode is attained and the origami pattern is well followed in all the 7 configurations. Figure 4.14 shows the crushed configurations of 2M_TH140, 2M_TH145, 2M_TH150, 2M_TH155, 2M_H160, 2M_H165, and 2M_TH170 respectively.

Fig. 4.14. All 7 Crushed Configurations of Origami with 2 Modules with θ from $140°$ to $170°$
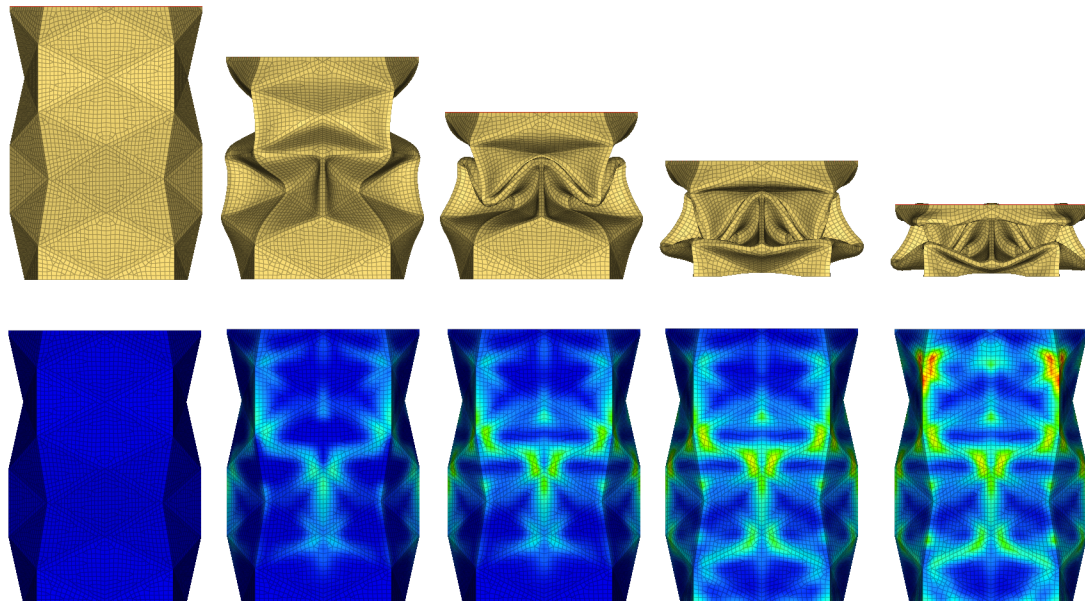

Fig. 4.15. Crushing Process and PEEQ Plot of 2MTH155 Origami Tube

In all the 7 configurations, the folding starts at the interaction between the two module and then propagates to both the end, which can be confirmed from the crushing process and PEEQ plot for origami tube 2M_TH155 in Figure 4.15. Though a large amount of plastic strain concentration can be seen in the topmost module, which is the one having contact with rigid mass with a velocity, responsible for dynamic loading.

Origami Tubes with 3 Modules

A similar collapse behavior was seen in all the 7 origami tube configurations with 3 modules, which can be seen in Figure 4.17, showing crushed configurations for 3M_TH140, 3M_TH145, 3M_TH150, 3M_TH155, 3M_TH160, 3M_TH165, and 3M_TH170. The predefined crushing pattern is seen to be followed completely with configurations from dihedral angle θ from 140° to 160°, which can be seen in Figure 4.16 (a) - (e). However, when θ reaches 165°, during the crushing process a lobe formation can be seen between the contact points of the modules. Leading to a underdeveloped collapsed pattern with local buckling, which can be seen in Figure 4.16 (f). As the θ value is further increased to 170°, the local buckling is seen to be more prominent and the resultant collapse mode can be seen in Figure 4.16 (g). Although the pattern is seen to be followed but the collapse mode is seen to be underdeveloped.

In all the 7 configurations of the 3 modules, the folding starts at the 2nd module and then propagates to both the end. This can be confirmed from the Figure 4.17, showing the crushing process and plastic strain hinge line propagation in origami tube with 3 modules, 3M_TH155. A large amount of plastic strain concentration which was seen in origami tubes with $M = 2$ whereas, in origami tubes with $M = 3$ the plastic strain are less severe. One reason for that will be increased plastic hinge length in tubes with $M = 3$. Hence dispersing the stress throughout the tube. Also it can be stated, almost negligible to none strain generation is seen on the surfaces of the

tubes and all the strain concentrations are seen on the mountain and valleys of the creasing pattern.

Fig. 4.16. All 7 Crushed Configurations of Origami with 3 Modules with θ from 140° to 170°
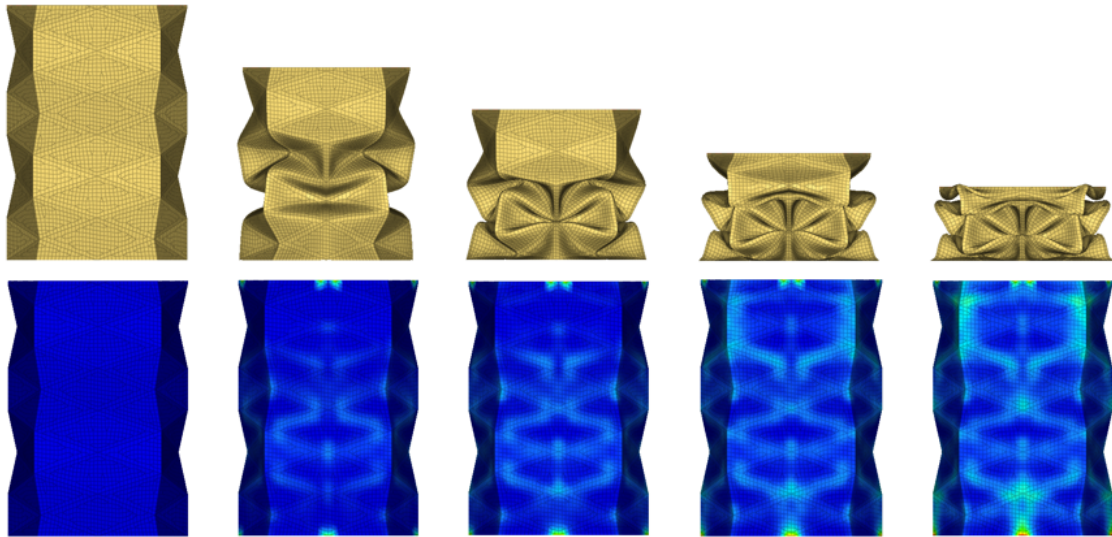
Fig. 4.17. Crushing Process and PEEQ Plot of 3MTH155 Origami Tube

Origami Tubes with 4 Modules

As M reaches 4, similar trend is seen as seen in tubes with 3 modules. The predefined crush pattern is completely followed by tubes with θ from 140° to 155°, as it can be confirmed in 4.18 from (a) to (d). When θ is 160°, an underdeveloped collapse is seen in module 4 which is the topmost module on the tube when seen in 4.18 (e). While at $\theta = 165°$, a local buckling lobe is seen to form at the connection point between module 1 and module 2, which later on alters the collapse mode as

seen in 4.18 (f). And when θ is 170°, two buckling lobes are generated along the tube. One seen at module 3 and 4 interaction and another at model 1 and 2 interaction.

Fig. 4.18. All 7 Crushed Configurations of Origami with 4 Modules with θ from 140° to 170°

Fig. 4.19. Crushing Process and PEEQ Plot of 4MTH155 Origami Tube

In all the 7 configurations of origami tube with $M = 4$, collapse starts with folding of module 2, 2nd module from the bottom, and subsequently folding of module 3, module 1 and eventually module 4. This can be confirmed from crushing process and PEEQ plot for 4M_TH155 from Figure 4.19. The strain plots are further less concentrated than that seen in tubes with 3 modules, especially the strain concentrations at the corner of each hexagonal pyramid element.

Origami Tubes with 5 Modules

Now with $M = 5$, all the configurations from θ of 140° to 150° completely follows the predefined collapse pattern, with the similar exception behavior seen in tubes with θ ranging from 160° to 170°. When θ is 160°, an incomplete collapse mode is seen with only module 5 and 2 seen to follow the creasing pattern and remaining modules are seen to buckle incompletely. But complete buckling behavior can be seen when θ is 165° and 170°, with two buckling lobes seen in module 4 and module 2, in turn disrupting the propagation of plastic hinge lines.
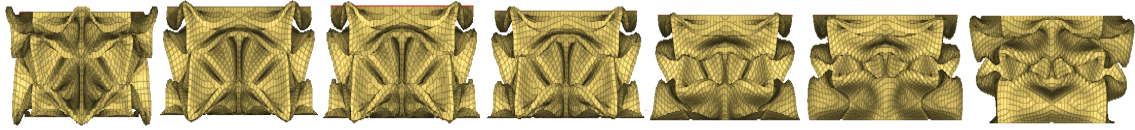

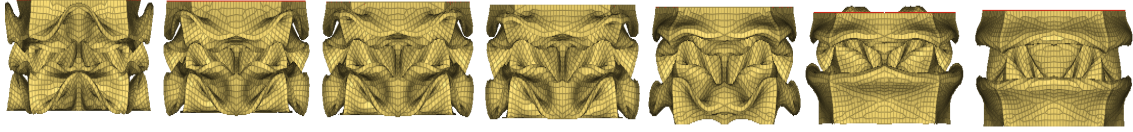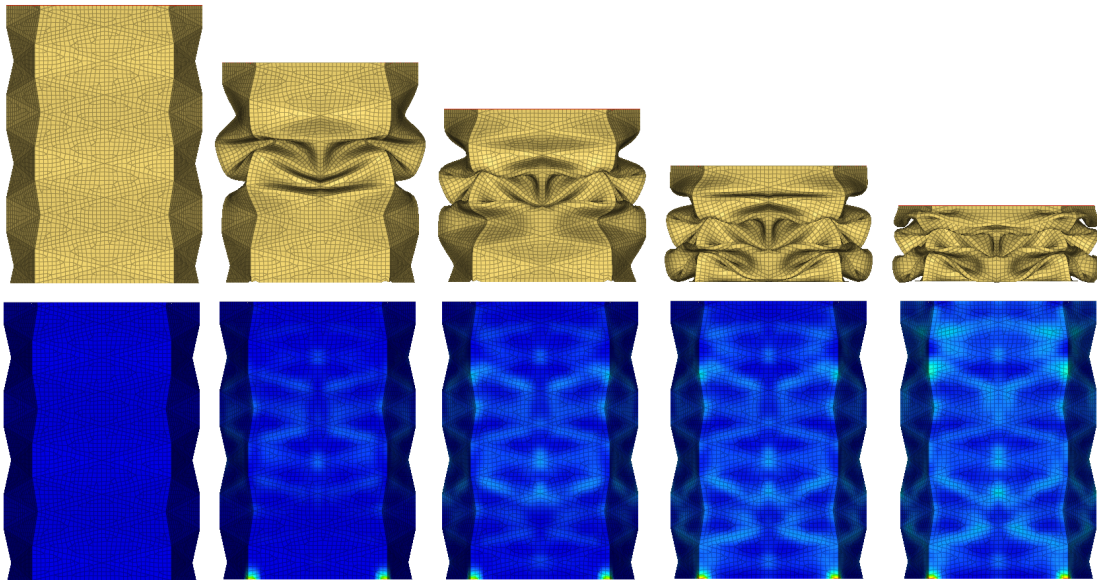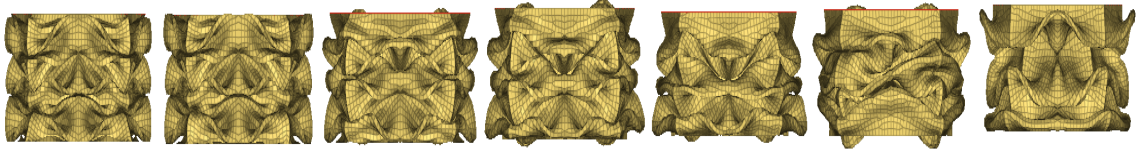Fig. 4.20. All 7 Crushed Configurations of Origami with 5 Modules with θ from 140° to 170°
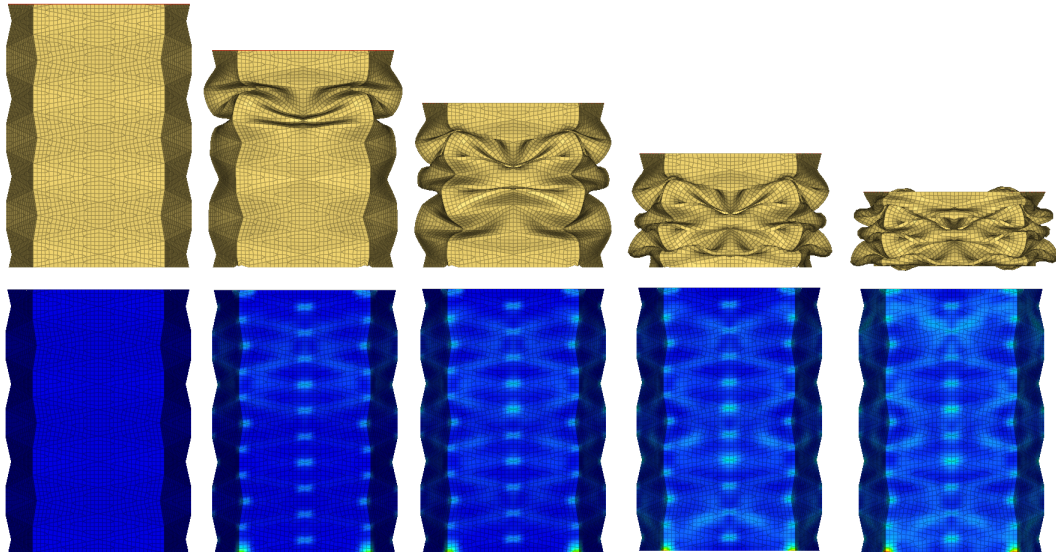
Fig. 4.21. Crushing Process and PEEQ Plot of 5MTH155 Origami Tube

In all the 7 configurations of origami tube with 5 modules, collapse occurs first in module 4 and subsequently happens in module 5, module 3, module 2, and lastly in module 1. The similar collapse pattern can be seen in Figure 4.21 showing the

crushing process and PEEQ plot for 5M_TH155 tube. In tubes with 5 modules, an slightly increased strain can be seen on the edges of the hexagon element when compared with tubes with 4 modules. But a noticeable strain concentrations on the corners of each hexagon element is noticed from the start of the crushing process.

Two conclusions can be drawn from all simulation results shown above.

1. Firstly, for tubes with same number of modules M, an predefined extensional collapse mode is always seen to be triggered when the dihedral angle θ is lower. The extensional collapse mode is promised to triggered until a specific dihedral angle θ. Once that critical angle is crossed, the collapse patterns are either seen to be underdeveloped or the predefined pattern is completely not followed, like when angle is 165° and 170° in tubes with $M = 3, 4, 5$ modules. The judgements made here for judging the collapse mode is purely based on visual inspection, as there is no other way to exactly state if the collapse is completely or partially followed.

2. When dihedral angle θ is in the range of 140 to 155, complete collapse can be seen in each origami configuration of all modules. When number of modules rises above 3, the creasing pattern is not followed instances can be seen at lower angles. Hence it can be stated, as the number of modules are increased, the critical dihedral angle gets lowered. Which can be seen, as the critical dihedral angle for tubes with 2, 3, 4 and 5 module are seen to be 170°, 165°, 160° and 160° respectively. Therefore we can conclude, a larger number of modules makes it difficult for the crushing pattern to be followed.

Now let us focus on the energy absorption properties of the tubes. All the numerical data from the all the 28 simulations are tabulated in Figure 4.8. Following observations can be made from those results.

Firstly, in each module it can be seen, as the dihedral angle θ increases the P_{mean} value also increases, provided the extensional collapse mode is triggered. Figure 4.22 shows the variation trend of P_{mean} verses θ for all the modules. For example, at M
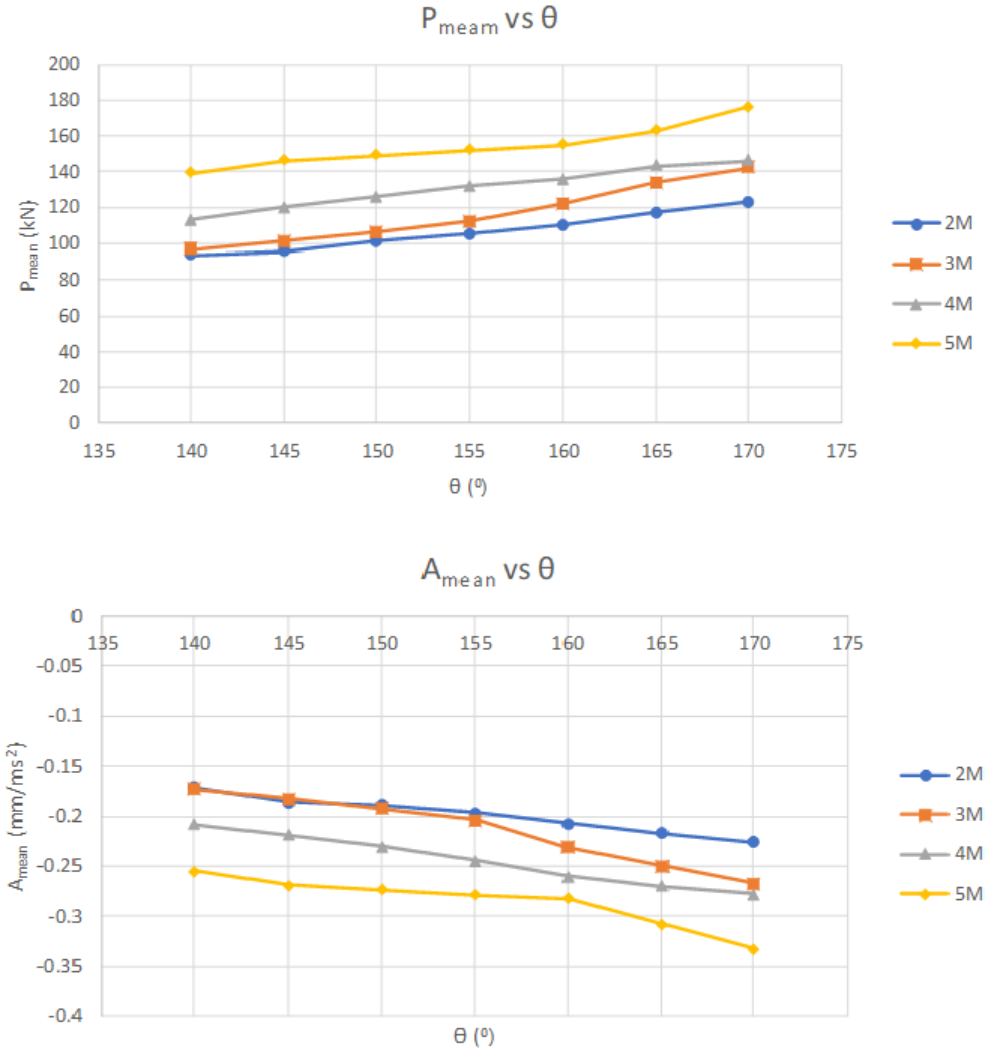
Fig. 4.22. Effect of θ on P_{mean} and A_{mean}

$= 2$, the P_{mean} increases as θ increases from 140° to 170°. While similar increasing trend for P_{mean} can be seen for $M = 3, 4$, and 5. The rise in the mean crushing values can be justified as the θ determines the rotation of stationary plastic hinge lines and corner areas swept by travelling plastic hinge lines, hence lager the θ greater will be the P_{mean} value. Similar trend is seen in deceleration plots too in Figure 4.22. For any module it can be confirmed, as the θ is increased, the deceleration values also increases, in turn showing a linear dependency on the dihedral angle.

Secondly, P_{max} also shows similar correlation to θ. It can be confirmed from the P_{max} verses θ plot 4.23, on any module, as the θ value increases the P_{max} value also increases. Since higher amount of energy is needed to trigger the buckling as the θ approaches to 180°. Similar trend is seen in deceleration plots too in Figure 4.23. For any module it can be confirmed, as the θ is increased, the deceleration values also increases, in turn showing a linear dependency on the dihedral angle.
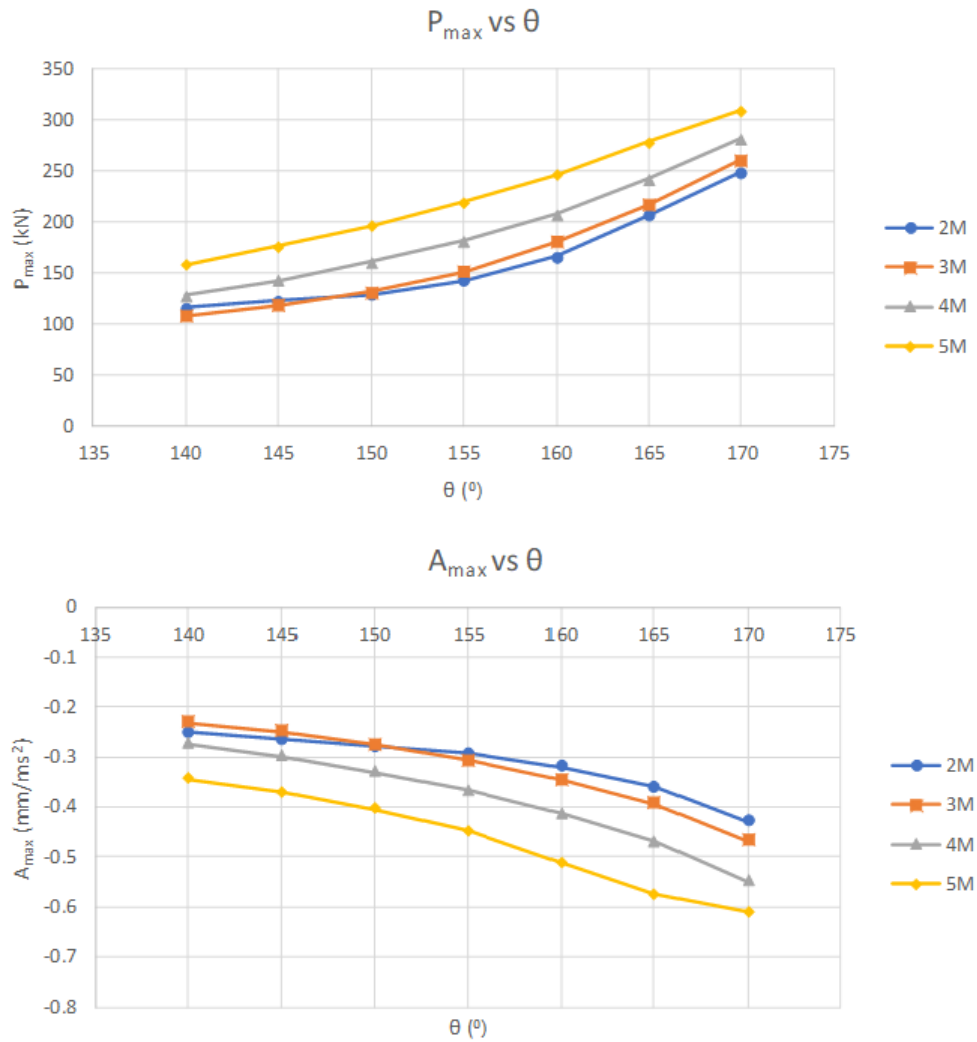
Fig. 4.23. Effect of θ on P_{max} and A_{max}

Thirdly, when θ is kept constant, and tubes with different modules are compared, an increase in P_{mean} value is noticed as seen in Figure 4.22 For example, with $\theta =$ 155°, when we compare tubes with $M = $ 2, 3, 4, and 5 we can see a rise in mean crushing forces, indicating increase in energy absorption capacity. But at the same time increase in deceleration is also noticed.

Fourthly, similar correlation was seen with P_{max} values, as seen in Figure 4.23 For example, with Theta $= $ 140°, when we compare tubes with $M = $ 2, 3, 4, and 5 we can see a rise in peak crushing forces, indicating as the number of folds are increased which results in folds overlaps which causes higher crushing resistance. Increase in number of modules also affects the collapse mode. With tubes with 2 modules, the collapse pattern was triggered at every angle from 140° to 170°. With tubes with 3 modules, after 165° the predefined collapse mode was not attained, leading to a under developed fold pattern. While in with 4 and 5 modules, after 160° and 155° respectively, some of the modules in the tube collapses with mixed collapse mode. But at the same time increase in deceleration is also noticed.

Lastly, out of all the 28 origami designs, every design has shown an noticeable reduction in P_{max} and A_{max} than that of the conventional square tube design with some reduction in P_{mean} and A_{mean} too.

4.6.3   Effect of Hexagonal Dimension b

For studying the effect of vertical dimension b of hexagon element, origami tube 2M_TH155 was considered. The dimension b is governed by equation 4.1 and equation 4.3 and plays a critical role in energy absorption and extensional collapse behavior. When b will be equal to zero, the side of the square tube will be an prefolded rhombus, while when b will be equal to its vertical diagonal x_1, it form a prefolded square. Hence if b is very high, close to its vertical diagonal x_1, the desired extensional mode can't be attained and if $b = 0$ then the peak crushing forces will be lower and the desired collapse mode will be attained but the energy absorption capacity will be too low

as less amount of work will be needed in overcoming the buckling forces to initiate folds. In addition, the amount of rotation in plastic hinge lines will also be drastically reduced. Throughout the study, the width is kept constant at 60 mm. And the total unfolded length of the sheet is kept at 120 mm. A total of 9 origami configurations are evaluated with dimension b varied from 10 mm to 50 mm in increments of 5 mm. All other parameters like uncompressed length of the tube, surface area and hence mass of the tube are all kept constant. Figure 4.10 lists all the 9 configurations with their simulation results.
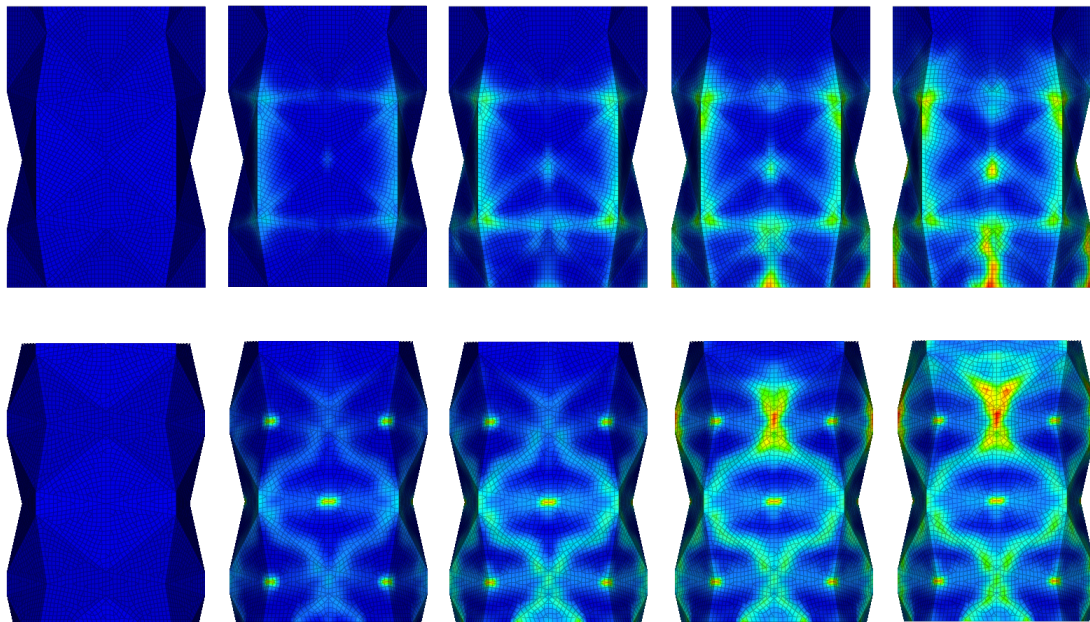
Fig. 4.24. PEEQ Plot for Origami Tubes with $b = 50$ mm (top) and $b = 10$ mm (bottom)

Figure 4.24 shows PEEQ plot for origami tube with $b = 50$ mm and $b = 10$ mm We can clearly see a difference in the formation and propagation of hinge line. In tube with $b = 50$ mm, the majority of crushing load is taken by the vertical edges of the hexagon. And besides that the tube does not collapses in the desired extensional mode. While in tube with $b = 10$ mm, the loads are taken by all the edges of the hexagon besides the vertical edges. And the tube is seen to completely collapse with

extensional mode Hence the optimum value of b is found around $b = 30$ mm, where all the six edges are responsible for taking the load, hence the stress distribution in tubes with $b = 30$ mm is low. Hence it can be seen the value of b affects the generation and propagation of plastic hinge lines.
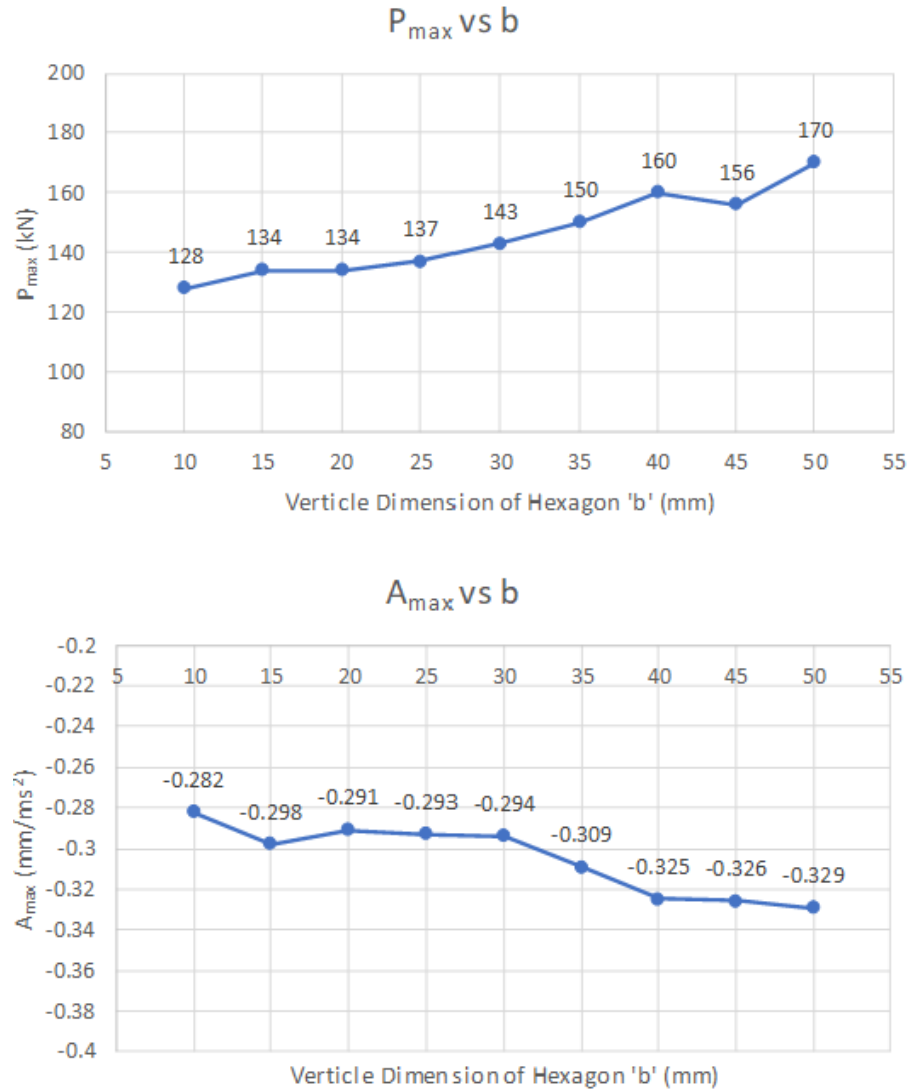
Fig. 4.25. Effect of dimension b on P_{max} and A_{max}

Also similar conclusion can be drawn by looking at the numerical data. A correlation can be seen with P_{max} values and dimension b, as seen in Figure 4.25 So when the value of b is lower the P_{max} values are lower, as less amount of energy is needed

for initiating the buckling. Similar trend is seen in the maximum deceleration plot too.

4.7 Comparison with Full Diamond Mode Pattern

In origami crash structures, full diamond mode have shown promising results in increasing the crash efficiency. Hence in this section, the performance of the origami pattern with hexagonal extensional collapse element is compared with origami pattern developed for full diamond collapse and also with square tube collapse for reference. Figure 4.26 shows a origami pattern developed for full diamond collapse by Jiayao Ma in [4].
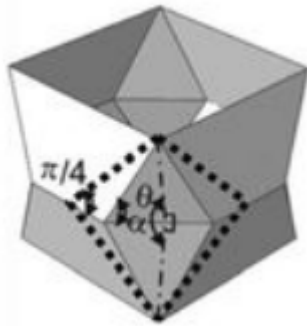
Fig. 4.26. Module of Full Diamond Mode [4]

A parametric study was done on the full diamond pattern and Figure 4.27 below shows all the simulation results for it. The dynamic Finite element formulation was kept same, with same 2 mm thickness. Also, the unfolded sheet dimensions are the same, 240 mm x 120 mm, to keep the comparison even. Both the origami designs are compared at 155° angle, since 155° was seen to be the common angle for both the designs where predefined collapse mode was achieved for all the modules. Also it was noticed, with 120 mm in tube length, the performance of the tubes are better when there are 3 to 4 modules. Hence for comparison only these two modules numbers are considered.

Model	l	θ	Modules	Thk	c/l	P$_{max}$	P$_{mean}$	A$_{max}$	A$_{mean}$
	(mm)	°		(mm)		(kN)	(kN)	(mm/ms^2)	(mm/ms^2)
A0			1	2		347.6	136.8	0.67	0.27
A1_3	60	140	2	2	0.83	133.8	126.5	0.31	0.25
A1_4	60	145	2	2	0.75	143.1	135.6	0.31	0.25
A1_5	60	150	2	2	0.6	159.5	149.6	0.3	0.3
A1_7	60	155	2	2	0.50	178.2	158.8	0.36	0.31
A1_8	60	160	2	2	0.42	186.2	164.5	0.37	0.31
A1_9	60	165	2	2	0.34	190.4	173.0	0.38	0.34
A1_10	60	170	2	2	0.2	202.3	167.8	0.4	0.3
A2_3	40	140	3	2	0.83	129.9	116.9	0.28	0.23
A2_4	40	145	3	2	0.75	135.2	123.6	0.29	0.24
A2_5	40	150	3	2	0.6	146.1	137.3	0.3	0.3
A2_7	40	155	3	2	0.50	155.7	154.4	0.34	0.31
A2_8	40	160	3	2	0.42	165.1	159.0	0.36	0.32
A2_9	40	165	3	2	0.34	170.8	159.0	0.37	0.31
A2_10	40	170	3	2	0.2	192.0	138.7	0.4	0.3
A3_3	30	140	4	2	0.83	131.6	124.9	0.29	0.25
A3_4	30	145	4	2	0.75	138.5	131.7	0.31	0.26
A3_5	30	150	4	2	0.6	149.3	144.7	0.3	0.3
A3_7	30	155	4	2	0.50	160.9	155.6	0.36	0.31
A3_8	30	160	4	2	0.42	174.2	160.1	0.38	0.32
A3_9	30	165	4	2	0.34	180.5	155.6	0.39	0.31
A3_10	30	170	4	2	0.2	202.9	142.4	0.4	0.3
A4_3	24	140	5	2	0.83	139.7	137.7	0.31	0.27
A4_4	24	145	5	2	0.75	145.8	139.9	0.33	0.27
A4_5	24	150	5	2	0.6	155.9	149.6	0.4	0.3
A4_7	24	155	5	2	0.50	168.1	159.5	0.38	0.31
A4_8	24	160	5	2	0.42	176.9	153.6	0.39	0.30
A4_9	24	165	5	2	0.34	185.5	153.4	0.39	0.30
A4_10	24	170	5	2	0.2	213.7	150.7	0.4	0.3

Fig. 4.27. Parametric Study on Full Diamond Mode

Figure 4.28 shows the typical crushing process and PEEQ plot for full diamond mode with 155° dihedral angle with 3 modules. It can be stated, the crushing starts with 2nd module and then gradually travels to both the end of tubes as the crushing progresses. Similar behavior was seen in origami tube with extensional collapse mode, as seen in Figure 4.17. In the deformation of the origami tube with Full Diamond pattern, large stress concentrations are seen over edges of diamond fold. Also, most of the edges showed negligible strain formation. This leads to conclusion that the entire energy absorption is focused on the corner edges like seen in square tubes in Figure 3.8. When compared with origami tube with extensional collapse mode, the strain formation are seen to be dispersed throughout the surface of the tube, which

can be seen in Figure 4.17. Also it can be confirmed, the length of traveling plastic hinge line is greater in proposed origami pattern with extensional collapse mode.
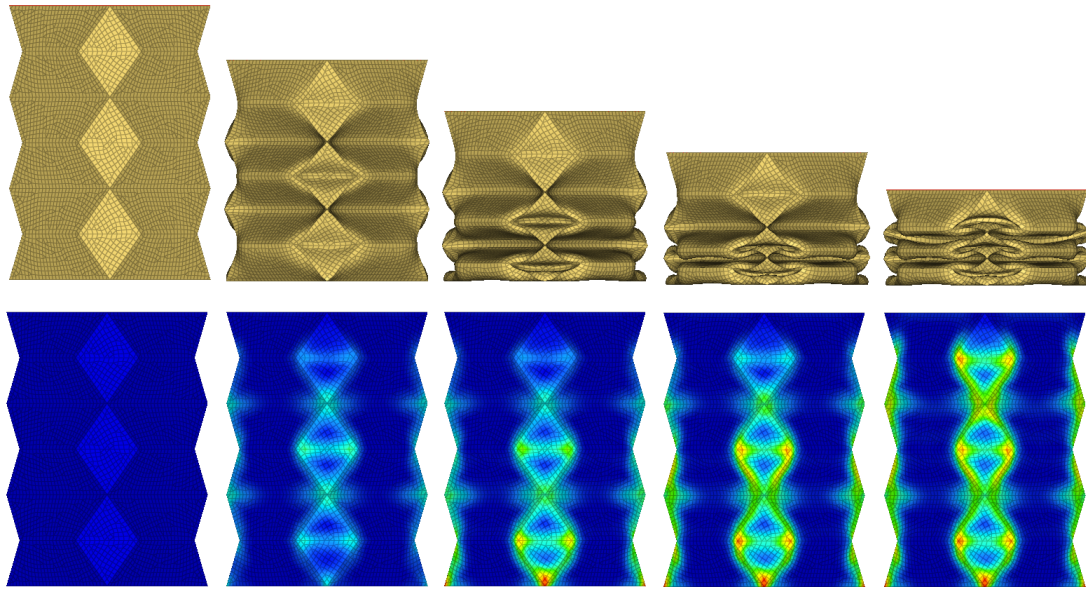
Fig. 4.28. Crushing process and PEEQ Plot for Full Diamond mode

Figure 4.29 and 4.30 shows the performance comparison of origami tube with extensional collapse mode (ECM), full diamond mode (FDM) and the conventional square tube. It can be seen, significant amount of energy is needed to initiate buckle in square tube. While both the origami designs shows significant drop in the peak crushing force. Same conclusion can be stated from the deceleration plot. Both the origami tubes have 3 modules, but still there is no excitation in the plots suggesting smooth transition of forces from one module to other. Square tube showed a peak of 327 kN in crushing force, while tube with extensional collapse mode and full diamond mode showed 152 kN and 155 kN respectively. With origami tube with extensional collapse mode we are seeing 52% in peak crushing force when compared with square tubes. And about 2% drop when compared to full diamond collapse mode, which shows similar about similar crash performance for peak crushing forces.

Similarly, with deceleration, square tube showed a similar trend with high peak deceleration of 0.7 mm/ms^2, while tube with extensional collapse mode and full di-
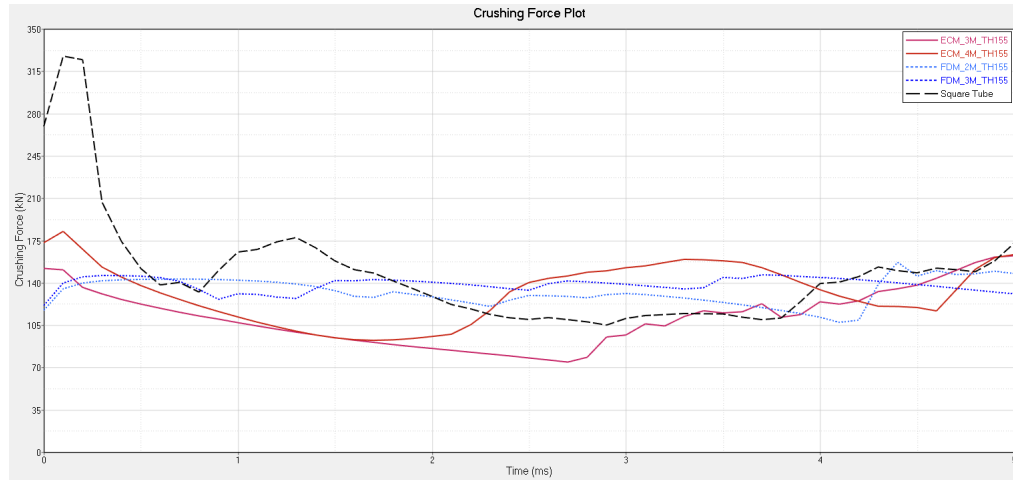
Fig. 4.29. Crushing Force Plot for Hexagonal Extensional mode and Full Diamond mode
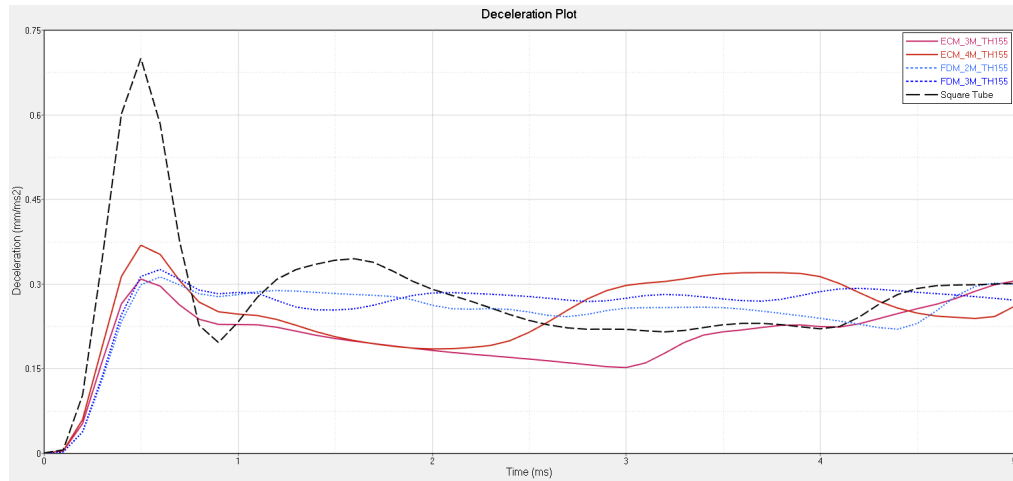
Fig. 4.30. Deceleration Plot for Hexagonal Extensional mode and Full Diamond mode

amond mode recorded 0.30 and 0.34 mm/ms^2 respectively. Hence demonstrating a 29% drop in deceleration with square tubes and about 11% drop when compared with full diamond mode.

5. SUMMARY AND FUTURE WORK

5.1 Summary

In this thesis, a new origami pattern is developed for thin walled structures as an efficient solution for energy absorption. The important accomplishments are summarized in the sections below.

A conventional square tube was first studied with specific width to thickness ratios to find type of collapse modes seen in high speed crash. A series of dynamic crash testing was done to reveal the fold patterns. It was verified symmetric modes always get triggered when the width to thickness ratio was greater than 30. But due to in plane stretching extensional modes have more energy absorption capacity but are normally dominant when width to thickness ratio is below 7.5 i.e., when either tube has smaller width or higher thickness. Hence in tubes with higher width to thickness ratio, extensional collapse mode was not seen be appearing. Therefore there was need seen to develop extensional mode that can be induced forcefully.

A new type of thin-walled tubular energy absorption device known as the origami tube which has origami pattern pre-manufactured on the surface has been developed and analyzed. For the origami pattern for a square tubes, a set of independent geometric parameters has been identified. The origami pattern on the surface of the origami tube acts as a form of geometric imperfection to reduce the initial buckling force and, more importantly, as a failure mode inducer to trigger the extensional mode in a tube which is more crash efficient because it increases the number of travelling plastic hinge lines on each side of the tube. In addition, the origami pattern have several additional properties. It is designed in a modular way so that origami tubes of various sizes can be easily obtained by changing the number of modules axially.

The surface of the tube with origami patterns is developable so that the origami tube can be conveniently and accurately constructed out of a flat sheet of material.

An extensive numerical study of the performances of origami tubes with various configurations when subjected to dynamic axial crushing has been carried out. The results show that the extensional collapse mode can be successfully induced in a square origami tube, and both low peak force and low deceleration is achieved in a single tube with the new design. A parametric study has been conducted on square origami tubes to investigate the effects of a series of geometric parameters. It is found that by properly selecting the pattern geometry, the peak crushing force can be lowered by over 40% in comparison with that of a conventional square tube while still maintaining similar mean crushing forces. The results demonstrate that the extensional mode can be always be triggered in origami tubes provided that a proper dihedral angle is selected, leading to both low peak force and high mean crushing force. The developed origami pattern is also compared with the full diamond collapse mode, and seen to show similar performance.

5.2   Future Work

In this dissertation, a novel type of origami pattern with improved crashworthiness capability was discussed. However, along the way, many interesting aspects were identified for future work which are summarized below.

1. **Testing the design under oblique loading and with different cross section:** In this research, the origami pattern was created over a square cross section tube only. And the study can be extended to different cross sectional shapes like hexagon or octagon. Also, the entire study was done with axial loading but in reality most of the impacts are not 100% axial. So a origami tube with proposed origami pattern with varying cross section and module length can be developed and evaluated over oblique impact.

2. **Develop an origami tube with modules with variable thickness and module length:** In this research, the thickness of the tube was kept constant at 2mm. But by creating the same tube from modules with different thicknesses and different lengths, the collapse mode can be further controlled.

3. **Including effect of uncertainty:** In this research, it was assumed that the values of the model parameters and their properties were accurate. But in real world conditions, values are uncertain. Hence the effect of uncertainty of model parameters and their properties, on the origami design and crash performance can be explored.

4. **Include more design variables:** In this dissertation, only three parameters were explored in parametric study of the proposed origami tube, like theta, number of modules M, and dimension b. Additional parameters like width to thickness ratio w/t, can be used to evaluate and further improve the performance of this design.

5. **Include more design objectives:** In this work, crushing force and deceleration are the two crashworthiness indicators that were extensively explored. However the study can be expanded by capturing the performance over crashworthy indicator like specific energy absorption.

6. **Defining Progressive Collapse Index (PCI):** While performing parametric study, 42 crash simulations were done in total, in turn a metadata has been created. This meta data can be used in machine learning and predicting PCI.

7. **Defining Fracture Model:** In this study, all the FEA models were developed without fracture definitions so as to be able to compare with different origami designs. Hence to understand the true capability of the current proposed origami structure under dynamic loading, a study will be performed with fracture definitions included.

REFERENCES

REFERENCES

[1] M. Peden, R. Scurfield, D. Sleet, D. Mohan, A. A. Hyder, E. Jarawan, C. D. Mathers *et al.*, "World report on road traffic injury prevention," pp. 3–6, 2004.

[2] A. Alghamdi, "Collapsible impact energy absorbers: an overview," *Thin-walled structures*, vol. 39, no. 2, pp. 189–213, 2001.

[3] G. Lu and Yu, "Energy absorption of structures and materials," *Elsevier*, pp. 10–19, 2003.

[4] J. Ma and Z. You, "Energy absorption of thin-walled square tubes with a pre-folded origami patternpart i: geometry and numerical simulation," *Journal of Applied Mechanics*, vol. 81, no. 1, p. 011003, 2014.

[5] W. Abramowicz and N. Jones, "Dynamic progressive buckling of circular and square tubes," *International Journal of Impact Engineering*, vol. 4, no. 4, pp. 243–270, 1986.

[6] T. Y. Reddy and S. Reid, "Phenomena associated with the crushing of metal tubes between rigid plates," *International Journal of Solids and Structures*, vol. 16, no. 6, pp. 545–562, 1980.

[7] G. Lu, "A study of the crushing of tubes by two indenters," *International journal of mechanical sciences*, vol. 35, no. 3-4, pp. 267–278, 1993.

[8] H. Al-Qureshi *et al.*, "Mechanics of static and dynamic inversion processes," *International journal of mechanical sciences*, vol. 39, no. 2, pp. 147–161, 1997.

[9] T. Reddy and S. Reid, "Axial splitting of circular metal tubes," *International Journal of Mechanical Sciences*, vol. 28, no. 2, pp. 111–131, 1986.

[10] R. A. Mayville, K. N. Johnson, R. G. Stringfellow, and D. C. Tyrell, "The development of a rail passenger coach car crush zone," *IEEE/ASME 2003 Joint Rail Conference*, pp. 55–61, 2003.

[11] E. Martinez, D. Tyrell, B. Perlman *et al.*, "Development of crash energy management designs for existing passenger rail vehicles," *ASME 2004 Joint Rail Conference*, pp. 63–67, 2004.

[12] D. Tyrell, K. Jacobsen, E. Martinez, and A. B. Perlman, "Train-to-train impact test of crash energy management passenger rail equipment: structural results," *ASME 2006 international mechanical engineering congress and exposition*, pp. 35–44, 2006.

[13] A. Airoldi, J. Gerardus, C. Bergamelli, and M. Sanvito, "Triggering system for the plastic collapse of a metal structural element," *US Patent 7,566,031*, 2009.

[14] J. D. Reid, J. R. Rohde, and D. L. Sicking, "Box-beam bursting energy absorbing terminal," *Journal of transportation engineering*, vol. 128, no. 3, pp. 287–294, 2002.

[15] AASHTO-ARTBA-AGC, "Guide to standardized highway barrier hardware,," *American Association of State Highway and Transportation Officials, Washington, DC*, pp. 773–777, 1995.

[16] P. W. Rothemund, "Folding dna to create nanoscale shapes and patterns," *Nature*, vol. 440, no. 7082, p. 297, 2006.

[17] S. D. Guest, "Deployable structures: concepts and analysis," Ph.D. dissertation, University of Cambridge, 1994.

[18] S. D. Guest and S. Pellegrino, "The folding of triangulated cylinders, part i: geometric considerations," *Journal of applied mechanics*, vol. 61, no. 4, pp. 773–777, 1994.

[19] P. S. Guest, Simon D, "The folding of triangulated cylinders, part iii: experiments," *Transactions-American Society of Mechanical Engineers Journal of Applied Mechanics*, vol. 63, pp. 77–83, 1996.

[20] R. Barker and S. Guest, "Inflatable triangulated cylinders," *IUTAM-IASS Symposium on Deployable Structures: Theory and Applications*, pp. 17–26, 2000.

[21] H. Tsunoda and Y. Senbokuya, "Rigidizable membranes for space inflatable structures," *43rd AIAA/ASME/ASCE/AHS/ASC Structures, Structural Dynamics, and Materials Conference*, pp. 1367–1373, 2002.

[22] Z. You and N. Cole, "Self-locking bi-stable deployable booms," *47th AIAA/ASME/ASCE/AHS/ASC Structures, Structural Dynamics, and Materials Conference 14th AIAA/ASME/AHS Adaptive Structures Conference 7th*, pp. 1685–1689, 2006.

[23] N. Jones, "Structural impact," *Cambridge university press*, pp. 54–63, 2011.

[24] R. A. Galganski, "Crashworthiness design of hsggt vehicles," *Proceedings of the 1993 IEEE/ASME Joint Railroad Conference*, pp. 121–130, 1993.

[25] J. A. Newman, "Head injury criteria in automotive crash testing," *SAE Transactions*, pp. 4098–4115, 1980.

[26] T. Frank and K. Gruber, "Numerical simulation of frontal impact and offset collisions," *CRAY Channels, Cray Research Inc*, pp. 2–6, 1992.

[27] NHTSA, "Federal motor vehicle safety standards and regulations," http://www.nhtsa.dot.gov/cars/rules/import/fmvss/index.html, 2018, [Online; accessed 18-January-2019].

[28] CMVSR, "Canadian motor vehicle safety standard and regulations," http://www.tc.gc.ca/actsregulations/regulations/crc-c1038/menu.html, 2018, [Online; accessed 16-January-2019].

[29] ECMT, "European vehicle safety standard regulations for crash testing," http://www.crashnetwork/regulations/ece-regulations/ece-regulations.html, 2018, [Online; accessed 16-January-2019].

[30] W. T. Hollowell, H. C. Gabler, S. L. Stucki, S. Summers, and J. R. Hackney, "Updated review of potential test procedures for fmvss no. 208," *NHTSA Docket*, pp. 6407–6, 1999.

[31] IIHS, "Side impact crashworthiness evaluation crash test protocol (version x)," https://www.iihs.org/iihs/ratings/technical-information/technical-protocols, 2017, [Online; accessed 19-January-2019].

[32] M. Richter, D. Otte, T. Pohlemann, C. Krettek, and M. Blauth, "Whiplash-type neck distortion in restrained car drivers: frequency, causes and long-term results," *European Spine Journal*, vol. 9, no. 2, pp. 109–117, 2000.

[33] NHTSA, "Laboratory test procedure for rear impact fmvss301r," https://www.nhtsa.gov/sites/nhtsa.dot.gov/files/tp-301r-02.pdf, 2007, [Online; accessed 20-January-2019].

[34] U. W. Seiffert and L. Wech, "Automotive safety handbook," *SAE International*, pp. 109–117, 2007.

[35] M. El-Gindy and L. Ilosvai, "An experimental investigation into vehicle response during steering and braking manoeuvres," *International Journal of Vehicle Design*, vol. 2, no. 4, pp. 463–469, 1981.

[36] M. El-Gindy and X. Tong, "Stability and braking performance analysis of bus/pony-trailer combination vehicles," *International Journal of Heavy Vehicle Systems*, vol. 8, no. 3-4, pp. 285–300, 2001.

[37] S. Shinde, "Structural optimization of thin walled tubular structure for crashworthiness," Master's thesis, IUPUI, 2014.

[38] S. P. Timoshenko and J. M. Gere, "Theory of elastic stability," *Courier Corporation*, pp. 174–299, 2009.

[39] A. Robertson, "The strength of tubular struts," *Proceedings of the Royal Society of London. Series A, Containing Papers of a Mathematical and Physical Character*, vol. 121, no. 788, pp. 558–585, 1928.

[40] E. E. Lundquist, "Strength tests of thin-walled duralumin cylinders in pure bending," *National Aeronautics and Space Administration*, pp. 1–16, 1933.

[41] T. Allan, "Experimental and analytical investigation of the behaviour of cylindrical tubes subject to axial compressive forces," *Journal of Mechanical Engineering Science*, vol. 10, no. 2, pp. 182–197, 1968.

[42] Q. Meng, S. Al-Hassani, and P. Soden, "Axial crushing of square tubes," *International Journal of Mechanical Sciences*, vol. 25, no. 9-10, pp. 747–773, 1983.

[43] T. Wierzbicki and W. Abramowicz, "On the crushing mechanics of thin-walled structures," *Journal of Applied mechanics*, vol. 50, no. 4a, pp. 727–734, 1983.

[44] P. H. Tehrani and I. Ferestadeh, "Studying energy absorption in tapered thick walled tubes," *Latin American Journal of Solids and Structures*, vol. 12, no. 1, pp. 173–204, 2015.

[45] W. Abramowicz and N. Jones, "Dynamic axial crushing of square tubes," *International Journal of Impact Engineering*, vol. 2, no. 2, pp. 179–208, 1984.

[46] W. Chen and T. Wierzbicki, "Relative merits of single-cell, multi-cell and foam-filled thin-walled structures in energy absorption," *Thin-Walled Structures*, vol. 39, no. 4, pp. 287–306, 2001.

[47] W. Abramowicz and N. Jones, "Dynamic axial crushing of circular tubes," *International Journal of Impact Engineering*, vol. 2, no. 3, pp. 263–281, 1984.

[48] N. Jones and W. Abramowicz, "Static and dynamic axial crushing of circular and square tubes," *Metal forming and impact mechanics*, pp. 225–247, 1985.

[49] D. Karagiozova, "Dynamic buckling of elastic–plastic square tubes under axial impacti: stress wave propagation phenomenon," *International Journal of Impact Engineering*, vol. 30, no. 2, pp. 143–166, 2004.

[50] D. Karagiozova and N. Jones, "Dynamic buckling of elastic–plastic square tubes under axial impactii: structural response," *International Journal of Impact Engineering*, vol. 30, no. 2, pp. 167–192, 2004.

[51] K. Murase and H. Wada, "Numerical study on the transition of plastic buckling modes for circular tubes subjected to an axial impact load," *International journal of impact engineering*, vol. 30, no. 8-9, pp. 1131–1146, 2004.

[52] D. Karagiozova, M. Alves, and N. Jones, "Inertia effects in axisymmetrically deformed cylindrical shells under axial impact," *International Journal of Impact Engineering*, vol. 24, no. 10, pp. 1083–1115, 2000.

[53] D. Karagiozova and N. Jones, "Influence of stress waves on the dynamic progressive and dynamic plastic buckling of cylindrical shells," *International Journal of Solids and Structures*, vol. 38, no. 38-39, pp. 6723–6749, 2001.

[54] N. Karagiozova, Jones, "On dynamic buckling phenomena in axially loaded elastic–plastic cylindrical shells," *International Journal of Non-Linear Mechanics*, vol. 37, no. 7, pp. 1223–1238, 2002.

[55] H. K. Ibrahim, "Design optimization of vehicle structures for crashworthiness improvement," Ph.D. dissertation, Concordia University, 2009.

[56] W. Abramowicz and N. Jones, "Transition from initial global bending to progressive buckling of tubes loaded statically and dynamically," *International Journal of Impact Engineering*, vol. 19, no. 5-6, pp. 415–437, 1997.

[57] I. Eren, Y. Gür, and Z. Aksoy, "Finite element analysis of collapse of front side rails with new types of crush initiators," *International journal of automotive technology*, vol. 10, no. 4, pp. 451–457, 2009.

[58] L. Abah, A. Limam, and M. Dejeammes, "Effects of cutouts on static and dynamic behaviour of square aluminium extrusions," *WIT Transactions on The Built Environment*, vol. 35, p. 88, 1970.

[59] S. Lee, C. Hahn, M. Rhee, and J.-E. Oh, "Effect of triggering on the energy absorption capacity of axially compressed aluminum tubes," *Materials & design*, vol. 20, no. 1, pp. 31–40, 1999.

[60] H. El-Hage, P. Mallick, and N. Zamani, "A numerical study on the quasi-static axial crush characteristics of square aluminum tubes with chamfering and other triggering mechanisms," *International Journal of Crashworthiness*, vol. 10, no. 2, pp. 183–196, 2005.

[61] N. Chase, R. Averill, and R. Sidhu, "Design optimization of progressively crushing rails," *SAE Technical*, pp. 47–54, 2009.

[62] A. Mamalis, D. Manolakos, S. Saigal, G. Viegelahn, and W. Johnson, "Extensible plastic collapse of thin-wall frusta as energy absorbers," *International journal of mechanical sciences*, vol. 28, no. 4, pp. 219–229, 1986.

[63] S. Hosseinipour and G. Daneshi, "Energy absorbtion and mean crushing load of thin-walled grooved tubes under axial compression," *Thin-walled structures*, vol. 41, no. 1, pp. 31–46, 2003.

[64] A. A. Singace and H. El-Sobky, "Behaviour of axially crushed corrugated tubes," *International Journal of Mechanical Sciences*, vol. 39, no. 3, pp. 249–268, 1997.

[65] X. Zhang, H. Su, and T. Yu, "Energy absorption of an axially crushed square tube with a buckling initiator," *International Journal of Impact Engineering*, vol. 36, no. 3, pp. 402–417, 2009.

[66] M. Shakeri, R. Mirzaeifar, and S. Salehghaffari, "New insights into the collapsing of cylindrical thin-walled tubes under axial impact load," *Proceedings of the Institution of Mechanical Engineers, Part C: Journal of Mechanical Engineering Science*, vol. 221, no. 8, pp. 869–885, 2007.

[67] T. Adachi, A. Tomiyama, W. Araki, and A. Yamaji, "Energy absorption of a thin-walled cylinder with ribs subjected to axial impact," *International journal of impact engineering*, vol. 35, no. 2, pp. 65–79, 2008.

[68] K. Andrews, G. England, and E. Ghani, "Classification of the axial collapse of cylindrical tubes under quasi-static loading," *International Journal of Mechanical Sciences*, vol. 25, no. 9-10, pp. 687–696, 1983.

[69] K. Lee, S. Kim, and I. Yang, "The energy absorption control characteristics of al thin-walled tube under quasi-static axial compression," *Journal of materials processing technology*, vol. 201, no. 1-3, pp. 445–449, 2008.

[70] X. Zhang, G. Cheng, Z. You, and H. Zhang, "Energy absorption of axially compressed thin-walled square tubes with patterns," *Thin-Walled Structures*, vol. 45, no. 9, pp. 737–746, 2007.

[71] W. Abramowicz and T. Wierzbicki, "Axial crushing of multicorner sheet metal columns," *Journal of Applied Mechanics*, vol. 56, no. 1, pp. 113–120, 1989.

[72] A. Mamalis, D. Manolakos, A. Baldoukas, and G. Viegelahn, "Energy dissipation and associated failure modes when axially loading polygonal thin-walled cylinders," *Thin-Walled Structures*, vol. 12, no. 1, pp. 17–34, 1991.

[73] M. Yamashita, M. Gotoh, and Y. Sawairi, "Axial crush of hollow cylindrical structures with various polygonal cross-sections: Numerical simulation and experiment," *Journal of Materials Processing Technology*, vol. 140, no. 1-3, pp. 59–64, 2003.

[74] A. Najafi and M. Rais-Rohani, "Influence of cross-sectional geometry on crush characteristics of multi-cell prismatic columns," *49th AIAA/ASME/ASCE/AHS/ASC Structures, Structural Dynamics, and Materials Conference*, p. 2014, 2008.

[75] H.-S. Kim, "New extruded multi-cell aluminum profile for maximum crash energy absorption and weight efficiency," *Thin-Walled Structures*, vol. 40, no. 4, pp. 311–327, 2002.

[76] X. Zhang, G. Cheng, and H. Zhang, "Theoretical prediction and numerical simulation of multi-cell square thin-walled structures," *Thin-Walled Structures*, vol. 44, no. 11, pp. 1185–1191, 2006.

[77] G. Nagel and D. Thambiratnam, "Computer simulation and energy absorption of tapered thin-walled rectangular tubes," *Thin-walled structures*, vol. 43, no. 8, pp. 1225–1242, 2005.

[78] G. M. Nagel and D. P. Thambiratnam, "Dynamic simulation and energy absorption of tapered thin-walled tubes under oblique impact loading," *International Journal of Impact Engineering*, vol. 32, no. 10, pp. 1595–1620, 2006.

[79] A. Mamalis and W. Johnson, "The quasi-static crumpling of thin-walled circular cylinders and frusta under axial compression," *International Journal of Mechanical Sciences*, vol. 25, no. 9-10, pp. 713–732, 1983.

[80] G. Sun, S. Li, Q. Liu, G. Li, and Q. Li, "Experimental study on crashworthiness of empty/aluminum foam/honeycomb-filled cfrp tubes," *Composite Structures*, vol. 152, pp. 969–993, 2016.

[81] S. Santosa and T. Wierzbicki, "Crash behavior of box columns filled with aluminum honeycomb or foam," *Computers & Structures*, vol. 68, no. 4, pp. 343–367, 1998.

[82] H.-S. Kim, W. Chen, and T. Wierzbicki, "Weight and crash optimization of foam-filled three-dimensional s frame," *Computational mechanics*, vol. 28, no. 5, pp. 417–424, 2002.

[83] Zaidi, Akbar, and Simmathiri, "Progressive damage of double-cell square aluminium 6061-t5 alloy polystyrene foam-filled section," *2nd International Conference on Arts, Social Sciences Technology*, pp. 601–612, 2012.

[84] A. G. Hanssen, M. Langseth, and O. S. Hopperstad, "Static and dynamic crushing of circular aluminium extrusions with aluminium foam filler," *International Journal of Impact Engineering*, vol. 24, no. 5, pp. 475–507, 2000.

[85] X. Zhang and G. Cheng, "A comparative study of energy absorption characteristics of foam-filled and multi-cell square columns," *International Journal of Impact Engineering*, vol. 34, no. 11, pp. 1739–1752, 2007.

[86] L. Mirfendereski, M. Salimi, and S. Ziaei-Rad, "Parametric study and numerical analysis of empty and foam-filled thin-walled tubes under static and dynamic loadings," *International Journal of Mechanical Sciences*, vol. 50, no. 6, pp. 1042–1057, 2008.

[87] H. Zarei and M. Kröger, "Bending behavior of empty and foam-filled beams: Structural optimization," *International Journal of Impact Engineering*, vol. 35, no. 6, pp. 521–529, 2008.

[88] H. Zarei and Matthias, "Optimum honeycomb filled crash absorber design," *Materials & Design*, vol. 29, no. 1, pp. 193–204, 2008.

[89] Z. Ahmad, D. Thambiratnam, and A. Tan, "Dynamic energy absorption characteristics of foam-filled conical tubes under oblique impact loading," *International Journal of Impact Engineering*, vol. 37, no. 5, pp. 475–488, 2010.

[90] G. L. Farley and R. M. Jones, "Crushing characteristics of continuous fiber-reinforced composite tubes," *Journal of composite Materials*, vol. 26, no. 1, pp. 37–50, 1992.

[91] J. R. M. Farley, Gary L, "Prediction of the energy-absorption capability of composite tubes," *Journal of Composite Materials*, vol. 26, no. 3, pp. 388–404, 1992.

[92] G. L. Farley, "Analogy for the effect of material and geometrical variables on energy-absorption capability of composite tubes," *Journal of composite materials*, vol. 26, no. 1, pp. 78–89, 1992.

[93] A. Mamalis, D. Manolakos, G. Demosthenous, and M. Ioannidis, "The static and dynamic axial crumbling of thin-walled fibreglass composite square tubes," *Composites Part B: Engineering*, vol. 28, no. 4, pp. 439–451, 1997.

[94] D. I. M. Mamalis, Manolakos, "Analysis of failure mechanisms observed in axial collapse of thin-walled circular fibreglass composite tubes," *Thin-Walled Structures*, vol. 24, no. 4, pp. 335–352, 1996.

[95] T. Wierzbicki *et al.*, "Axial resistance and energy absorption of externally reinforced metal tubes," *Composites Part B: Engineering*, vol. 27, no. 5, pp. 387–394, 1996.

[96] Mamalis, Manolakos, Ioannidis, and Papapostolou, "On the response of thin-walled cfrp composite tubular components subjected to static and dynamic axial compressive loading: experimental," *Composite structures*, vol. 69, no. 4, pp. 407–420, 2005.

[97] H.-W. Song, Z.-M. Wan, Z.-M. Xie, and X.-W. Du, "Axial impact behavior and energy absorption efficiency of composite wrapped metal tubes," *International Journal of Impact Engineering*, vol. 24, no. 4, pp. 385–401, 2000.

[98] M. Bambach and M. Elchalakani, "Plastic mechanism analysis of steel shs strengthened with cfrp under large axial deformation," *Thin-walled structures*, vol. 45, no. 2, pp. 159–170, 2007.

[99] M. Bambach, M. Elchalakani, and X.-L. Zhao, "Composite steel–cfrp shs tubes under axial impact," *Composite Structures*, vol. 87, no. 3, pp. 282–292, 2009.

[100] X. Zhang, Z. Wen, and H. Zhang, "Axial crushing and optimal design of square tubes with graded thickness," *Thin-Walled Structures*, vol. 84, pp. 263–274, 2014.

[101] X. Zhang, H. Zhang, and Z. Wen, "Axial crushing of tapered circular tubes with graded thickness," *International Journal of Mechanical Sciences*, vol. 92, pp. 12–23, 2015.

[102] G. Sun, F. Xu, G. Li, and Q. Li, "Crashing analysis and multiobjective optimization for thin-walled structures with functionally graded thickness," *International Journal of Impact Engineering*, vol. 64, pp. 62–74, 2014.

[103] J. Song, Y. Chen, and G. Lu, "Axial crushing of thin-walled structures with origami patterns," *Thin-Walled Structures*, vol. 54, pp. 65–71, 2012.

[104] J. Ma, D. Hou, Y. Chen, and Z. You, "Quasi-static axial crushing of thin-walled tubes with a kite-shape rigid origami pattern: numerical simulation," *Thin-Walled Structures*, vol. 100, pp. 38–47, 2016.

[105] K. Yang, S. Xu, J. Shen, S. Zhou, and Y. M. Xie, "Energy absorption of thin-walled tubes with pre-folded origami patterns: Numerical simulation and experimental verification," *Thin-Walled Structures*, vol. 103, pp. 33–44, 2016.

[106] J. N. Reddy, "An introduction to nonlinear finite element analysis: with applications to heat transfer, fluid mechanics, and solid mechanics," *Oxford University Press*, pp. 249–278, 2014.

[107] S. Rao, "The finite element method in engineering," *Elsevier Science*, pp. 147–168, 2005.

[108] N. Liu, Nguyen, Thoi, and Trung, "Smoothed finite element methods," *CRC Press*, p. 123, 2010.

[109] AISI, "Material properties for dp600," https://www.autosteel.org/research/ahss-data-utilization/dp600, 2019, [Online; accessed 8-January-2019].

[110] Altair, "Radioss 14 theory manual," Radioss Help, 2018, [Online; accessed 8-November-2018].

[111] H. T. Yang, S. Saigal, A. Masud, and R. Kapania, "A survey of recent shell finite elements," *International Journal for numerical methods in engineering*, vol. 47, no. 1-3, pp. 101–127, 2000.

[112] Altair, "Radioss 14 user guide," https://www.autosteel.org/research/ahss-data-utilization/dp600, 2018, [Online; accessed 8-November-2018].

[113] M. Bari, "A finite element study of shell and solid element performance in crash-box simulations," *SAE Technical*, pp. 93–97, 2015.

[114] J. O. Hallquist *et al.*, "Ls-dyna theory manual," *Livermore software Technology corporation*, vol. 3, pp. 25–31, 2006.

[115] P. Bandi, D. Detwiler, and A. Tovar, "Design of progressively folding thin-walled tubular components using compliant mechanism synthesis," *Thin-Walled Structures*, vol. 95, pp. 208–220, 2015.

[116] R. Wagoner and M. Li, "Simulation of springback: through-thickness integration," *International Journal of Plasticity*, vol. 23, no. 3, pp. 345–360, 2007.

[117] W. Abramowicz, "Thin-walled structures as impact energy absorbers," *Thin-Walled Structures*, vol. 41, no. 2-3, pp. 91–107, 2003.

[118] C. Yang, "Dynamic progressive buckling of square tubes," *The 27th Conf. on Theoretical and Appl. Mech., Tainan, Taiwan, ROC*, pp. 36–43, 2003.

[119] K. Yang, S. Xu, S. Zhou, J. Shen, and Y. M. Xie, "Design of dimpled tubular structures for energy absorption," *Thin-Walled Structures*, vol. 112, pp. 31–40, 2017.